Dedicated

To the Memory
of my Mother

Jenny Kohn

Table of Contents

EFFECTS OF THE TRIP PHENOMENON ON THE TOUGHNESS OF HEAT TREATABLE ALLOY STEELS

Gabriel Kohn

Materials and Molecular Research Division, Lawrence Berkeley Laboratory
and Department of Materials Science and Engineering,
University of California, Berkeley, California 94720

ABSTRACT

It is shown that substantial amounts of untransformed austenite may be obtained in low alloy steels by a combination of alloy modification (addition of silicon) and heat treatment. In silicon modified AISI 4330 steel, the amount of untransformed austenite is varied by utilizing isothermal treatments both above and below the M_s. The stability of the untransformed austenite is found to be dependent on the amount of silicon and also on the tempering temperature. A magnetic saturation technique was utilized to monitor the transformation of the austenite under uniaxial tensile loading. An improvement in the plane strain fracture toughness (K_{Ic}) was observed when the retained austenite transformed with respect to strain. This improvement was optimized with particular combinations of stability and volume fractions of retained austenite. The addition of silicon resulted in an increase of both the strength and the fracture toughness (K_{Ic}) of the quenched and tempered AISI 4330 steel. Yield strengths in the range of 200-220 ksi and K_{Ic} values as high as 107 ksi$\sqrt{in}$ were obtained. The microstructure was characterized using both optical and electron microscopy and is correlated with the mechanical properties.

I. INTRODUCTION

In recent years a large research effort has been directed towards improving the strength and toughness of steels.[1-4,48-50] The needs of the advanced technology of our days call for both better strength-to-weight and toughness-to-weight ratios. Remarkable combinations of strength and toughness have been obtained in the so called "TRIP" (TRansformation Induced Plasticity) steels.[5-8] These are metastable austenitic high strength steels that undergo an austenite to martensite transformation when plastically deformed. The formation of martensite provides resistance to necking in a tension test and thus increases both uniform elongation and ultimate tensile strength. Toughness is promoted due to both the energy absorption capacity of the austenite to martensite transformation and the 3% volume expansion associated with the transformation. The expansion tends to relieve the triaxial state of stresses at the tip of a crack during straining. The mechanical properties of TRIP steels are strongly dependent on austenite stability. The influence of austenite stability on mechanical properties of TRIP steels has been discussed by Bhandarkar et al.[9] The main limitation to the wide use of TRIP steels is the difficult and expensive process involved in their commercial manufacturing.[10]

Heheman[11] and Babu,[12] among others have shown that substantial amounts of austenite can be retained in AISI 4300 type steels when they are isothermally transformed at temperatures near the M_s. Babu has also shown that additions of alloying elements, especially Si,

increase the amount of untransformed austenite retained at room temperature after cooling down from the isothermal transformation temperature. Additions of alloying elements are not the only way to increase the amount of retained austenite in these steels. Lai[13] et al have reported that increasing the austenitizing temperature from the conventional 870-900°C to 1200°C increases the amount of retained austenite in AISI 4340 steel. They have also reported a two-fold increase in the plane strain fracture toughness on increasing the austenitizing temperature. Improvements in strength and toughness in experimental Fe-Cr-C steels by additions of alloying elements and by increasing the austenitizing temperature were reported by Carlson et al.[51] In other steels, Webster[14,15] and Antolovich et al[16] have shown that the retained austenite enhances fracture toughness by blunting a propagating crack and by undergoing a phase transformation at the crack tip.

The main objective of the present investigation was to study the behavior of retained austenite under stress and strain in modified AISI 4300 type steels and to examine whether it is possible to incorporate the good properties of the TRIP steels in these steels.

The base steel chosen for the present investigation was a AISI 4330 steel. The choice was based on three main consideration. First, the steel is commercially available. Secondly, a wide base of information about it is available in the literature. Thirdly, choice of AISI 4330 rather than higher C content steels from the AISI 4300 family was based on the extensive work of Thomas[17,48] and Thomas and Das[18,19] who have shown that carbon contents of 0.4% and higher increase the amount of twinning in martensite and lower the fracture toughness.

The reasons for choosing Si as the modifying element were, first, it is an inexpensive alloying element. In addition, Si is known to be a strong solid solution hardener[20,21] and is also known in its ability to retard the softening which occurs upon tempering.[22-25] The influence of Si on the tempering response of steel is explained by an alteration of the activity of carbon in the iron matrix[26] in a manner which retards the nucleation and growth of iron-carbides.[21,23] As shown by Babu,[12] yet another effect of Si is that it promotes retention of austenite in AISI 4300 type steels. By adding varying amounts of Si it was possible to obtain various amounts of retained austenite in the steels.

In the present investigation, the relative stability of the austenite with respect to stress or strain was examined in steels transformed at temperatures near the M_s, and the influence of the TRIP phenomenon, (when it occurred) on mechanical properties was established. Optical and electron microscopy were employed to correlate microstructure and mechanical properties.

II. EXPERIMENTAL PROCEDURE

A. Materials Preparation

1. Alloy Preparation

The steels used in the present investigation were prepared from commercial aircraft quality AISI 4330 steel. The chemical composition of the steel is given in Table 1. The steel was received in the form of a 1.5" dia. round bars in the "as-annealed" condition. It was remelted in a vacuum induction furnace and steels having Si contents of 1.0, 2.0 and 3.0 wt% were obtained. Sections of one ingot of each heat were chemically analyzed for all the major elements while the C and Si contents were determined in all the ingots. The compositions of the steels are also listed in Table 1.

The ingots were upset and cross forged to 2.75" wide by 1.0" thick bars and homogenized in vacuum for 24 hours at 1200°C.

2. Heat Treatment and Specimen Preparation

All specimen blanks were cut from the forged stock and had roughly the same size in order to keep the heating and cooling rates as similar as possible. The austenitizing treatment was carried out in a vertical alumina tube furnace in which a continuous argon flow was maintained. The duration of the austenitizing anneal was 1 hour after which the bottom lid of the tube was removed, and the specimen dropped into the quenching medium which was either agitated molten salt (for the isothermal treatments) or agitated oil (for the quenched and tempered treatments). Following the isothermal treatments, the specimens were

air cooled or, in a few cases, cooled to liquid nitrogen. Tempering treatments were carried out in salt baths. Test specimens were rough machined from heat treated blanks prior to tempering and then machined to their final dimensions. It was expected that the final machining following tempering would minimize the residual stresses and surface defects that may have resulted from the prior heat treatments.

The relative orientation of the specimen and the forged ingot is given in Fig. 1a.

B. Mechanical Testing

1. Hardness Tests

A Wilson hardness testing machine was used for hardness measurements on the Rockwell "C" scale. The reported results represent the average of at least 3 readings on each sample. Measurements were taken from the surface of flat tensile specimens and from pieces sectioned from the plane strain fracture toughness specimens.

2. Tensile Tests

The room temperature longitudinal tensile properties were determined using sheet tensile specimens having a 1.0" gauge length, a thickness of 0.05" and a gauge section width of 0.125" (Fig. 1b). In some cases additional tests were conducted using 1.0" gauge length 0.25" diameter ASTM specified round specimens (Fig. 2b). The tensile specimens were austenitized in the form of blocks 0.7×0.7×2.75" in size. This was done in order that heating and cooling rates in the tensile specimens would approach the rates in 0.7" thick fracture toughness specimens.

Sheet tensile specimens were obtained by slicing the 0.7" thick blanks with a water cooled cutoff wheel to form blanks 0.7×0.1×2.75" is size, then tempering and wet grinding to final dimensions. The round tensile specimens were tempered in the thick blank form and then ground to final dimensions.

The sheet tensile specimens, which were also used to detect the $\gamma \rightarrow \alpha$ transformation as described in a later section, were tested at a strain rate of 0.02 %/min. using a 5000 Kg capacity Instron machine. The yield strength was determined at 0.2% offset and the plastic strain to failure was obtained from the load vs crosshead displacement curve. The round tensile specimens were tested on a 300,000 lb (300 Kip) capacity MTS Universal Tensile Testing machine at a strain rate of 0.02% per minute. The yield strength was determined again using the 0.2% strain offset method and the plastic strain to failure was measured both from the recording chart and from the gauge section of the broken specimen.

3. Fracture Toughness Tests

Room temperature fracture toughness tests were performed according to ASTM specifications E-399-72. The specimens were of the compact tension type (CTS) as shown in Fig. 1c. The thickness of the specimens varied between 0.60 and 0.95".

The specimens were heat treated after being machined to their final dimensions except for their thickness (which was .040" oversize).

After heat treatment the specimens were wet ground to their final thickness, at the same time removing the decarburized layer. The 0.008" wide slot was then introduced by grinding. Subsequently a fatigue

crack was started at the tip of the 0.008" slot. The fatigue crack growth rate was chosen such that an average of 20,000 fatigue cycles was enough to introduce the standard crack length of 0.10". The fatigue precracked specimens were fractured using a MTS 300 Kip capacity Universal Tensile Testing machine. The ram speed was .0005 in./sec which ensured a stress intensity loading rate within the ASTM specified range.

A crack opening displacement (COD) gauge was used to monitor crack length during the test. The critical crack length at which instability occurred was determined from the load - COD plot, and the critical stress intensity K_Q was calculated and its validity as a plane strain fracture toughness value K_{Ic} was established according to standard ASTM procedures.

4. Impact Tests

Room temperature longitudinal impact properties were determined using a pendulum impact machine adjusted to a 60 ft-lb capacity. The tests were performed according to ASTM E-23-72 specifications. The Charpy V-notch specimen dimensions are shown in Fig. 2a.

C. Measurement of Phase Transformation Characteristics

1. Magnetic Saturation Technique

The amount of austenite to martensite phase transformation produced during tensile testing was measured using a magnetic saturation technique (Fig. 3). The saturation induction of each specimen was measured before and during straining on the Instron machine. Standard specimens of different compositions were austenitized, oil quenched and

then tempered at 650°C for 1 hour in order to transform any retained austenite. These standards were checked by x-rays and considered to be 100% magnetic. The magnetic saturation readings of each tensile specimen were compared to that of the standards and the amounts of austenite and martensite were determined. Detailed information concerning magnetic saturation in iron and the technique used can be found elsewhere.[26-29]

Since the determination of the amount of retained austenite using the magnetic saturation technique depended on many factors, the error in the measured value could not be estimated accurately using error propagation methods. However, in duplicate tests, the measured amounts of retained austenite varied by not more than ± 1%. This would result in confidence levels of ± 20% for specimens containing around 5% austenite and confidence levels of ± 5% for specimens containing about 20% austenite. In all cases, however, the relative changes in the amounts of phases within the same specimen were determined very accurately and the relative error was estimated to be not more than ± 1%. The minimum amount of austenite which could be detected in any given specimen was around 1%.

2. Dilatometry

A Theta Dilatronic IIIR model dilatometer was used in the present investigation. All measurements were carried out using hollow cylindrical specimens 0.4" long, 0.187" outer diameter, and 0.125" inner diameter. The heating rate was 900 °C/min, the austenitizing time at 900°C was 15 min and the cooling rate was 100 °C/sec.

The M_s, M_f, A_s, and A_f temperatures of all the alloys investigated were determined from the dilatometric curves and are given in Table 2.

The dilatometer was also used to follow the kinetics of the austenite decomposition in the course of the various isothermal heat treatments and to determine the relative amounts of phases present at the end of each isothermal heat treatment. The relative amounts of the athermal and isothermal decomposition products were determined by comparing the relative amounts of volume expansion at each stage.

3. X-Ray Analysis

In addition to the magnetic saturation technique, x-ray analysis was used for the retained austenite measurements. A Picker biplane diffractometer with a Cu tube operated at 40 KV and 14 mA was used. The florescent radiation was eliminated by the use of a LiF monochromator. Specimens used fof the x-ray analysis were sliced from the fracture toughness specimens and then polished using standard metallographic techniques.

The amounts of retained austenite were calculated by comparing the intensities of the 220_γ, 311_γ, and 211_α peaks using the method described by Cullity.[29] Comparison of the results obtained by x-ray and magnetic saturation techniques showed good agreement when the amount of retained austenite was 10% or greater. When the amount of austenite was smaller, the γ peaks were rather diffuse and x-ray analysis gave smaller values for the amount of austenite than the values obtained by the magnetic technique.

D. Microscopy

1. Scanning Electron Microscopy

Fracture surfaces were observed using a JEOLCO JSM-U3 Scanning Electron Microscopy (SEM) operated at 25 KV and an AMR 1000 SEM operated at 20 KV. The AMR 1000 Scanning Electron Microscopy had an Energy Dispersive Analysis of X-rays unit (EDAX model 711) attached to it which enabled semi-quantitive analysis of the chemical composition of very small areas from the observed specimen.

2. Optical Microscopy

Specimens for optical microscopy were cut from either the fracture toughness specimens or from the flat tensile specimens. They were mounted in Koldmount and abraded on silicon carbide paper down to 600 grit and then polished on a 1 μm diamond abrasive wheel. Specimens were etched in either nital (2-5%) or picral for 10-30 sec. A Carl Zeiss Ultraphot II metallograph was used for the examination of microstructures.

3. Transmission Electron Microscopy

Thin foils for TEM studies were prepared by cutting thin slices (.020-.030" thick) off the fracture toughness specimens using an abrasive wheel, chemically thinning the slices down to .002" using a solution containing 5% hydroflouric acid in hydrogen peroxide, and then polishing. A twin jet electropolishing unit operated at 30-50 V and 30-40 mA was used. The polishing solution was acetic-chromic acid (75g, CrO_3, 400 cc Acetic Acid, 20 cc H_2O). A Hitachi HU 125 and a Philips EM301 electron microscopes were used to observe the microstructure of the foils.

III. RESULTS AND DISCUSSION

A. Mechanical Properties

1. Isothermal Transformation at 350°C

The mechanical properties, as a function of tempering temperature, of steels isothermally transformed at 350°C for 1 hr. following austenitizing at 900°C for 1 hr. are summarized in Figs. 4 and 5 and also in Table 3. The amount of retained austenite as a function of Si content is shown in Fig. 6. The transformation behavior of retained austenite upon straining in tension and as a function of tempering temperature is shown in Figs. 7-10.

The results indicated that for the untempered steels, the higher the Si content the higher was the volume fraction of austenite retained on cooling to ambient temperature from the isothermal hold, the higher was the ultimate tensile strength and the hardness, the lower was the yield strength, and the higher was the total elongation. This behavior may be explained by the following known effects of Si on steels:

1) A significant concentration of Si (e.g. >1%) prevents the growth of carbides,[21,23,30] thereby maintaining a high carbon concentration in austenite. This results in chemical stabilization of the austenites[11,30] leading to greater amounts of retained austenite with concomitant lower yield strengths and higher ductility. This effect increases with greater Si content.

2) The presence of Si increases the strength of martensite by solid solution effects[31] resulting in higher strengths in steels with greater Si content.

Tempering these steels for 1 hour in the temperature range of 250°C to 400°C does not have a large effect on the amount of austenite which is retained upon cooling to room temperature. Tempering at higher temperatures, (up to 650°C) however, reduces the volume fraction of austenite as can be expected from known tempering behavior.[25,52] Tempering these steels does not change the relative stability of the austenite with respect to uniaxial loading and for each composition the amount of austenite which undergoes transformation remains constant.

The plane strain fracture toughness after transformation at 350°C was higher for the steel containing 2.0 wt%Si than for the steel with 3.0 wt%Si for all tempering temperatures up to 400°C. After tempering at 400°C for 1 hour an even higher plane strain fracture toughness was obtained for the steel modified with 1.0 wt%Si. This result may seem unusual since the steel having the lowest yield strength would normally be expected to have the highest fracture toughness. The behavior of the 3.0 wt%Si steel can be explained by considering the role of Si in these steels. Si is known to be a ferrite stabilizer[1,33] and even though the dilatometer results indicated that at 900°C the steel having 3.0 wt%Si is in a single austenite phase, it is possible that due to the difference in size between the CTS and the dilatometer specimen, the CTS was not austenitized completely and some untransformed ferrite was retained in the structure (As can be seen in Fig. 54).

The retained ferrite is a softer phase and gives less resistance to tearing, causing the lower toughness.

A second explanation for the decrease in toughness w' the general increase in the Si content (and judging from the quasi-cleavage mode of fracture of the 2.0 and 3.0 wt%Si steel shown in Figs. 35 and 36 probably a more important one) is the carbon enrichment of austenite during the isothermal transformation at 350°C. It is well known that during the bainite transformation carbon partitions from ferrite to austenite.[11,34] This carbon may either remain in solution or precipitate as carbides. However, due to the presence of Si which retards the growth of carbides most of the carbon may still be in solution in the austenite. Upon loading these steels in tension part of this high carbon austenite transforms to carbon rich martensite which is known to be brittle.[17-19] An estimation can be made of the amount of carbon in the austenite by assuming that the carbon content of bainite is between 0.2% to 0.25% as has been shown by Matas and Hehemann.[30] If the initial concentration of carbon in the steel was 0.3 wt%, and after transformation at 350°C there is 80% bainite with a carbon content of 0.25% then the carbon content in the austenite is 0.5%. Calculations based on diffusion data of carbon in α iron taken from Speich[46] and Smith[47] have shown that the diffusion distance of carbon during the isothermal hold is ~45 μm. This distance is large enough to allow carbon concentration to build up in the retained austenite. Previous studies have shown that 0.4% is the maximum allowable concentration of carbon in austenite which will not transform

to brittle martensite.[17-19] The results obtained from the specimens isothermally transformed at 350°C and tempered at 400°C show that the modified steel having the least amount of retained austenite, i.e. the steel containing 1.0 wt%Si has both the highest yield strength and the highest toughness while the steels having successively higher amounts of austenite due to their higher Si content have successively lower toughnesses.

In order to verify the effect of the untransformed high carbon austenite on the mechanical properties of these steels, tensile and CTS blanks of the alloy containing 2.0 wt%Si were transformed at 350°C and immediately quenched in liquid nitrogen (LN) and held until they cooled down to LN temperature (-196°C). The effect of refrigeration was to transform part of the austenite to martensite. The tensile properties and the amount of untransformed austenite of the LN-quenched steel are shown in Table 4 and in Figs. 11 and 12 respectively for all tempering temperatures and the plane strain fracture toughness is plotted in Fig. 4 for the steel tempered at 400°C.

While the amount of untransformed austenite prior to testing was lower in the LN quenched alloy and its yield strength consequently higher, the plane strain fracture toughness increased from 85 ksi$\sqrt{in}$ to 101 ksi$\sqrt{in}$. The results indicate that reducing the amount of brittle martensite which formed when the austenite transformed on loading and replacing it with a high carbon but tempered martensite increased the toughness of the alloy.

2. Isothermal Transformation at 250°C

The tensile strength of all the modified alloys isothermally transformed at 350°C was considerably lower than that obtained for the oil quenched alloys. In order to increase the strength of the steels an isothermal transformation temperature, lower then the M_s temperature of the steels, was chosen. The isothermal temperature 250°C is approximately 50°C below the M_s temperature of all four steels investigated. The mechanical properties of the steels isothermally transformed at 250°C are shown in Figs. 13 and 14 and in Table 5 as a function of the tempering temperature. The amount of untransformed austenite and its transformation behavior upon loading in uniaxial tension are summarized in Figs. 15 through 20.

The isothermal transformation of these steels below the M_s temperature introduces varying amounts of martensite (depending on their composition) into the microstructure. The amount of untransformed austenite increased with increasing Si content and the yield strength decreased accordingly. The effect of the retained austenite on the yield strength is best observed by comparing the results obtained from untempered specimens and specimens tempered at 250°C, with the results obtained from specimens tempered at higher temperatures. During tensile stressing the yield strength (which is measured at 0.2% strain offset) will decrease if martensite forms under the applied load (as has been demonstrated for "TRIP" steels[22]). The stability of the austenite with respect to stress, as measured by the vertical distance between the plotted lines in Figs. 14-17, in the first group of specimens was by far

smaller than that in the second group. This results in the drastic increase of the yield strength observed when tempering the tensile specimens at a temperature higher than 250°C.

Two reasons can lead to this difference in austenite stability. First, the specimens in the first group, i.e. untempered specimens and specimens tempered at 250°C are likely to have unrelieved stresses resulting from quenching. These stresses coupled with the loading stresses can trigger the $\gamma \rightarrow \alpha$ transformation at a load lower than that required for the initiation of transformation in specimens of the second group. Secondly, a difference in stability of retained austenite arises from its response to tempering. Measurements of the amount of retained austenite before and after tempering have shown that part of the austenite undergoes a phase transformation during the tempering treatment. The results are plotted in Fig. 16. The results show that maximum amount of austenite decomposition occurred during tempering at 300°C. Since this decomposition involves a 3% volume expansion the remaining untransformed austenite is constrained by a compressive stress that can mechanically stabilize the austenite.

It is interesting to note that the temperature at which the maximum amount of the retained austenite transformed, i.e. 300°C, is very close to the M_s temperature of these steels. Apparently at this temperature the thermodynamic driving force for the transformation is strong enough and the kinetics of carbide growth, which deplete the austenite of carbon, are rapid enough to cause this maximum in austenite transformation.

The ultimate tensile strength of all of the four alloys decreased continuously with increasing tempering temperature. While the unmodified steel had the highest yield strength, the steel containing 3.0 wt%Si had the highest tensile strength. The change in ultimate tensile strength with variation in Si content can be attributed both to the effect of the TRIP phenomenon which is largest in this steel and to the solid solution strengthening of the Si.

The carbon content of the austenite retained after transformation at 250°C is different from that obtained by transforming the steels at 350°C. When the steel is quenched into the salt bath at 250°C about 30 to 40 percent (depending on composition of the austenite) transforms to martensite. Since the martensitic transformation is a diffusionless transformation the carbon content of the martensite is the same as that of the parent austenite, in this case 0.3 wt%.
After the initial martensitic transformation has taken place, an isothermal transformation occurs as indicated by a volume expansion in a dilatometer specimen. The exact nature of the isothermal transformation product was not determined in this investigation, but the volume change indicated that there was a structural change from fcc to bcc or bct. This would suggest that the isothermal product was either bainite (which has a carbon content of 0.2 - 0.25%[30]) or martensite (with a carbon content of 0.3%), or both. In any case, the untransformed austenite can become enriched with carbon only if carbon partitioning occurs from the bainitic product. Therefore, the austenite carbon content would not exceed 0.4%. As previously mentioned, this

is the maximum allowable amount of carbon in austenite which would not transform to brittle martensite. Apparently, the presence of relatively low carbon content austenite in the steels isothermally transformed at 250°C leads to fracture toughness values higher than these obtained for steels isothermally transformed at 350°C.

While the yield strengths of the modified steels were approximately the same after isothermal transformation at 250°C and 1 hour tempering at temperatures equal to and greater than 250°C, the plane strain fracture toughness of the steel containing 2.0 wt%Si was higher than that of the other two modified steels. This was possibly due to the presence of austenite having optimum stability. It appeared that transformation of austenite under load in the 2.0 wt%Si steel resulted in a balance between the beneficial effects due to energy absorption and relief of stresses at the crack tip on the one hand, and the detrimental effects due to brittle phase formation on the other.

The plot of %elongation vs the tempering temperature (Fig. 13) indicated that an increase in the amount of Si in the steel led to an increase in the total elongation to fracture. The increase was attributed to the formation of strain induced martensite which increases the resistance to necking and enhances the elongation.

3. Isothermal Transformation at 200°C

Isothermal transformation at 200°C led to the formation of a greater volume fraction of martensite than formed at the higher temperatures and the volume fractions of retained austenite and isothermal product (which will be refered to as bainite) were lowered

concomitantly. The amounts of phases present are shown in Table 7. This resulted in increases in both the yield strength and the ultimate tensile strength. The yield and ultimate tensile strengths increased also with increase in Si content. The mechanical properties of steels isothermally transformed at 200°C are plotted as a function of tempering temperature in Figs. 21 and 22 and also given in Table 8. The amount and transformation behavior of untransformed austenite in the steels are shown in Figs. 23 through 26.

The low temperature isothermal transformation leads to increases in the yield strengths of the alloys as a result of the introduction of more martensite into the structure. With this heat treatment the modified alloys display yield strengths exceeding 200 ksi. The results also indicate that the solid solution strengthening effect of the Si prevailed over its previously described softening effect resulting from austenite retention.

The ultimate tensile strength of the steels also increased upon lowering the isothermal transformation temperature and again the steel containing the higher Si content had a higher tensile strength. The values obtained for the steel containing 3.0 wt%Si were as high as 280 ksi in the as-transformed condition and 260 ksi after tempering at 400°C.

Even though the yield and ultimate strengths of all the steels increased by transforming at 200°C the fracture toughness did not decrease. In fact, in most cases the plane strain fracture toughness was greater than that obtained for specimens transformed at 250°C.

An optimum combination of strength and plane strain fracture toughness was obtained for the 2.0 wt% steel tempered at 400°C following isothermal transformation at 200°C. The yield strength was 207 ksi, the ultimate strength was 240 ksi, the plane strain fracture toughness was 102 ksi$\sqrt{in.}$ and the room temperature CVN impact energy was 28 ft-lbs. The good combination of strength and toughness were attributed to several factors: At the lower isothermal transformation temperature the driving force for the initial martensitic transformation was larger than that at the higher isothermal transformation temperature resulting both in a larger volume fraction of martensite and in a finer lath or packet size. The fine structure is probably due to the fact that at the lower temperature more martensite nuclei actively take part in the transformation and since the size of a single lath is determined only by the distance from the site of its nucleation to the nearest obstacle for growth, the impingement of the laths against each other results in a finer structure. Both the higher martensite content and the fine structures are factors which increase toughness.[35,36]

To examine whether retained austenite had any additional effect on the mechanical properties of steels isothermally transformed at 200°C, specimens of the 2.0 wt% steel were isothermally transformed at 200°C and immediately quenched to liquid nitrogen. This resulted in the transformation of part of the untransformed austenite into martensite. The specimens were then tempered for 1 hr. at temperatures up to 400°C. The tensile properties and the transformation behavior of untransformed austenite are illustrated in Table 9 and Figs. 27 and 28 for all

tempering temperatures. The plane strain fracture toughness of the specimen tempered at 400°C is plotted in Fig. 21. The toughness of the specimen tempered at 400°C was appreciably lower than that of a specimen which had not been quenched to liquid nitrogen. The lower toughness was attributed to the lower amount of austenite in the specimen quenched to liquid nitrogen.

The role of the retained austenite may also be seen by observing the difference in toughness between the specimen of the 2.0 wt%Si steel tempered at 250°C and 300°C following isothermal transformation at 200°C and air cooling. The toughness was lower for the specimen tempered at the higher tempering temperature (Fig. 21). This reduction in toughness seemed to correlate well with the greater stability of the austenite in the steel tempered at 300°C as compared to the austenite stability in the steel tempered at 250°C (Fig. 25). As in the case of specimens isothermally transformed at 250°C; optimum combinations of strength and toughness were obtained for specimens transformed at 200°C when the specimens were tempered in the temperature range of 250°C to 400°C.

All the alloys isothermally transformed at 200°C exhibited lower toughness in the as transformed condition than in the tempered condition. This indicated that the residual stresses coupled with the relatively large instability of austenite (with respect to an applied stress) and the large amount of brittle martensite forming by the deformation induced transformation of austenite have a detrimental effect on the resistance of the alloys to crack propagation.

4. Quenched and Tempered Steels

Commercially AISI 4330 steel is commonly used in the quenched and tempered condition. It was of interest therefore, to study the effect of Si additions on the mechanical perperties of the steel after it was quenched and tempered. The mechanical properties are plotted in Figs. 29 and 30 and are also shown in Table 10. The amount and transformation behavior of retained austenite in the quenched and tempered steels are plotted in Fig. 32 through 34.

By comparing the results obtained for specimens of commercial AISI 4330 steel with those obtained for the Si modified steels, two important effects of Si additions were observed:

1) The strength and the plane strain fracture toughness of the modified steels were higher than those of commercial AISI 4330 steel.

2) The "martensite embrittlement" range as seen from Fig. 29 was shifted from around 300°C in the commercial steel to around 500°C in the modified steels.

The strengthening effect of the Si is so dramatic that the yield strength of the 3.0 wt%Si steel was higher in some cases than the ultimate tensile strength of the unmodified steel; and yet, the plane strain fracture toughness was not much lower and, in some cases, (as quenched, and 300°C temper) was even higher.

The effect of Si on toughness can be explained on the basis of its effect on the growth of carbides. The "tempered martensite" embrittlement is associated with the formation of carbide films at lath boundaries.[25] By retarding the growth of those carbides the Si modified

steel can be tempered at higher temperatures and thus stress relieved more effectively.[37]

In the quenched and tempered condition, as was the case in the isothermally transformed condition, the steel modified with 2.0 wt%Si showed the best combinations of tensile strength and fracture toughness. The values of 220 ksi for yield strength 260 ksi for tensile strength, and 107 ksi$\sqrt{in}$ for plane strain fracture toughness and CVN impact energy of 28 ft-lb. represent a typical good combination of properties.

B. Microscopy

1. Scanning Electron Microscopy

Scanning electron microscopy was used to study the surface of specimens which had been tested for fracture toughness, in order to characterize their mode of failure. Three basic modes of fractures, as described by Beachem and Pelloux,[38] were observed in all the specimens. These were:

a. Dimpled rupture or microvoid coalescence

b. Quasi-cleavage

c. Cleavage.

Since different areas of most specimens showed different modes of fracture an attempt was made to select only those fractographs which show the dominant mode of fracture in each specimen.

The fractographs shown in Figs. 35 through 37 are representative fractographs taken from specimens which have been isothermally transformed at 350°C. It is interesting to note that all specimens except the one

which was refrigerated to liquid nitrogen temperature (Fig. 37b) show quasi-cleavage as the main mode of fracture. The presence of this mode of fracture, both in the untempered specimens Fig. 35 and in the tempered specimens (Fig. 36 and Fig. 37a), is also associated with high fracture toughness (over 100 ksi$\sqrt{in}$ in the case of the 1.0 wt%Si steel). The fracture appearance was attributed to the presence of retained austenite (in amounts as high as 20% in the 3.0 wt%Si steels). As mentioned earlier, the retained austenite was very rich in carbon and presumably transformed to a carbon rich martensite which is brittle, particularly when untempered.

The size of the quasi-cleavage facets shown in all the fractographs is at least an order of magnitude larger than the size of the retained austenite films (as shown in the TEM micrographs in a different section). It seems, though, that the fractographs give us evidence, on a macroscopic scale, about the behavior of the material on a microscopic scale. The detrimental effect of retained austenite on fracture toughness was also evident from the fractograph in Fig. 37b. The fractograph was obtained from a 2.0 wt%Si steel which was cooled down to liquid nitrogen temperature (-196°C) immediately following isothermal transformation at 350°C. A part of the retained austenite transformed when the steel was cooled to -196°C and the plane strain fracture toughness increased from 85 to 100 ksi$\sqrt{in}$. Fractographs of the specimen showed a considerable amount of dimpled rupture which is a mode of fracture usually associated with high energy absorption.

In fracture specimens of steels isothermally transformed below the M_s, the fracture morphology was mainly dimpled rupture with some quasi-cleavage features. The fractographs of specimens transformed at 250°C are shown in Fig. 38 through 40.

In specimens which were isothermally transformed at 200°C the main mode of fracture was dimpled rupture with very few quasi-cleavage areas. Here, as in the case of specimens isothermally transformed at 250°C, the as cooled specimens had high toughness. This was due to tempering, during isothermal hold, of the martensite which formed on quenching from the austenitizing temperature to the isothermal hold temperature. A typical fracture surface of the as-cooled specimens is shown in Fig. 41 which is a fractograph of a 3.0 wt%Si specimen. The main mode of fracture - microvoid coalescence - was also found in tempered specimens as evident in Figs. 42, 43, 44, and 45. On the basis of these fractographs it was concluded that tempering the modified steels at temperatures as high as 400°C did not change their mode of fracture.

The unmodified steel, on the other hand, showed a drastic change in the mode of fracture when tempered at 400°C as seen in Fig. 45b. The dominant mode of fracture in this specimen was quasi-cleavage with very little dimpled rupture. This difference in fracture mode between the modified and unmodified steels was due to the effect of silicon on the "tempered martensite embrittlement" range in these steels. While there was no evidence of embrittlement, (represented by quasi-cleavage mode of fracture), in the modified steels when tempered at 400°C, the unmodified 4330 steel clearly showed evidence of embrittlement.

The same changes in mode of fracture, which were observed in the unmodified steel isothermally transformed at 200°C, were also seen in the quenched and tempered specimens. Figures 46 and 47 show a sequence of fractographs taken from specimens of the unmodified steel which were oil quenched and tempered at various temperatures. While the as-quenched specimens and the specimens quenched and tempered at 250°C (Fig. 46) show dimpled rupture, the specimens tempered at 300°C and 400°C (Fig. 47) feature mainly a quasi-cleavage mode of fracture which indicated that these steels were embrittled by the tempering at temperatures higher than 250°C. The same was not true for the modified steels. All quenched and tempered specimens of modified steels showed a ductile rupture mode of fracture as long as the tempering temperature did not exceed 400°C. Typical fractographs are shown in Figs. 48 through 50. Strong evidence of embrittlement and intergranular cracking is seen in Fig. 51 which is a fractograph of a 2.0 wt%Si steel tempered at 500°C. The intergranular cracking can be seen both in the fatigue precracked area Fig. 51b and in the fast fracture area of the specimen Fig. 51a. It is interesting to note that the embrittlement in the modified steel occurred following tempering at a temperature high enough to transform a large volume fraction of retained austenite to ferrite and carbide.

Various types of inclusions were observed in all the steels used in the present investigation. The inclusions apparently served as crack initiation sites in specimens loaded in tension. Tearing of the matrix around inclusions resulted in the formation of the cup-like dimples observed on fracture surfaces. Inclusions were observed at the bottom

of these dimples. Most of these inclusions have been analyzed to be MnS particles but their actual composition may vary. Figure 52a shows a SEM fractograph illustrating inclusion in a 3.0 wt%Si steel specimen. The EDAX output obtained from the inclusion is shown in Fig. 52b. The peaks (from left to right) are from Al, Si, Ca, Mn, FeK_{α} and FeK_{β}. Figure 53 shows a different area of the same specimen with an inclusion which contains Si, Cr, Mn, and Fe.

2. Optical Microscopy

Using the optical microscopy, it is very difficult, if not impossible, to differentiate between lower bainite and martensitic structures in steels. Therefore, no attempt was made to use optical micrographs to differentiate between the isothermal and the athermal transformation products in the structure as it appears in the optical micrographs. Optical microscopy was used mainly to characterize the grain size of the specimens after heat-treatment and to provide general information about the microstructures involved.

A representative set of micrographs of specimens isothermally transformed at 350°C is shown in Figs. 54 and 55. The prior austenite grain sizes of all the specimens were almost the same (ASTM 7) as that shown in Fig. 54a.

Figure 54b is a micrograph of a 3.0 wt%Si in which light spheres of untransformed ferrite can be observed. The bainite laths are clearly seen but the morphology of the austenite, which is known to be present

in the steel, cannot be determined from these micrographs and electron transmission microscopy had to be used for this purpose (see next section).

The next two micrographs (Fig. 55a,b) show the structure of the steels after tempering at 400°C, in which the carbides that formed during the tempering stage can be seen.

The microstructures which were obtained after transformation below the M_S temperature were all very similar to each other. The main difference between the isothermally transformed and oil quenched structures was in the relative sizes of the laths which were smaller in the oil quenched specimens. This was explained by the lower transformation temperature which increases the driving force for the transformation and leads to a larger number of lath nuclei growing simultaneously. The impingement on each other of the growing laths stops their growth and a finer transformation product is obtained. Examples of the microstructures obtained by isothermal transformation at 200°C and by oil quenching are shown in Figs. 56 through 58. Figure 56a and b are optical micrographs of a 2.0 wt%Si steel isothermally transformed at 200°C and tempered at 300°C and 400°C respectively. The structure is a fine mixture of martensite and the isothermal product which formed during the isothermal hold. In the 3.0 wt%Si steel Fig. 47 a few traces of untransformed ferrite can be clearly seen (marked by an arrow).

The martensitic structure Fig. 58 is a mixture of lath and plate martensite with the lath structure being the dominant feature. The

retained austenite, while present, could not be detected from these pictures.

3. Transmission Electron Microscopy

Electron microscopy studies were employed to characterize the microstructure and to determine the morphology and distribution of retained austenite. It was observed that retained austenite was distributed as thin films around either bainite or martensite laths. This observation is in agreement with other studies of similar steels.[34] The same morphology of the untransformed austenite was found in all the steels of the present investigation irrespective of their composition and heat treatment. No large "bulks" of austenite were found even in the steels containing up to 20 wt% of untransformed austenite.

Figure 59 shows the transmission electron micrographs of a 2.0 wt%Si steel transformed at 350°C and tempered at 400°C. The microstructure is very similar to the one reported by Huang and Thomas[39] for a similar Si steel. The dark field micrograph of the austenite spot (Fig. 59b) shows reversal of contrast of austenite areas. It is evident that the films of retained austenite follow the laths boundaries and then bend into the bainite matrix. The two other dark field micrographs Fig. 59c,d show two twin-related bainite laths - a feature which was occasionally observed in these structures.

The next series of electron micrographs shows the microstructure of the 2.0 wt%Si steel isothermally transformed below the M_s temperature. (This composition was chosen since that steel had the best combination of properties). Figures 60 through 62 show the microstructure of a

specimen which was transformed at 200 and air cooled. The general structure is that of dislocated lath martensite with retained austenite films between the laths. This can be best seen in the bright and dark field micrographs of Fig. 60.

Analysis of the diffraction pattern, given in the line drawing of Fig. 68c (see Ref. 52) shows that the orientation between the austenite and martensite has the Kurdjumov-Sachs relationship[40] i.e. $(111)_\gamma \| (011)_\alpha$, $(110)_\gamma \| (\bar{1}11)_\alpha$. Occasional martensite twinning was observed as illustrated in Fig. 61. Some of the laths contained very fine wavy precipitates as illustrated both in Fig. 60 and Fig. 62. The precipitates were so fine that they did not give rise to a distinct diffraction pattern and so they were not unambiguously identified. The habit plane of the precipitates was not any of the known habit planes for ε carbides or cementite[41-43] and this too contributed to the difficulty in identification.

Figures 63 through 65 show the microstructure of the 2.0 wt%Si steel having undergone the same heat treatment plus tempering at 400°C. While the retained austenite is still present, the carbides are coarser in size and are evident in the dark field image of a carbide diffraction spot (Fig. 63). Analysis of the diffraction pattern showed that the matrix orientation was [110]. The carbide spot which was used to obtain the dark field image of the carbides was indexed as a $(0\bar{2}2)$ cementite reflection. Two other carbide diffraction spots were identified as (042) and $(02\bar{2})$ cementite (see Fig. 63c). The long axis of the carbides is perpendicular to the 112 direction of the matrix indicating

that they have probably been nucleated on twin boundaries. This was in agreement with the observations made by Kelly and Nutting[44] and by Huang and Thomas.[45]

The two electron micrographs Fig. 66 and Fig. 67 show the structure of the 2.0 wt%Si steel quenched and tempered at 300°C. The microstructure is that of a dislocated lath martensite with carbides present in some of the laths. Untransformed austenite was present in small quantities and can be clearly seen in the dark field micrograph of Fig. 66. Some evidence of microtwinning can be seen in the bright field image of this figure but the twinning was not extensive and most of the structure was similar to that shown in Fig. 67.

4. Summary

Isothermal transformation above the M_s (300°C), i.e. at 350°C resulted in steels having various levels of retained austenite. The higher the amount of silicon in the steel the higher was the amount of retained austenite which was retained as thin films between the bainite or martensite laths. The mechanical properties of the steels transformed at 350°C were characterized by low yield strengths ranging from 140 to 180 ksi and moderate ultimate strengths in the range of 200 to 220 ksi. The ductility increased with increasing amounts of retained austenite while the plane strain fracture toughness decreased as the amount of austenite increased. The dominant mode of fracture in all the modified steels was quasi-cleavage thereby reflecting the detrimental effect on toughness of the carbon enriched retained austenite which transformed, during testing, to martensite. Isothermally

transforming the steels at temperatures below their M_s temperature did not change the morphology of the austenite. The amount of the austenite and its carbon content, however, decreased with the decrease in isothermal transformation temperature.

A marked improvement in properties was observed at the lower isothermal transformation temperatures, accompanied by a change in the mode of fracture from mainly quasi-cleavage for steels transformed at the higher temperature to mainly dimpled rupture for steels transformed at the lower temperature. This was attributed both to the introduction of martensite into the microstructure and to the beneficial effects of the $\gamma \rightarrow \alpha$ transformation, during testing, of a low carbon austenite.

A selected number of experimental results obtained in the present investigation are plotted in Figs. 69 and 70. The figures are plots of the bands of toughness vs. yield strength or ultimate strength for several steels. It is seen that the strength-toughness combination of steels in the present investigation compared favorably with the expensive maraging steels.

IV. CONCLUSIONS

The steels studied in the present investigation were AISI 4330 and AISI 4330 modified with additions of 1.0, 2.0 and 3.0 wt%Si. All steels were austenitized 1 hour at 900°C and then transformed at various temperatures. The general conclusions which pertain both to steels isothermally transformed below and above the M_s temperature are:

1. The amount of austenite which was retained in steels cooled to room temperature from the isothermal transformation temperature increased with an increase in the Si content.

2. The untransformed austenite was retained as thin films around bainite or martensite laths.

3. During tempering some of the retained austenite underwent a phase transformation. A peak in the amount transformed during tempering was observed to occur around the 300°C tempering temperature. Most of the retained austenite decomposed after tempering around 600-650°C for ½ hour.

4. The stability of the retained austenite to stress/strain increased with increased in the tempering temperature up to 350-400°C and then decreased.

5. The higher the amount of retained austenite the larger was the ductility of the steel.

6. The higher the amount of Si the higher was the tensile strength.

The conclusions which can be drawn from the results of transformation at 350°C are:

1. The higher the amount of retained austenite the lower was the yield strength of the steel.

2. The higher the amount of (carbon rich) austenite the lower was the plane strain fracture toughness of the steel.

The conclusion from the investigation of sepcimens transformed below the M_s temperature are:

1. The transformation of the austenite (less enriched in carbon) under stress/strain had a beneficial effect on the plane strain fracture toughness of the steels.

2. Optimum combination of amount and stability to stress/strain of the austenite were observed in steels modified with 2.0 wt%Si and these were the steels with the best mechanical properties.

3. Best combination of strength and toughness, i.e. 220 ksi yield strength and 107 ksi$\sqrt{in}$ plane strain fracture toughness were observed in the 2.0 wt%Si steel which was oil quenched and tempered at 300°C.

4. Good combination of properties were also obtained for steels isothermally transformed at 200°C. The best values were 208 ksi yield strength with 102 ksi$\sqrt{in}$. plane strain fracture toughness.

5. Si additions to AISI 4330 steel shifted the "martensite embrittlement" range to higher temperatures (from 250-300°C to around 500°C).

REFERENCES

1. Bain, E.C. and Paxton, H.W., Alloying Elements in Steel (American Society for Metals, Metals Park, Ohio, 1966).
2. Thomas, G., Zackay, V.F., and Parker, E.R., Substructure and High Strength Metals, Sagamore Conference, NY, 1965. Syracuse University Press 3-39 (1966).
3. Parker, E.R., Zackay, V.F., Lai, G.Y., and Horn, R.M., Untempered Ultra-High Strength Steels of High Fracture Toughness, LBL-2715. Lawrence Berkeley Laboratory, University of California, Berkeley, April 1974. Also in Alloy Design, Tien, J.K. and Ansell, G.S., editors, Academic Press (1975).
4. Zackay, V.F. and Parker, E.R., Alloy Design for Fracture Toughness, LBL-2782, Lawrence Berkeley Laboratory, University of California, Berkeley, June 1974.
5. Gerberich, W.W., Hemmings, P.L., and Zackay, V.F., Met. Trans. 2, 2243 (1971).
6. Antolovich, S.D. and Singh, B., Met. Trans. 2, 2135 (1971).
7. Gerberich, W.W., Hemmings, P.L., Merz, M.D., and Zackay, V.F., Trans. ASM, 61, 843 (1968).
8. Gerberich, W.W., Hemmings, P.L., Zackay, V.F., and Parker, E.R., Fracture 1969, Pratt, P.L., ed., Chapman and Hall, Ltd., London, 288 (1969).
9. Bhandarkar, D., Zackay, V.F., and Parker, E.R., Stability and Mechanical Properties of Some Metastable Steels, Met. Trans. 3, 2619 (1972).

10. Zackay, V.F., Thermomechanical Processing, to be published in Materials Science and Engineering, and also LBL-4982, Lawrence Berkeley Laboratory, University of California, Berkeley, April 1976.

11. Hehemann, R.F., Phase Transformations (American Society for Metals, Ohio, 1970), p. 409.

12. Babu, B.N.P., An Investigation of Bainite Transformation in Medium Carbon Low Alloy Steels (D. Eng. Thesis), LBL-2772, August 1974.

13. Lai, G.Y., Wood, W.E., Clark, R.A., Zackay, V.F., and Parker, E.R., Met. Trans. 5, 1663 (1974).

14. Webster, D., Trans. ASM 61, 816 (1968).

15. Webster, D., Met. Trans. 2, 2097 (1971).

16. Antolovich, S.D., Saxena, A., and Chanani, G.R., Met. Trans. 5, 633 (1974).

17. Thomas, G., Met. Trans. 2, 2373 (1971).

18. Das, S.K. and Thomas, G., Trans. ASM, 62, 659 (1969).

19. Thomas, G. and Das, S.K., J. Iron Steel Inst. 209, 801 (1971).

20. Shih, C.H., Averbach, B.L. and Cohen, M., Trans. ASM 48, 86 (1958).

21. Altstetter, C.J., Cohen, M., Averbach, B.L., Trans. ASM 55, 287 (1962).

22. Allten, A.G. and Payson, P., Trans. ASM 45, 498 (1953).

23. Owen, W.S., Trans. ASM 46, 812 (1954).

24. Keh, A.S. and Leslie, W.C., Materials Science Research, Vol. 1, Plenum Press, New York, 1963, 208.

25. Speich, G.R. and Leslie, W.C., Met. Trans. 3, 1043 (1972).

26. Bozorth, R.M., Ferromagnetism, New York: D. Van Nostrand Co. (1951).

27. Hoselitz, K., Ferromagnetic Properties of Metals and Alloys, Oxford, England: Clarendon Press (1952).

28. de Miramon, B., Quantitative Investigation of Strain Induced Strengthening in Steel, M.S. Thesis, UCRL-17849, University of California, Berkeley, California, September 1967.

29. Cullity, B.P., Elements of X-Ray Diffraction (Addison-Wesley, Reading, MA, 1956), 391.

30. Matas, S. and Hehemann, R.F., Trans AIME, 221, 176 (1961).

31. Ziegler, N.A., Meinhart, W.L. and Goldsmith, J.R., Trans. ASM 40, 617 (1948).

32. Zackay, V.F., Bhandarkar, M.D. and Parker, E.R., The Role of Deformation Induced Phase Transformations in the Plasticity of Some Iron-Base Alloys, LBL-2775, Lawrence Berkeley Laboratory, University of California, Berkeley, August 1974.

33. Sato, A., Metallographic Investigation of the Iron-Silicon-Carbon Alloys, Technical Report, Tohoku., Vol. 9, 515-565 (1929-1930).

34. Bhat, M.S., Research in progress, Lawrence Berkeley Laboratory, Berkeley, California.

35. Turkalo, A.M., Trans. AIME 218, 24 (1960).

36. Jin, S., Hwang, S.K., and Morris, Jr., J.W., The Effect of Grain Size and Retained Austenite on the Ductile-Brittle Transition of a Titanium-Gettered Iron Alloy, LBL-3576, Lawrence Berkeley Laboratory, University of California, Berkeley, April 1975.

37. Wylie, E.A., The Effect of Tempering on the Strength and Toughness of a Series of Fe-Cr-Si-C Alloys, LBL-4574 (M.S. Thesis) Lawrence Berkeley Laboratory, University of California, Berkeley, January 1976.

38. Beachem, C.D. and Pelloux, R.M.N., Fracture Toughness Testing and Its Applications, ASTM STP 381, (American Society for Testing and Materials, Philadelphia), 210 (1965).

39. Huang, D.H., Bainitic Transformation in Steels, LBL-3713 (Ph.D. thesis) Lawrence Berkeley Laboratory, University of California, Berkeley, May 1975.

40. Kurdjumov, G. and Sachs, G., Z. Physik, 64, 325 (1930).

41. Jack, K.H., JISI 169, 26 (1951).

42. Isaichev, I.V., Zhur, Tekhn. Fiziki 17, 835 (1947).

43. Bagaryatskii, Yu. A., Doklady, Akademiia Nauk SSSR 73, 1161 (1950).

44. Kelly, P.M., and Nutting, J., Proc. Royal Soc. A259, 45 (1960).

45. Huang, D.H. and Thomas, G., Met. Trans. 2, 1587 (1971).

46. Speich, G.R., Tempering of Low-Carbon Martensite, Trans. AIME, 2553 (1969).

47. Smith, R.P., The Diffusivity and Solubility of Carbon in Alpha-Iron, Trans. AIME 224, 105 (1962).

48. Thomas, G., The Role of Electron Microscopy in Design of Strong, Tough, Economical Structural Steels, Iron & Steel Int. 46, 451-461 (1973).

49. Zackay, V.F., Parker, E.R., Morris, Jr., J. W., and Thomas, G., Mat. Sci. and Engn. 16, 201-221 (1974).

50. Thomas, G., Utilization and Limitations of Phase Transformations and Microstructures in Alloy Design for Strength and Toughness, LBL-4175, Lawrence Berkeley Laboratory, University of California, Berkeley, September, 1975.

51. Carlson, M.F., Rao, B.V.N., Ritchie. R.O., and Thomas G., Improvements in Strength and Toughness of Experimental Fe-Cr-C Steels, LBL-5111, Lawrence Berkeley Laboratory, University of California, Berkeley, April 1976.

52. McMahon, J. and Thomas, G., Third Int. Conf. on Strength of Metals and Alloys, Microstructure and Design of Alloys, Cambridge, England, 1, 180-184 (1973).

Table 1. Composition of Alloys

Alloy	Composition										
	C	Mn	P	S	Si	Cr	Ni	Mo	Va	Cu	Fe
AISI 4330	.29	.98	.011	.008	.29	.89	1.84	.47	.10	.11	Bal.
4330+1.0Si	.30	"	"	"	1.36	"	"	"	"	"	"
4330+2.0Si	.28	"	"	"	2.25	"	"	"	"	"	"
4330+3.0Si	.28	"	"	"	3.26	"	"	"	"	"	"

Table 2. Transformation temperatures for AISI 4330 steel with and without Si austenitized at 900°C.

%Si	A_s °C	A_f °C	M_s °C	M_f °C
0	650	820	320	170
1.0	690	870	320	160
2.0	710	890	310	160
3.0	710	890	300	160

Table 3. Mechanical properties of AISI 4330 steel with and without Si austenitized 1 hour at 900°C, isothermally transformed 1 hour at 350°C and tempered 1 hour.

Wt%Si	Tempering Temperature °C	Hardness R_c	Tensile Properties			Fracture Properties			
			0.2% Yield Strength KSI	Ultimate Tensile Strength KSI	%Elongation 1.6 in. Gauge Length	K_{IC} Fracture Toughness KSI $\sqrt{inch}$	Specimen Width Inches	$2.5(\frac{K_{IC}}{\sigma_{ys}})^2$	K_{max}/K_Q
0%	-		176	206	6.5				
	250		174	207	6.7				
	300		176	204	6.8				
	350		168	203	6.8				
	400		167	198	7.2	71	.79	.45	1.0
1%	-		169	211	10.6	119(K_Q)	.71	1.15	1.14
	250		165	215	10.2	140(K_Q)	7.1	1.6	1.28
	300		172	212	9.5				
	350		167	211	10.2				
	400		169	209	10.8	111	.94	1.08	1.06
2%	-		161	217	13.8	85	.72	.70	1.24
	250		153	216	13.8	76	.72	.62	1.46
	300		158	215	13.2				
	350		154	216	13.6				
	400		159	214	13.4	85	.94	.71	1.12
3%	-		142	232	14.8	59	.66	.43	1.13
	250		150	231	14.8	54	.66	.32	1.29
	300		147	229	15.7				
	350		149	231	13.5				
	400		151	231	15.5	77	.94	.65	1.12

Table 4. Mechanical properties of AISI 4330 steel +2.0 %wtSi austenitized 1 hour at 900°C, isothermally transformed 1 hour at 350° quenched to liquid nitrogen (-196°C) and tempered 1 hour.

Tempering Temperature °C	Hardness R_c	0.2% Yield Strength KSI	Ultimate Tensile Strength KSI	%Elongation 1.0 in. Gauge Length	K_{IC} Fracture Toughness KSI$\sqrt{inch}$	Specimen Width Inches	$2.5\left(\frac{K_{IC}}{\sigma_{ys}}\right)^2$	K_{max}/K_Q
-	44.0	158	219	14.0				
250	42.9	156	217	14.5				
300	43.3	161	214	14.2				
350	44.0	157	216	15.5				
400	43.2	167	214	13.6	101	.66	.91	1.18
450	39.3	157	205	11.8				

Table 5. Mechanical properties of AISI 4330 steel with and without Si austenitized 1 hour at 900°C, isothermally transformed 1 hour at 250°C.and tempered 1 hour.

			Tensile Properties			Fracture Properties.			
Wt%Si	Tempering Temperature °C	Hardness R_c	0.2% Yield Strength KSI	Ultimate Tensile Strength KSI	%Elongation 1.0 in. Gauge Length	K_{IC} Fracture Toughness KSI $\sqrt{inch}$	Specimen Width Inches	$2.5(\frac{K_{IC}}{\sigma_{ys}})^2$	K_{max}/K_Q
0%	-	49.3	179	243	7.9	57	.82	.26	1.03
	250	48.5	195	242	7.2	55	.81	.20	1.01
	300	47.0	199	240	6.2				
	350	47.0	204	235	5.8				
	400	45.5	200	224	5.4	66	.82	.27	1.04
1%	-	48.0	159	240	8.0	88	.67	.77	1.12
	250	47.9	162	240	10.0	92	.67	.81	1.03
	300	47.5	191	230	7.7				
	350	46.3	192	225	9.2				
	400	46.2	189	219	10.0	75	.94	.39	1.07
2%	-	47.8	151	245	10.5	85	.84	.79	1.12
	250	47.6	159	240	10.3	100	.80	.99	1.06
	300	46.9	193	235	11.7				
	350	47.0	192	229	12.7				
	400	46.9	194	228	14.4	84	.94	.47	1.08
3%	-	49.4	143	259	11.4	72	.67	.63	1.03
	250	48.8	157	246	13.4	76	.67	.59	1.04
	300	48.5	186	240	15.8				
	350	48.3	190	238	16.7				
	400	48.2	192	235	18.0	67	.94	.30	1.10

Table 6. Phase percentages of 250°C isothermally held AISI 4330 Steel with and without Si.

Silicon %	Martensite %	Bainite %	Retained Austenite %
Unmodified	41	51	8
1.0	36	48	16
2.0	38	44	18
3.0	42	38	20

Table. 7. Phase Percentages of 200°C Isothermally held AISI 4330 Steel with and without Si.

Silicon %	Martensite %	Bainite %	Retained Austenite %
Unmodified	60	27	13
1.0	65	25	10
2.0	67	22	11
3.0	62	27	11

Table 8 Mechanical properties of 4?SI 4330 steel with and without Si austenitized 1 hour at 900°C, isothermally transformed 1 hour at 200°C and tempered 1 hour.

Wt%Si	Tempering Temperature °C	Hardness R_c	Tensile Properties: 0.2% Yield Strength KSI	Tensile Properties: Ultimate Tensile Strength KSI	Tensile Properties: %Elongation 1.0 in. Gauge Length	Fracture Properties: K_{Ic} Fracture Toughness KSI$\sqrt{inch}$	Fracture Properties: Specimen* Width Inches	Fracture Properties: $2.5(\frac{K_{IC}}{\sigma_{ys}})^2$	Fracture Properties: K_{max}/K_Q
0%	-	49.2	154	253	8.0	57	.77	.34	1.04
	250	48.3	196	243	7.0	73	.81	.35	1.04
	300	46.7	194	229	6.8				
	350	45.9	190	220	7.2				
	400	44.3	187	211	7.0	70	.80	.35	1.00
1%	-	50.8	165	263	10.4	71	.67	.46	1.06
	250	49.8	191	245	8.3	104	.87	.74	1.03
	300	49.0	203	245	7.1				
	350	48.0	203	236	6.3				
	400	47.2	196	227	10.0	92	.71	.55	1.15
2%	-	50.4	195	270	8.6	77	.80	.39	1.21
	250	49.7	196	251	8.3	100	.80	.65	1.03
	300	49.8	202	246	7.0	94	.66	.54	1.02
	350	49.7	204	244	8.6				
	400	49.2	208	240	5.6	102	.93	.60	1.02
3%	-	52.6	195	279	8.0	60	.84	.24	1.02
	250	51.5	210	267	7.6	62	.84	.22	1.00
	300	51.6	210	261	7.6				
	350	51.2	209	257	6.8				
	400	51.0	224	257	6.4	83	.93	.35	1.01

Table 9. Mechanical properties of AISI 4330 steel +2.0 wt%Si austenitized 1 hour at 900°C, isothermally transformed 1 hour at 200°C, quenched to liquid nitrogen (-196°C) and tempered 1 hour.

Tempering Temperature °C	Hardness R_c	0.2% Yield Strength KSI	Ultimate Tensile Strength KSI	%Elongation 1.0 in. Gauge Length	K_{IC} Fracture Toughness KSI$\sqrt{inch}$	Specimen Width Inches	$2.5\left(\frac{K_{IC}}{\sigma_{ys}}\right)^2$	K_{max}/K_Q
-	50.2	203	271	7.9				
250	50.9	216	263	6.0				
300	49.4	214	259	7.0				
400	48.9	222	253	6.7	76	.66	.29	1.00

Table 10. Mechanical properties of AISI 4330 steel with and without Si austenitized 1 hour at 900°C oil quenched and tempered 1 hour.

			Tensile Properties			Fracture Properties			
Wt%Si	Tempering Temperature °C	Hardness R_c	0.2% Yield Strength KSI	Ultimate Tensile Strength KSI	%Elongation 1.0 in. Gauge Length	K_{IC} Fracture Toughness KSI$\sqrt{inch}$	Specimen Width Inches	$2.5(\frac{K_{IC}}{\sigma_{ys}})^2$	K_{max}/K_Q
0%	-	51.9	189	267	8.0	36	.80	.09	1.11
	250	49.6	210	246	6.0	78	.77	.34	1.04
	300	48.3	204	244	6.3	57	.80	.14	1.05
	350	46.4	200	234	6.5				
	400	45.4	200	224	6.6	91	.78	.52	1.05
1%	-	50.6	218	282	7.4	97	.72	.50	1.15
	250	49.1	219	259	6.3				
	300	48.9	214	253	5.8	104	.67	.60	1.03
	350	48.6	203	238	6.0				
	400	47.4	204	233	7.9	89	.94	.48	1.01
2%	-	53.0	217	282	6.4	74	.84	.29	1.03
	250	50.9	216	258	5.4				
	300	50.7	221	263	5.6	107	.84	.59	1.01
	350	51.0	216	256	6.6				
	400	49.7	220	252	6.3	91	.93	.43	1.01
	500					55	.66		1.01
3%	-	53.6	234	305	6.9	41	.67	.08	1.05
	250	52.8	233	282	6.8				
	300	52.0	232	274	7.5	73	.67	.25	1.06
	350	52.0	236	274	6.1				
	400	51.8	234	269	6.1	75	.93	.24	1.00
	450	50.1	226	260	6.7				

FIGURE CAPTIONS

Fig. 1. a) Orientation of specimens with respect to the forged bar, b) Dimensions of flat tensile specimens, c) Dimensions of compact tension specimens.

Fig. 2. Dimensions of a) Charpy V-notch specimens and b) round tensile specimens.

Fig. 3. Schematic diagram of magnetic saturation device (from Ref. 28).

Fig. 4. Mechanical properties of AISI 4330 steel with and without silicon isothermally transformed at 350°C.

Fig. 5. Hardnesses of AISI 4330 steel with and without silicon isothermally transformed at 350°C.

Fig. 6. Volume fraction of retained austenite vs. silicon additions for AISI 4330 steel isothermally transformed at 350°C.

Fig. 7. Variations in the volume fraction of retained austenite as a function of strain (during tensile testing) and tempering temperature for unmodified AISI 4330 steel isothermally transformed at 350°C.

Fig. 8. Variations in the volume fraction of retained austenite as a function of strain (during tensile testing) and tempering temperature for AISI 4330 steel plus 1.0 wt%Si isothermally transformed at 350°C.

Fig. 9. Variations in the volume fraction of retained austenite as a function of strain (during tensile testing) and tempering temperature for AISI 4330 steel plus 2.0 wt%Si isothermally transformed at 350°C.

Fig. 10. Variations in the volume fraction of retained austenite as a function of strain (during tensile testing) and tempering temperature for AISI 4330 steel plus 3.0 wt%Si isothermally transformed at 350°C.

Fig. 11. Mechanical properties of AISI 4330 steel plus 2.0 wt%Si isothermally transformed at 350°C and quenched in liquid nitrogen (-196°C).

Fig. 12. Variations in the volume fraction of retained austenite as a function of strain (during tensile testing) and tempering temperature for AISI 4330 steel plus 2.0 wt%Si isothermally transformed at 350°C and quenched in liquid nitrogen (-196°C).

Fig. 13. Mechanical properties of AISI 4330 steel with and without silicon isothermally transformed at 250°C.

Fig. 14. Hardnesses of AISI 4330 steel with and without silicon isothermally transformed at 250°C.

Fig. 15. Volume fraction of retained austenite vs. silicon additions for AISI 4330 steel isothermally transformed at 250°C.

Fig. 16. Variations in the volume fraction of retained austenite as a function of strain (during tensile testing) and tempering temperature for AISI 4330 steel with silicon additions isothermally transformed at 250°C. These measurements differ from other retained austenite measurements because the magnetic saturation blanks were .05"×.56"×2.75".

Fig. 17. Variations in the volume fraction of retained austenite as a function of strain (during tensile testing) and tempering temperature for unmodified AISI 4330 steel isothermally transformed at 250°C.

Fig. 18. Variations in the volume fraction of retained austenite as a function of strain (during tensile testing) and tempering temperature for AISI 4330 steel plus 1.0 wt%Si isothermally transformed at 250°C.

Fig. 19. Variations in the volume fraction of retained austenite as a function of strain (during tensile testing) and tempering temperature for AISI 4330 steel plus 2.0 wt%Si isothermally transformed at 250°C.

Fig. 20. Variations in the volume fraction of retained austenite as a function of strain (during tensile testing) and tempering temperature for AISI 4330 steel plus 3.0 wt%Si isothermally transformed at 250°C.

Fig. 21. Mechanical properties of AISI 4330 steel with and without silicon isothermally transformed at 200°C.

Fig. 22. Hardnesses of AISI 4330 steel with and without silicon isothermally transformed at 200°C.

Fig. 23. Variations in the volume fraction of retained austenite as a function of strain (during tensile testing) and tempering temperature for unmodified AISI 4330 steel isothermally transformed at 200°C.

Fig. 24. Variations in the volume fraction of retained austenite as a function of strain (during tensile testing) and tempering temperature for AISI 4330 steel plus 1.0 wt%Si isothermally transformed at 200°C.

Fig. 25. Variations in the volume fraction of retained austenite as a function of strain (during tensile testing) and tempering temperature for AISI 4330 steel plus 2.0 wt%Si isothermally transformed at 200°C.

Fig. 26. Variations in the volume fraction of retained austenite as a function of strain (during tensile testing) and tempering temperature for AISI 4330 steel plus 3.0 wt%Si isothermally transformed at 200°C.

Fig. 27. Mechanical properties of AISI 4330 steel plus 2.0 wt%Si isothermally transformed at 200°c and quenched in liquid nitrogen (-196°C).

Fig. 28. Variations in the volume fraction of retained austenite as a function of strain (during tensile testing) and tempering temperature for AISI 4330 steel plus 2.0 wt%Si isothermally transformed at 200°C and quenched in liquid nitrogen (-196°C).

Fig. 29. Mechanical properties of oil quenched AISI 4330 steel with and without silicon.

Fig. 30. Hardnesses of oil quenched AISI 4330 steel with and without silicon.

Fig. 31. Variations in the volume fraction of retained austenite as a function of strain (during tensile testing) and tempering temperature for oil quenched unmodified AISI 4330 steel.

Fig. 32. Variations in the volume fraction of retained austenite as a function of strain (during tensile testing) and tempering temperature for oil quenched AISI 4330 steel plus 1.0 wt%Si.

Fig. 33. Variations in the volume fraction of retained austenite as a function of strain (during tensile testing) and tempering temperature for oil quenched AISI 4330 steel plus 2.0 wt%Si.

Fig. 34. Variations in the volume fraction of retained austenite as a function of strain (during tensile testing) and tempering temperature for oil quenched AISI 4330 steel plus 3.0 wt%Si.

Fig. 35. SEM fractographs of fracture toughness specimens isothermally transformed at 350°C. a) AISI 4330 plus 2.0 wt%Si. b) AISI 4330 plus 3.0 wt%Si.

Fig. 36. SEM fractographs of fracture toughness specimens isothermally transformed at 350°C and tempered at 400°C. a) AISI 4330 plus 2.0 wt%Si. b) AISI 4330 plus 3.0 wt%Si.

Fig. 37. SEM fractographs of fracture toughness specimens isothermally transformed at 350°C. a) AISI 4330 plus 2.0 wt%Si tempered at 400°C. b) AISI 4330 plus 2.0 wt%Si refrigerated in LN and tempered at 400°C.

Fig. 38. SEM fractographs of fracture toughness specimens isothermally transformed at 250°C; untempered. a) AISI 4330 plus 1.0 wt%Si b) AISI 4330 plus 2.0 wt%Si.

Fig. 39. SEM fractographs of fracture toughness specimens isothermally transformed at 250°C, a) AISI 4330 plus 2.0 wt%Si tempered at 250°C. b) AISI 4330 plus 2.0 wt%Si tempered at 400°C.

Fig. 40. SEM fractorgraphs of fracture toughness specimens isothermally transformed at 250°C and tempered at 400°C. a) AISI 4330 plus 3.0 wt%Si.

Fig. 41. SEM fractograph of a AISI 4330 plus 3.0 wt%Si fracture toughness specimen isothermally transformed at 200°C; untempered.

Fig. 42. SEM fractographs of fracture toughness specimens isothermally transformed at 200°C and tempered at 250°C. a) AISI 4330 b) AISI 4330 plus 1.0 wt%Si.

Fig. 43. SEM fractographs of fracture toughness specimen isothermally transformed at 200°C. a) AISI 4330 plus 2.0 wt%Si tempered at 250°C b) AISI 4330 plus 2.0 wt%Si tempered at 300°C.

Fig. 44. SEM fractographs of fracture toughness specimens isothermally transformed at 200°C. a) AISI 4330 plus 2.0 wt%Si tempered at 400°C. b) AISI 4330 plus 2.0 wt%Si refrigerated to LN and tempered at 400°C.

Fig. 45. SEM fractographs of fracture toughness specimens isothermally transformed at 200°C. a) AISI 4330 plus 3.0 wt%Si tempered at 400°C. b) Unmodified AISI 4330 tempered at 400°C.

Fig. 46. SEM fractographs of unmodified AISI 4330 fracture toughness specimens, a) Oil quenched; untempered. b) Oil quenched and tempered at 250°C.

Fig. 47. SEM fractograph of unmodified AISI 4330 fracture toughness specimens a) Oil quenched and tempered at 400°C. b) Oil quenched and tempered at 300°C.

Fig. 48. SEM fractographs of oil quenched and untempered fracture toughness specimens. a) AISI 4330 plus 2.0 wt%Si; b) AISI 4330 plus 3.0 wt%Si.

Fig. 49. SEM fractographs of oil quenched and tempered at 300°C fracture toughness specimens of AISI 4330 plus 2.0 wt%Si steel a) General fracture appearance, b) View of inclusions causing tearing of the matrix around them.

Fig. 50. SEM fractographs of oil quenched fracture toughness specimens tempered at 400°C. a) AISI 4330 plus 2.0 wt%Si. b) AISI 4330 plus 1.0 wt%Si.

Fig. 51. SEM fractographs of oil quenched fracture toughness specimen tempered at 500°C. a) End of fatigue area, b) Center of specimen.

Fig. 52. a) SEM fractograph of the fatigue area of a oil quenched AISI 4330 plus 3.0 wt%Si fracture toughness specimen tempered at 300°C. b) EDAX analysis of the inclusion just right of center in fractograph. The peaks (from left to right) are Al, Si, Ca, Mn, FeK_{α} and FeK_{β}.

Fig. 53. a) SEM fractograph of oil quenched AISI 4330 plus 3.0 wt%Si fracture toughness specimen tempered at 300°C. b) EDAX analysis of the inclusion in the center of the picture (In dark hole at center). The peaks are Si, Cr, Mn, FeK_{α} and FeK_{β}.

Fig. 54. Optical micrographs of specimens isothermally transformed at 350°C. a) AISI 4330 plus 2.0 wt%Si tempered at 400°C. b) untempered AISI 4330 plus 3.0 wt%Si.

Fig. 55. Optical micrographs of AISI 4330 plus 2.0 wt%Si isothermally transformed at 350°C. a) tempered at 400°C. b) quenched to liquid nitrogen (-196°C) after isothermal transformation and then tempered at 400°C.

Fig. 56. Optical micrographs of AISI 4330 plus 2.0 wt%Si isothermally transformed at 200°C. a) tempered at 300°C, b) tempered at 400°C.

Fig. 57. Optical micrograph of AISI 4330 plus 3.0 wt%Si isothermally transformed at 200°C and tempered at 400°C.

Fig. 58. Optical micrographs of oil quenched untempered specimens. a) Unmodified AISI 4330, b) AISI 4330 plus 2.0 wt%Si.

Fig. 59. a) TEM micrograph of bainite obtained in AISI 4330 plus 2.0 wt%Si isothermally transformed at 350°C and tempered at 400°C, b) The retained austenite reverses contrast in the dark field image of the austenite spot. c) The selected area diffraction pattern and its indexing as a [311] bainite orientation. d) Twin related laths reverse contrast when the matrix and twin spots are imaged.

Fig. 60. a) TEM micrograph of AISI 4330 plus 2.0 wt%Si isothermally transformed at 200°C; untempered. b) The retained austenite reverses contrast in the dark field image of a $(002)_\gamma$ spot. c) The corresponding selected area diffraction pattern. The indexing is given in Fig. 68(c).

Fig. 61. a) TEM micrograph from of a different area of the specimen shown in Fig. 57. Microtwins can be observed. b) The corresponding selected area diffraction. The indexing is given in Fig. 68c.

Fig. 62. a) TEM micrograph of the same specimen shown in Fig. 57 showing wavy carbides. b) The corresponding selected area diffraction. The indexing is given in Fig. 65b.

Fig. 63. a) TEM micrograph of AISI 4330 plus 2.0 wt%Si isothermally transformed at 200°C and tempered at 400°C. b) Cementite precipitates can be seen by reversal of contrast of the $(0\bar{2}2)_C$ spot. c) The corresponding SAD pattern with its indexing.

Fig. 64. a) TEM micrograph from a different area of the specimen shown in Fig. 63. b) Retained austenite is seen by imaging the $(002)_\gamma$ spot. c) The corresponding SAD pattern. The indexing is given in Fig. 68c.

Fig. 65. a) Another TEM micrograph from the same specimen as in the previous two micrographs. b) Dark field image of $(200)_\gamma$ spot. c) The corresponding SAD pattern. The indexing given in Fig. 68d.

Fig. 66. a) TEM micrograph of AISI 4330 plus 2.0 wt%Si oil quenched and tempered at 300°C. Microtwins can be seen in some areas of the specimen. b) Some retained austenite can be seen along the martensite laths.

Fig. 67. a) Another TEM micrograph from the same specimen as in Fig. 66. Typical structure for quenched and tempered lath martensite. b) The corresponding SAD pattern. The indexing is given in Fig. 68a.

Fig. 68. Analysis of selected area diffraction patterns a) $[01\bar{1}]$ martensite orientation, b) [100] martensite orientation. c) [100] and [111] martensite orientations and [011] austenite orientation showing the Kurdjurmov-Sachs (K-S) orientation relationship viz. $(1\bar{1}0)_\gamma \parallel [\bar{1}\bar{1}1]_m$, $(111)_\gamma \parallel (011)_m$ between bct martensite and fcc γ. d) [011] austenite and [111] martensite orientations showing also the K-S orientation relationship.

Fig. 69. Plane strain fracture toughness vs. yield strength for AISI 4330 steel with silicon additions and for some other HSLA steels (AISI 4340 plus Al and AISI 4340 plus Al plus Si are from Ref. 34).

Fig. 70. Plane strain fracture toughness vs. ultimate tensile strength for AISI 4330 steel with silicon additions and for some other HSLA steels (AISI 4340 plus Al and AISI 4340 plus Al plus Si are from Ref. 34).

(a)

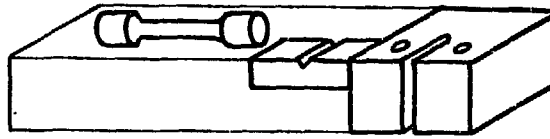

(b)

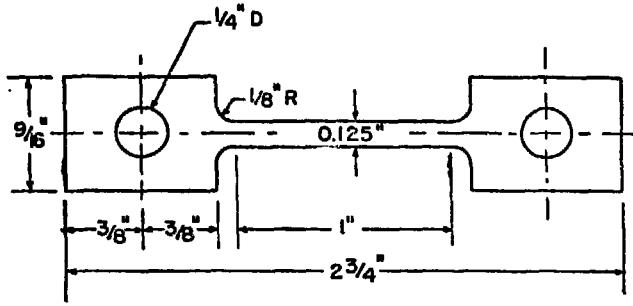

LONG GAGE TENSILE SPECIMEN.
SCALE: 2" = 1"

(c)

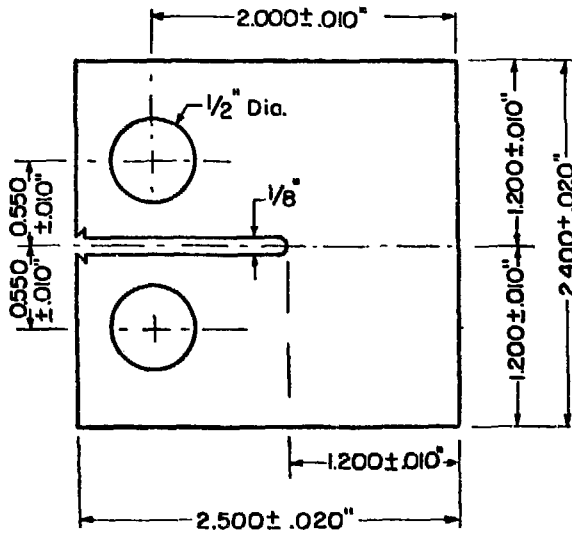

X8L 769-10410

Fig. 1.

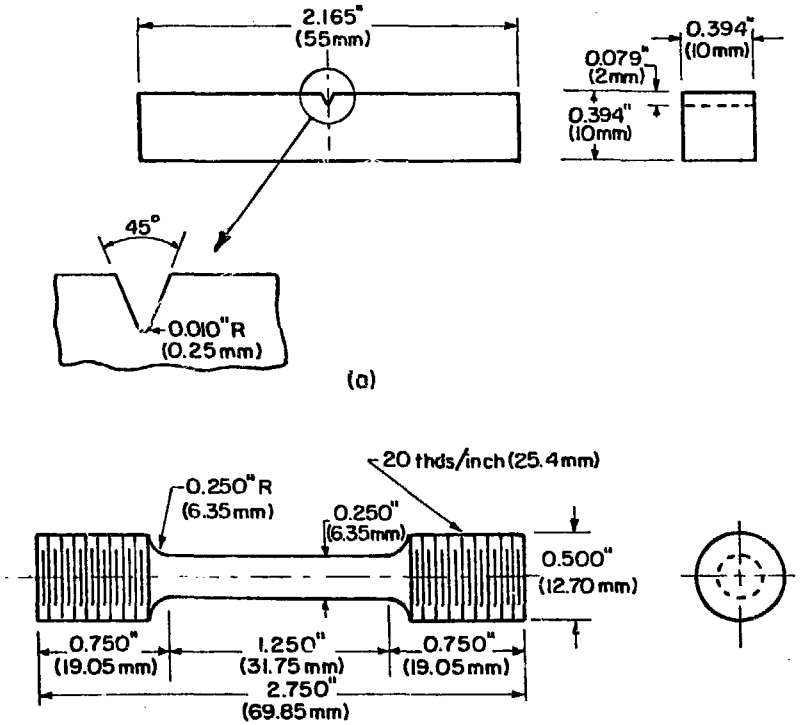

XBL 736-6280

Fig. 2.

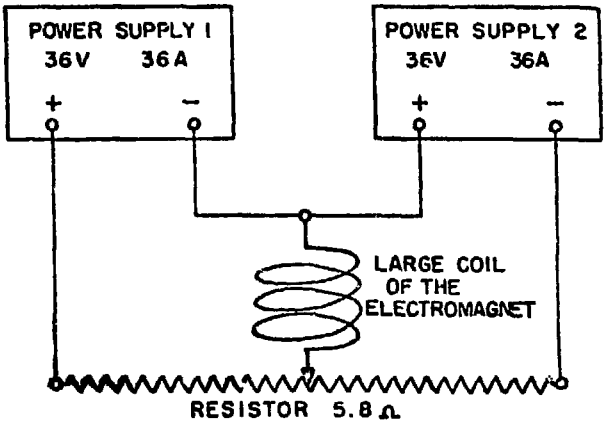

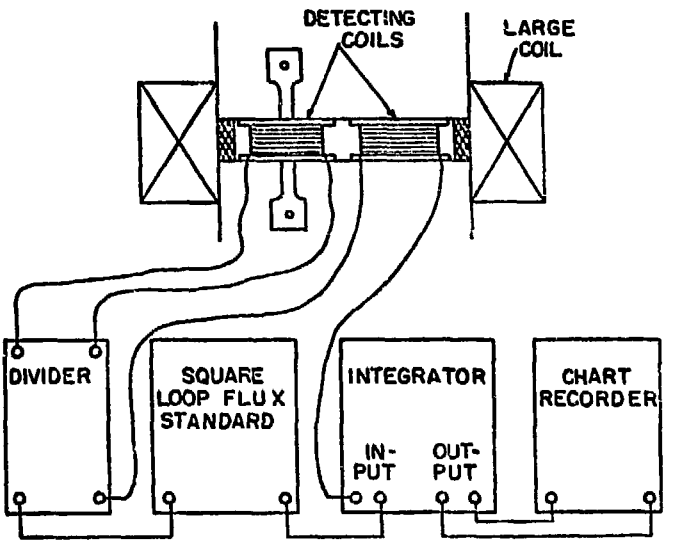

XBL 769-10409

Fig. 3.

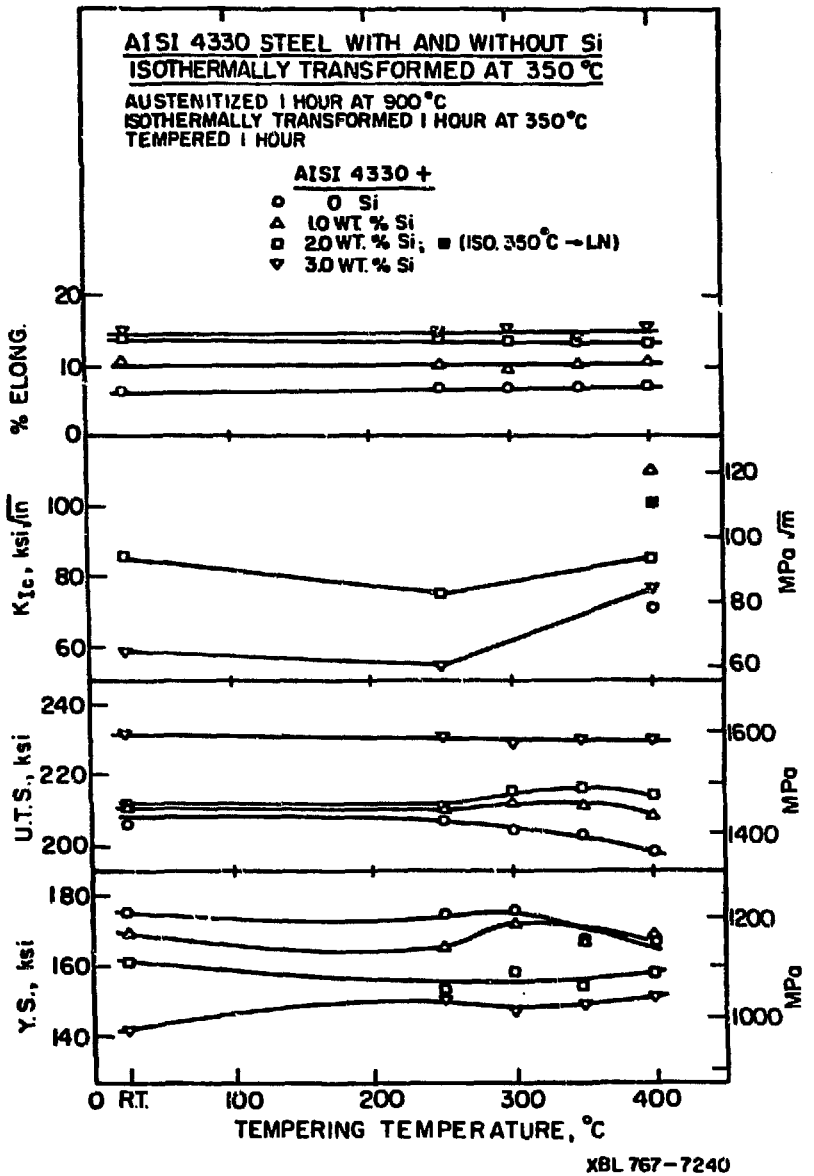
AISI 4330 STEEL WITH AND WITHOUT Si
ISOTHERMALLY TRANSFORMED AT 350 °C
AUSTENITIZED 1 HOUR AT 900°C
ISOTHERMALLY TRANSFORMED 1 HOUR AT 350°C
TEMPERED 1 HOUR
AISI 4330 +
0 Si
1.0 WT. % Si
2.0 WT. % Si; ■ (ISO. 350°C → LN)
3.0 WT. % Si
% ELONG.
K_{Ic}, ksi$\sqrt{in}$
MPa$\sqrt{m}$
U.T.S., ksi
MPa
Y.S., ksi
MPa
0 RT. 100 200 300 400
TEMPERING TEMPERATURE, °C
XBL 767-7240

Fig. 4.

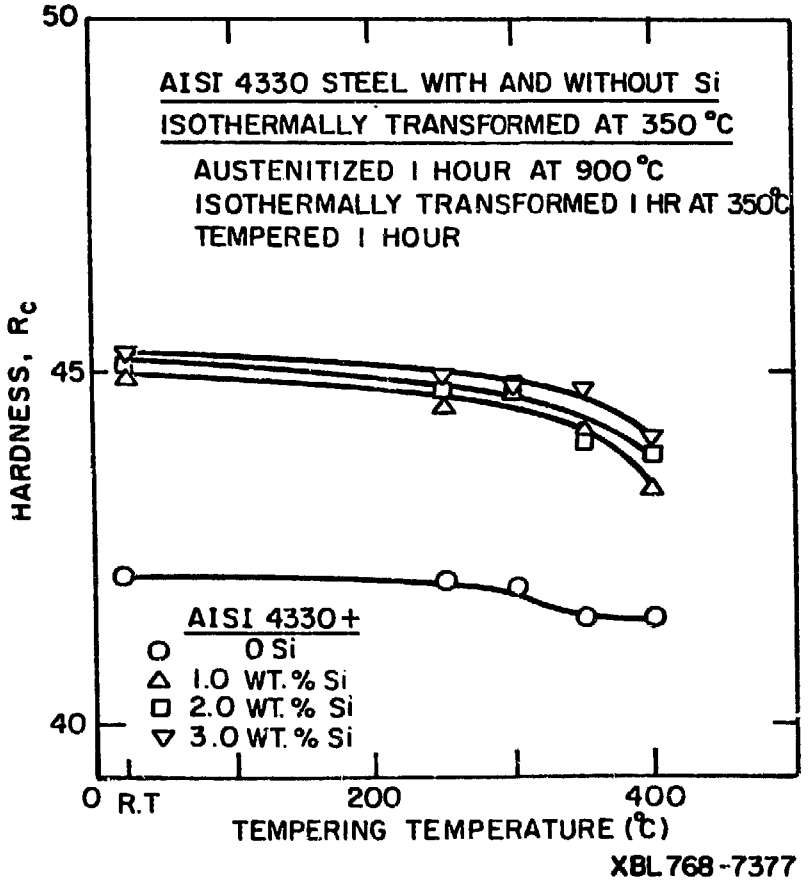
AISI 4330 STEEL WITH AND WITHOUT Si
ISOTHERMALLY TRANSFORMED AT 350 °C
AUSTENITIZED 1 HOUR AT 900 °C
ISOTHERMALLY TRANSFORMED 1 HR AT 350°C
TEMPERED 1 HOUR
HARDNESS, Rc
50
45
40
AISI 4330+
0 Si
1.0 WT.% Si
2.0 WT.% Si
3.0 WT.% Si
0 R.T
200
400
TEMPERING TEMPERATURE (°C)
XBL 768-7377

Fig. 5.

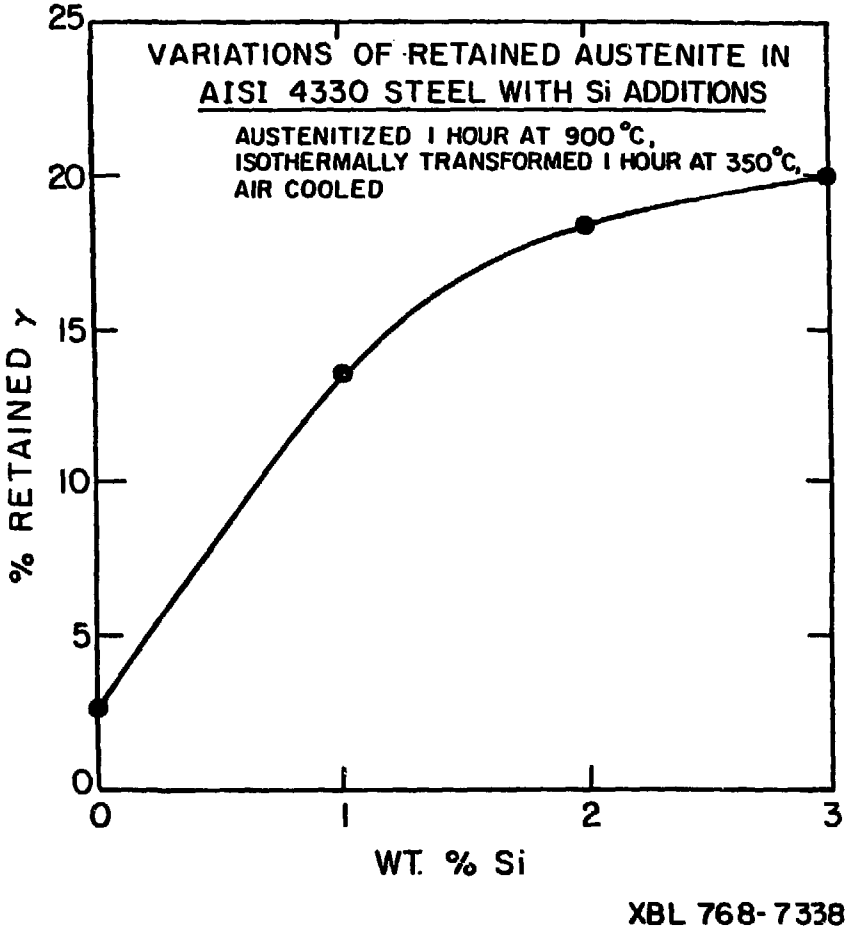
VARIATIONS OF RETAINED AUSTENITE IN
AISI 4330 STEEL WITH Si ADDITIONS
AUSTENITIZED 1 HOUR AT 900°C,
ISOTHERMALLY TRANSFORMED 1 HOUR AT 350°C,
AIR COOLED
% RETAINED γ
25
20
15
10
5
0
0
1
2
3
WT. % Si
XBL 768-7338

Fig. 6.

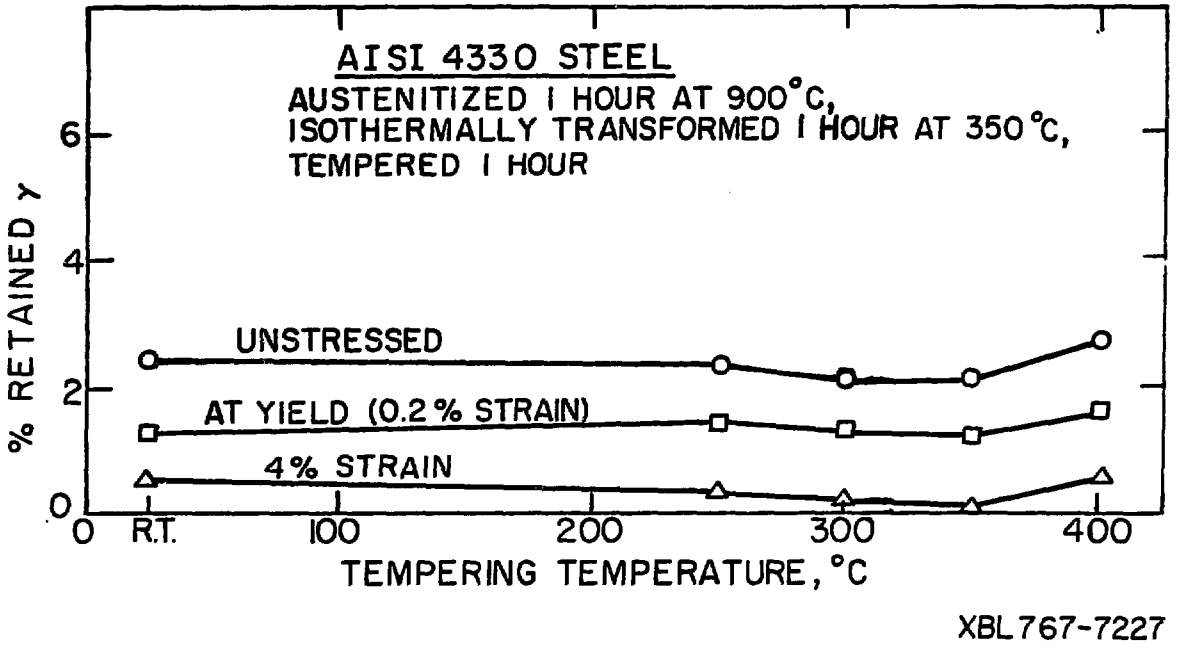
AISI 4330 STEEL
AUSTENITIZED 1 HOUR AT 900°C,
ISOTHERMALLY TRANSFORMED 1 HOUR AT 350°C,
TEMPERED 1 HOUR
% RETAINED γ
UNSTRESSED
AT YIELD (0.2% STRAIN)
4% STRAIN
0
2
4
6
0
R.T.
100
200
300
400
TEMPERING TEMPERATURE, °C
XBL767-7227

Fig. 7.

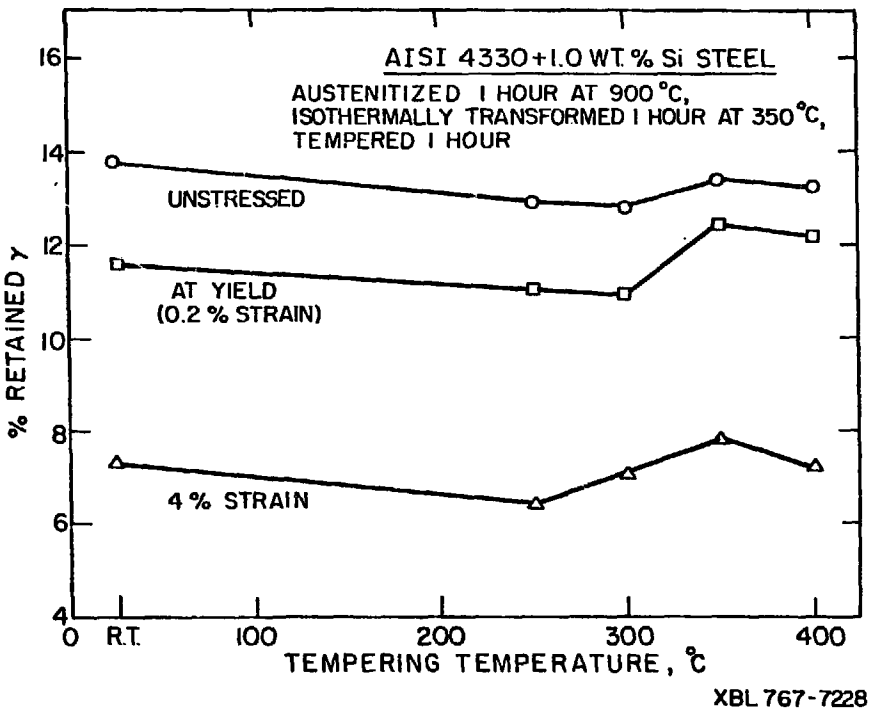
AISI 4330+1.0 WT.% Si STEEL
AUSTENITIZED 1 HOUR AT 900°C,
ISOTHERMALLY TRANSFORMED 1 HOUR AT 350°C,
TEMPERED 1 HOUR
UNSTRESSED
AT YIELD
(0.2 % STRAIN)
4 % STRAIN
% RETAINED γ
16
14
12
10
8
6
4
0
R.T.
100
200
300
400
TEMPERING TEMPERATURE, °C
XBL 767-7228

Fig. 8.

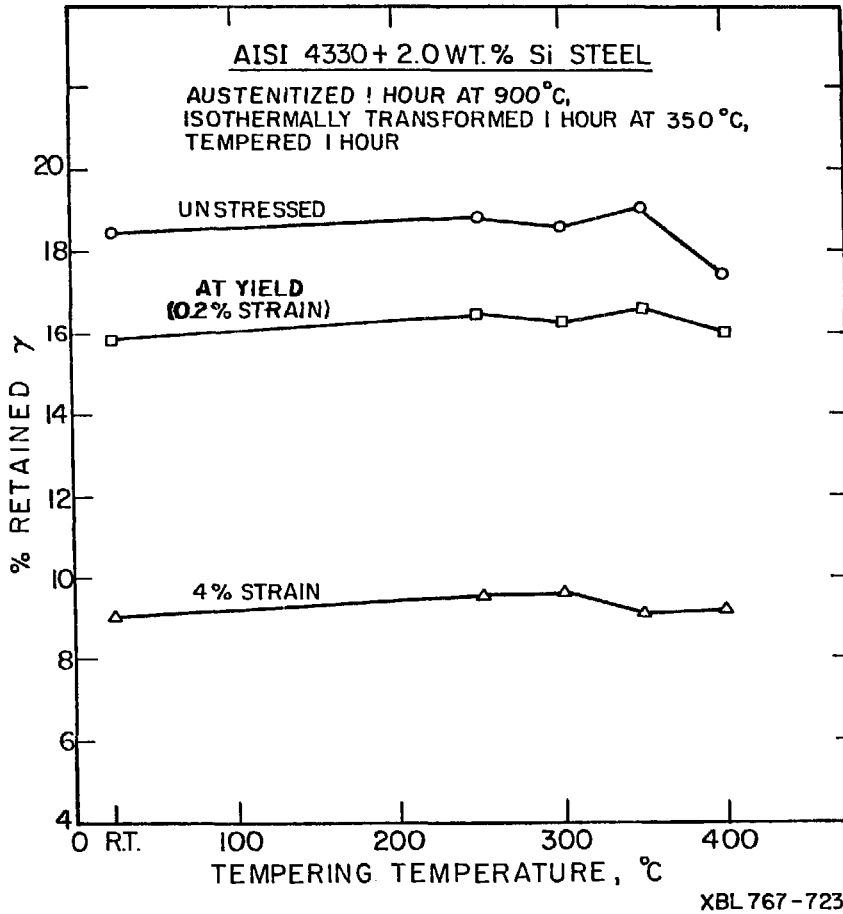
AISI 4330 + 2.0 WT.% Si STEEL
AUSTENITIZED 1 HOUR AT 900°C,
ISOTHERMALLY TRANSFORMED 1 HOUR AT 350°C,
TEMPERED 1 HOUR
UNSTRESSED
AT YIELD
(0.2% STRAIN)
4% STRAIN
% RETAINED γ
TEMPERING TEMPERATURE, °C
0 R.T.
100
200
300
400
4
6
8
10
12
14
16
18
20
XBL 767-7235

Fig. 9.

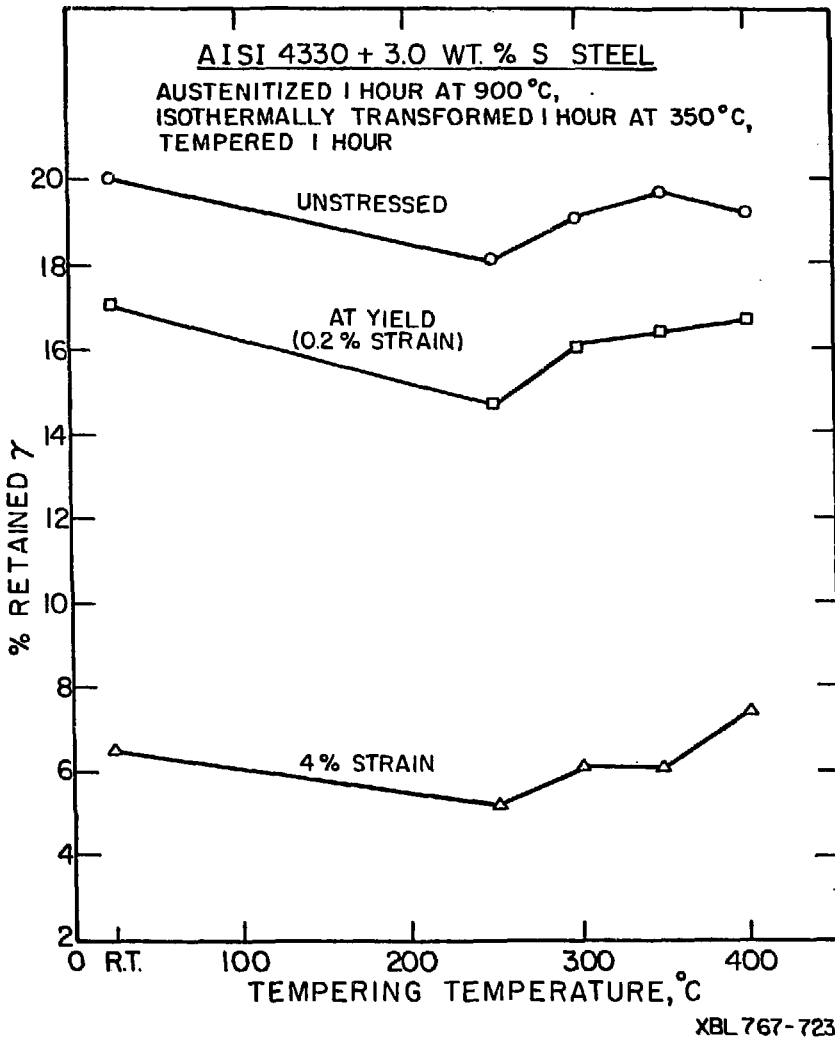
AISI 4330 + 3.0 WT. % S STEEL
AUSTENITIZED 1 HOUR AT 900°C,
ISOTHERMALLY TRANSFORMED 1 HOUR AT 350°C,
TEMPERED 1 HOUR
UNSTRESSED
AT YIELD
(0.2 % STRAIN)
4 % STRAIN
% RETAINED γ
20
18
16
14
12
10
8
6
4
2
0 R.T.
100
200
300
400
TEMPERING TEMPERATURE, °C
XBL 767-7236

Fig. 10.

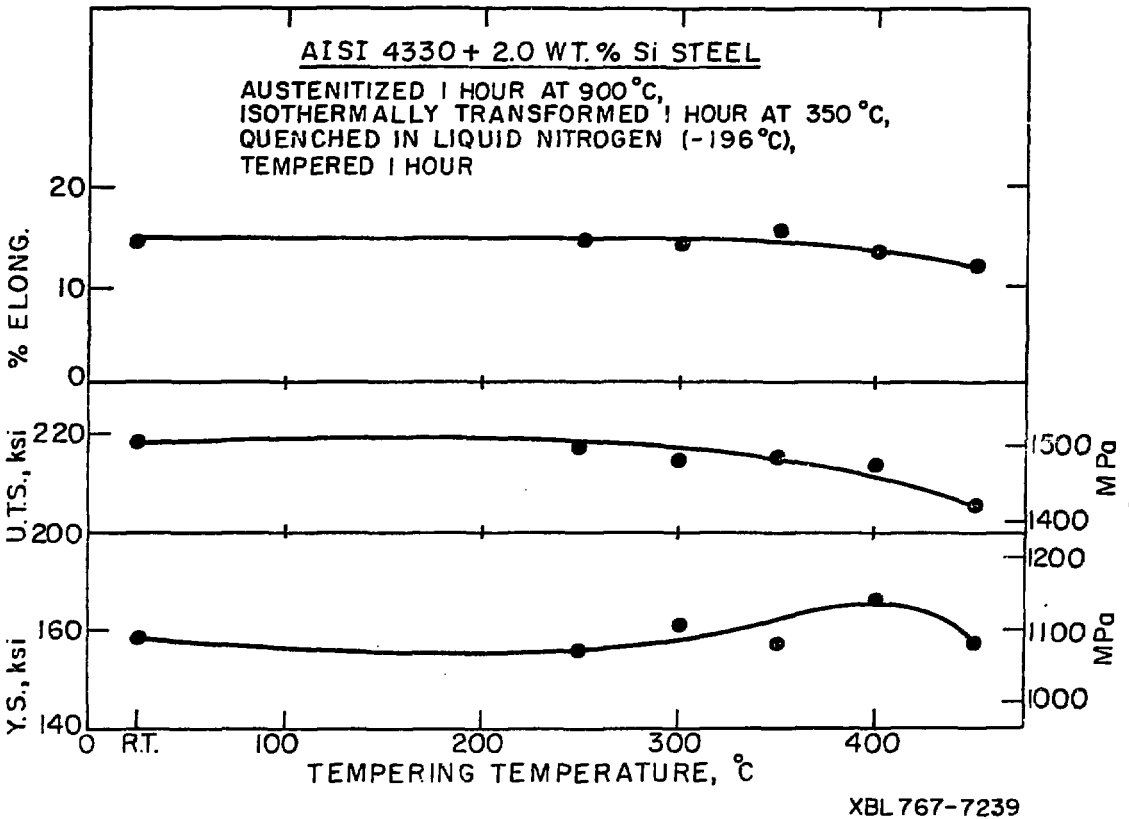
AISI 4330 + 2.0 WT.% Si STEEL
AUSTENITIZED 1 HOUR AT 900°C,
ISOTHERMALLY TRANSFORMED 1 HOUR AT 350°C,
QUENCHED IN LIQUID NITROGEN (-196°C),
TEMPERED 1 HOUR
% ELONG.
20
10
0
U.T.S., ksi
220
200
Y.S., ksi
160
140
1500
1400
1200
1100
1000
MPa
MPa
0
R.T.
100
200
300
400
TEMPERING TEMPERATURE, °C
XBL 767-7239

Fig. 11.

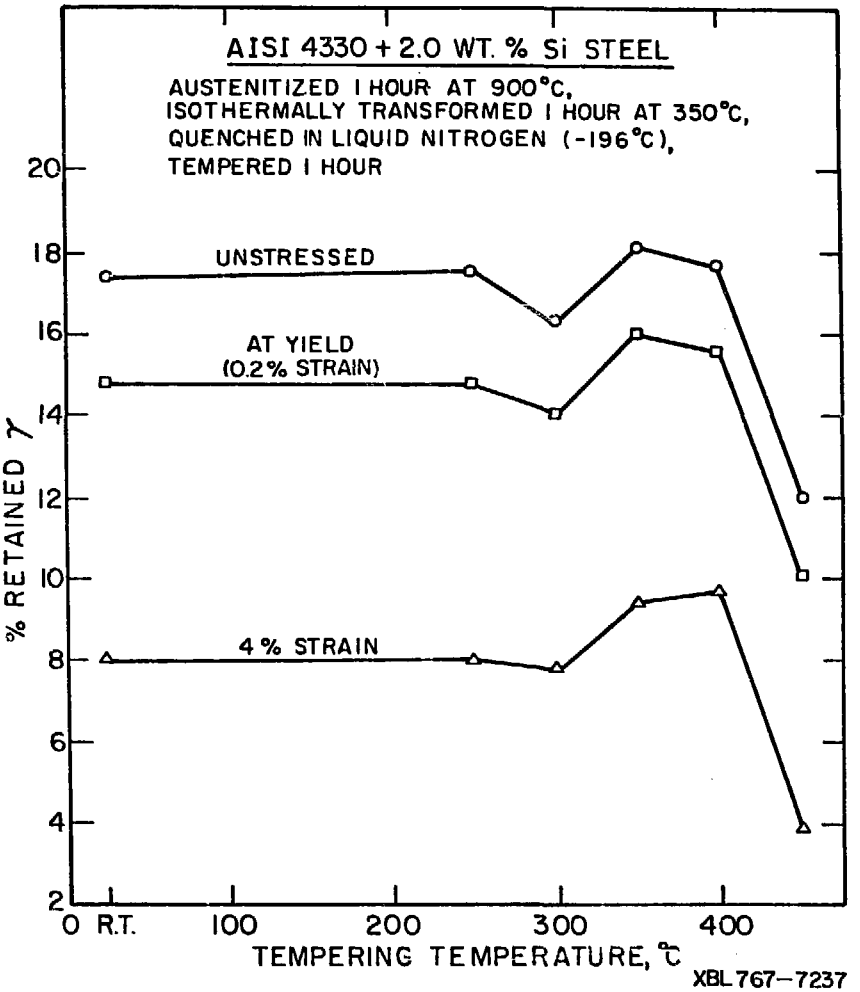
AISI 4330 + 2.0 WT. % Si STEEL
AUSTENITIZED 1 HOUR AT 900°C,
ISOTHERMALLY TRANSFORMED 1 HOUR AT 350°C,
QUENCHED IN LIQUID NITROGEN (-196°C),
TEMPERED 1 HOUR
UNSTRESSED
AT YIELD
(0.2% STRAIN)
4 % STRAIN
% RETAINED γ
TEMPERING TEMPERATURE, °C
0 R.T.
100
200
300
400
2
4
6
8
10
12
14
16
18
20
XBL767-7237

Fig. 12.

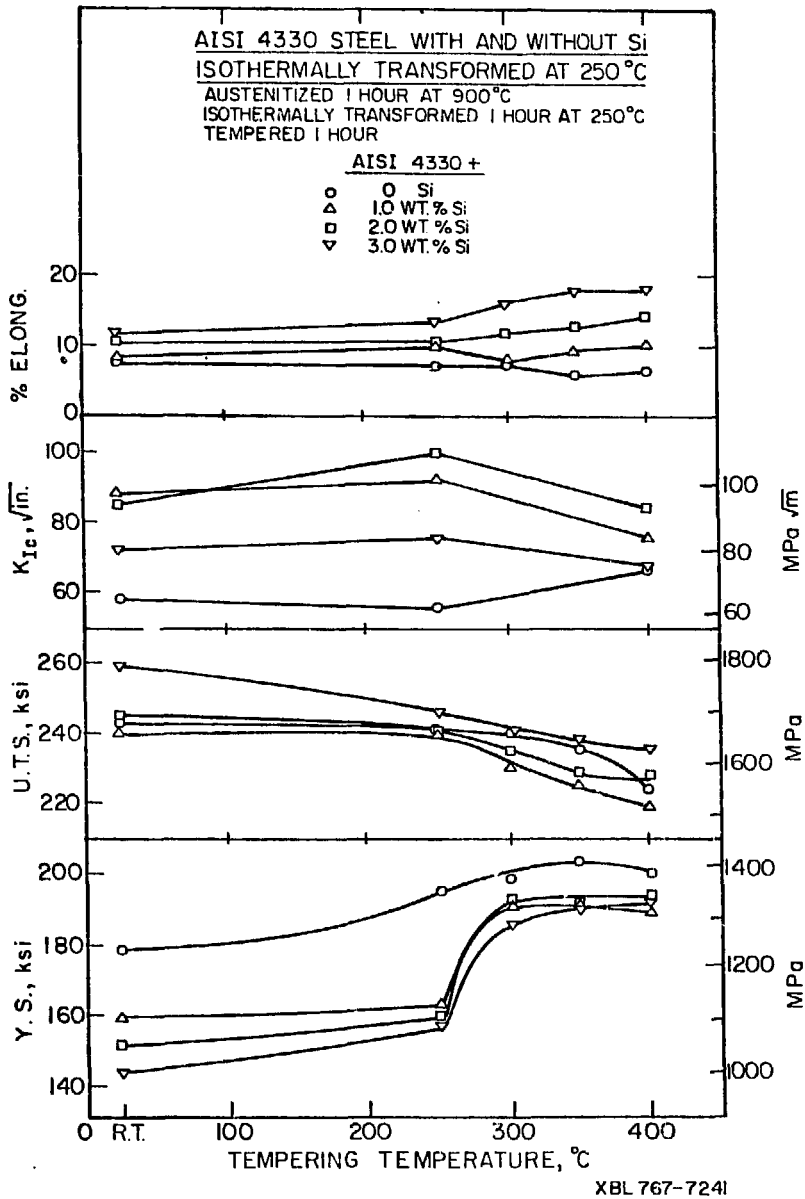
AISI 4330 STEEL WITH AND WITHOUT Si
ISOTHERMALLY TRANSFORMED AT 250°C
AUSTENITIZED 1 HOUR AT 900°C
ISOTHERMALLY TRANSFORMED 1 HOUR AT 250°C
TEMPERED 1 HOUR
AISI 4330 +
0 Si
1.0 WT.% Si
2.0 WT.% Si
3.0 WT.% Si
% ELONG.
K_{Ic}, $\sqrt{in.}$
MPa $\sqrt{m}$
U.T.S., ksi
MPa
Y.S., ksi
MPa
TEMPERING TEMPERATURE, °C
XBL 767-7241

Fig. 13.

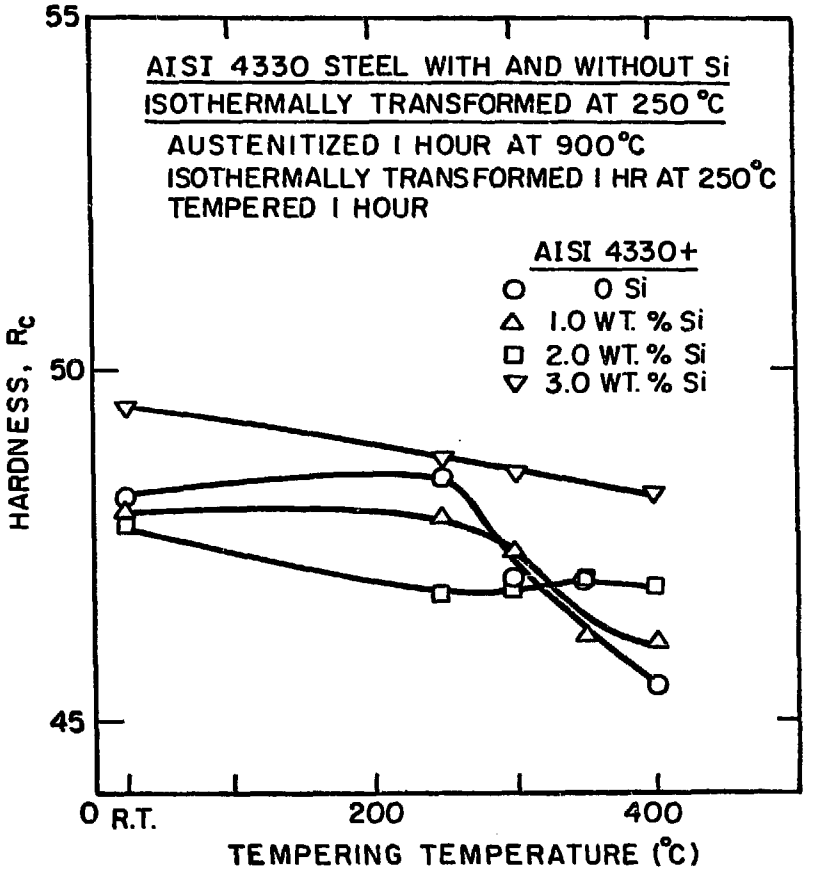

XBL 768-7376

Fig. 14.

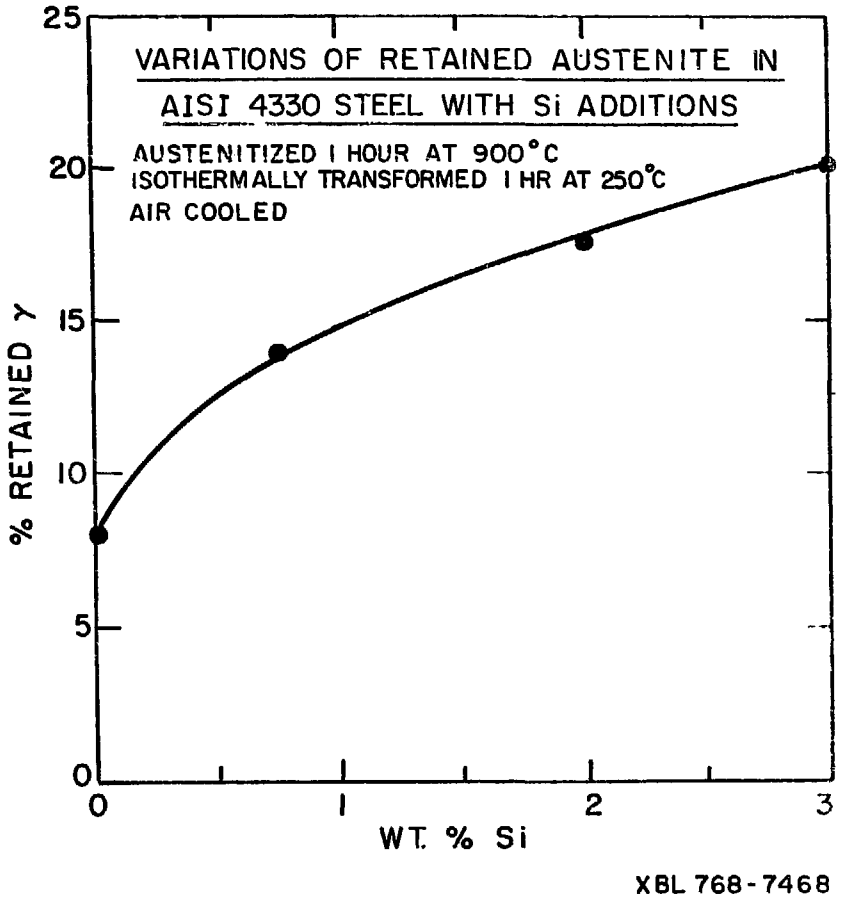
VARIATIONS OF RETAINED AUSTENITE IN
AISI 4330 STEEL WITH Si ADDITIONS
AUSTENITIZED 1 HOUR AT 900°C
ISOTHERMALLY TRANSFORMED 1 HR AT 250°C
AIR COOLED
% RETAINED γ
WT. % Si
0
5
10
15
20
25
0
1
2
3
XBL 768-7468

Fig. 15.

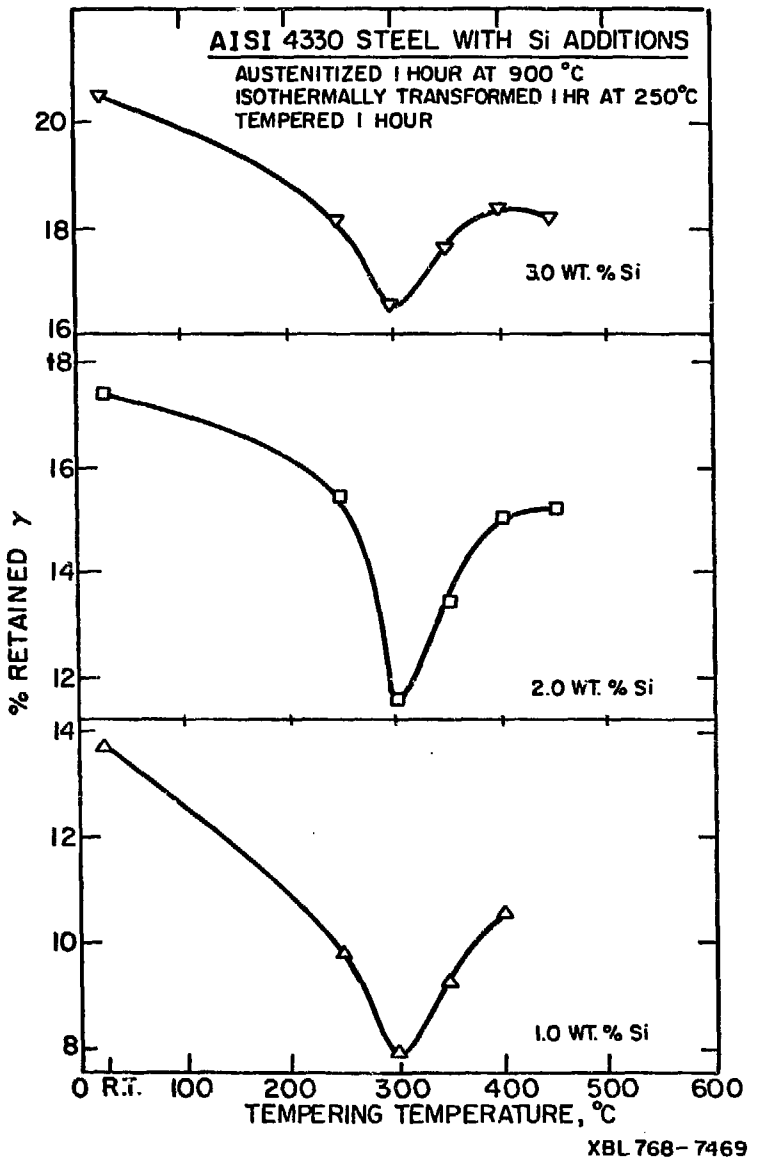
AISI 4330 STEEL WITH Si ADDITIONS
AUSTENITIZED 1 HOUR AT 900 °C
ISOTHERMALLY TRANSFORMED 1 HR AT 250°C
TEMPERED 1 HOUR
3.0 WT. % Si
2.0 WT. % Si
1.0 WT. % Si
% RETAINED γ
TEMPERING TEMPERATURE, °C
0 R.T. 100 200 300 400 500 600
20 18 16
18 16 14 12
14 12 10 8
XBL 768-7469

Fig. 16.

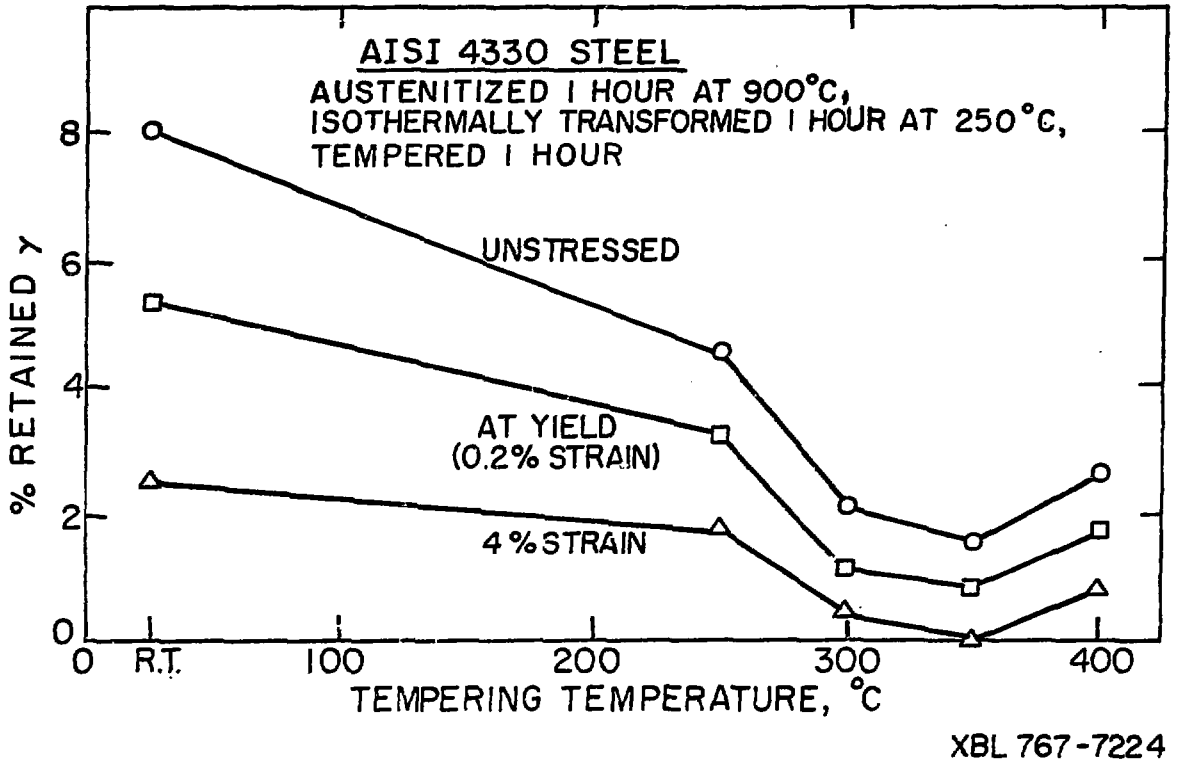
AISI 4330 STEEL
AUSTENITIZED 1 HOUR AT 900°C,
ISOTHERMALLY TRANSFORMED 1 HOUR AT 250°C,
TEMPERED 1 HOUR
UNSTRESSED
AT YIELD
(0.2% STRAIN)
4 % STRAIN
% RETAINED γ
0
2
4
6
8
0
R.T.
100
200
300
400
TEMPERING TEMPERATURE, °C
XBL 767-7224

Fig. 17.

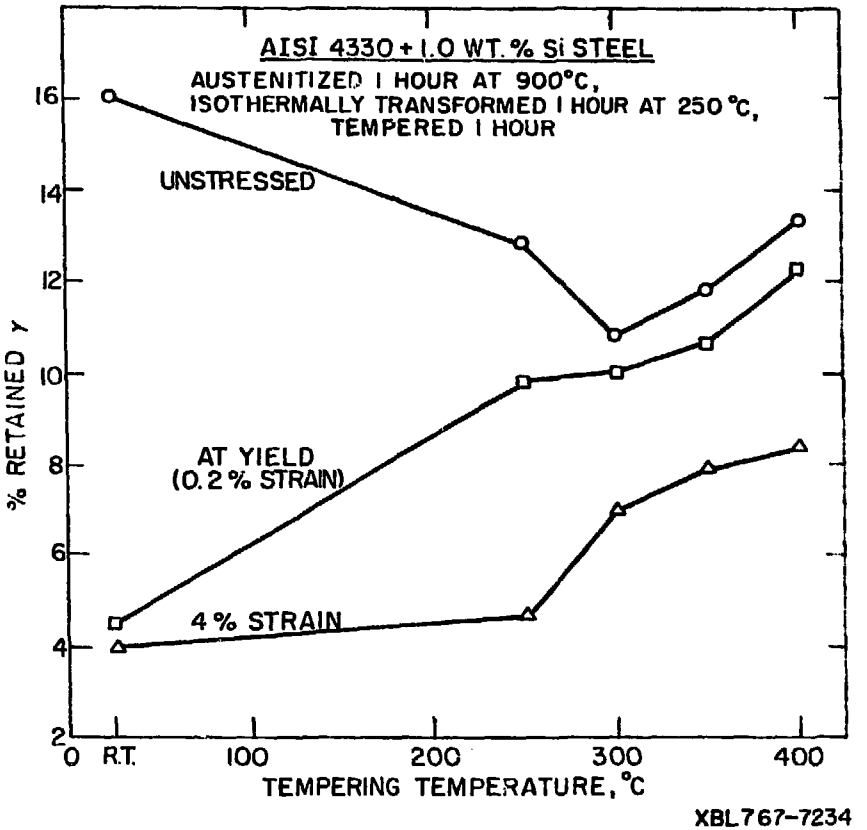
AISI 4330 + 1.0 WT. % Si STEEL
AUSTENITIZED 1 HOUR AT 900°C,
ISOTHERMALLY TRANSFORMED 1 HOUR AT 250 °C,
TEMPERED 1 HOUR
UNSTRESSED
AT YIELD
(0.2 % STRAIN)
4 % STRAIN
% RETAINED γ
16
14
12
10
8
6
4
2
0
R.T.
100
200
300
400
TEMPERING TEMPERATURE, °C
XBL767-7234

Fig. 18.

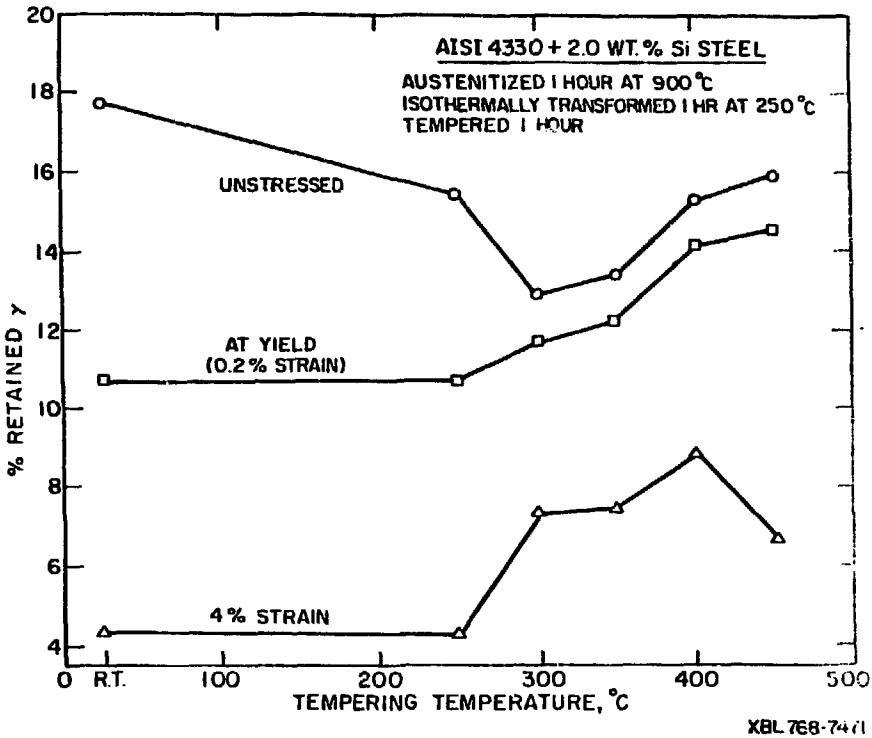
AISI 4330 + 2.0 WT.% Si STEEL
AUSTENITIZED 1 HOUR AT 900°C
ISOTHERMALLY TRANSFORMED 1 HR AT 250°C
TEMPERED 1 HOUR
UNSTRESSED
AT YIELD
(0.2% STRAIN)
4% STRAIN
% RETAINED γ
TEMPERING TEMPERATURE, °C
20
18
16
14
12
10
8
6
4
0
R.T.
100
200
300
400
500
XBL 768-7471

Fig. 19.

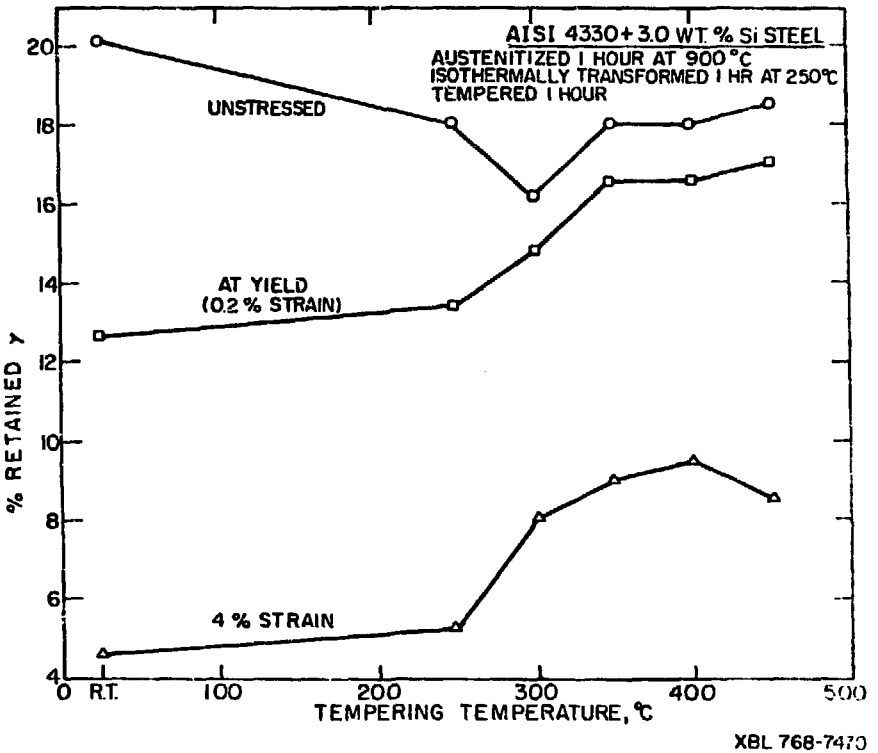
AISI 4330+3.0 WT.% Si STEEL
AUSTENITIZED 1 HOUR AT 900°C
ISOTHERMALLY TRANSFORMED 1 HR AT 250°C
TEMPERED 1 HOUR
UNSTRESSED
AT YIELD
(0.2 % STRAIN)
4 % STRAIN
% RETAINED γ
TEMPERING TEMPERATURE, °C
20
18
16
14
12
10
8
6
4
0
R.T.
100
200
300
400
500
XBL 768-7470

Fig. 20.

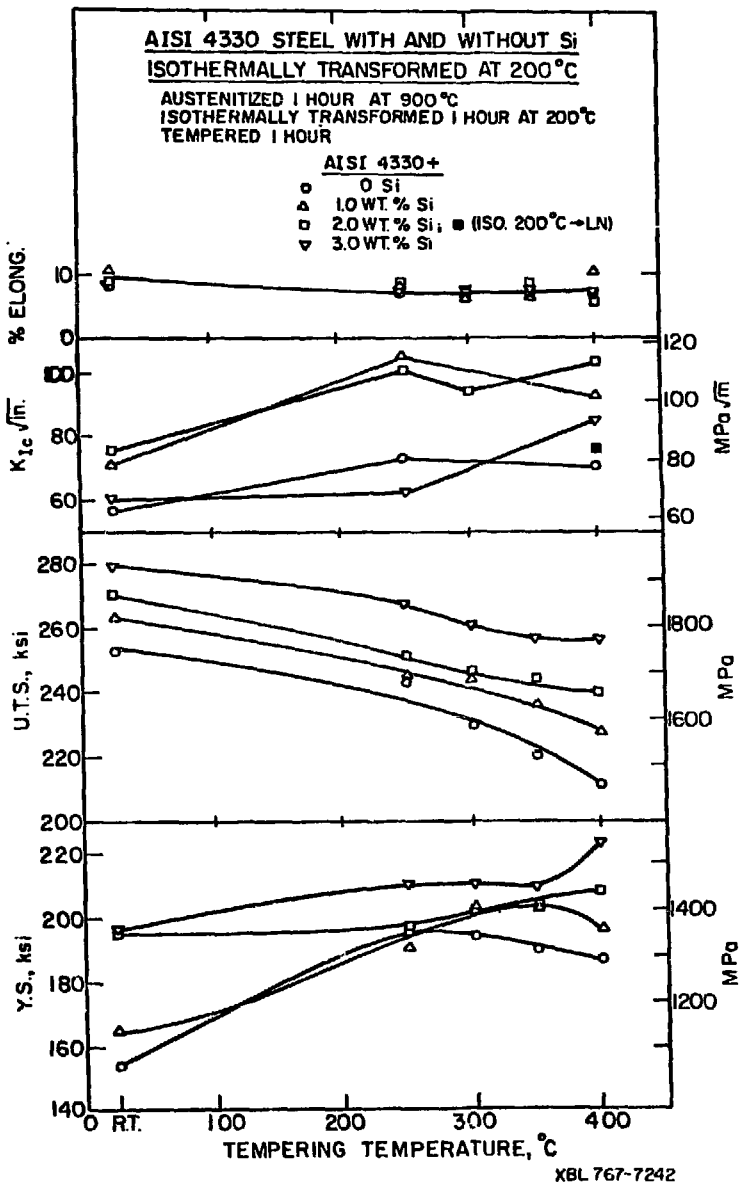
AISI 4330 STEEL WITH AND WITHOUT Si
ISOTHERMALLY TRANSFORMED AT 200°C
AUSTENITIZED 1 HOUR AT 900°C
ISOTHERMALLY TRANSFORMED 1 HOUR AT 200°C
TEMPERED 1 HOUR
AISI 4330+
0 Si
1.0 WT.% Si
2.0 WT.% Si; ■ (ISO. 200°C→LN)
3.0 WT.% Si
% ELONG.
$K_{1c}\sqrt{in.}$
MPa$\sqrt{m}$
U.T.S., ksi
MPa
Y.S., ksi
MPa
TEMPERING TEMPERATURE, °C
XBL 767-7242

Fig. 21.

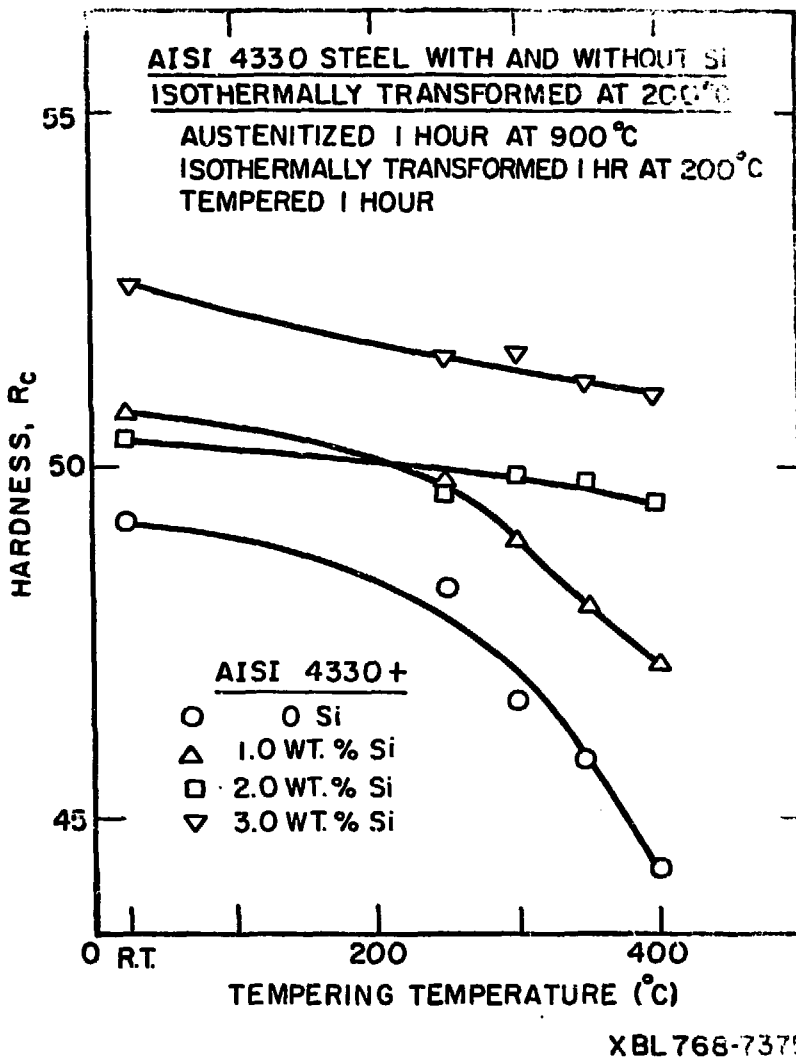
AISI 4330 STEEL WITH AND WITHOUT Si
ISOTHERMALLY TRANSFORMED AT 200°C
AUSTENITIZED 1 HOUR AT 900°C
ISOTHERMALLY TRANSFORMED 1 HR AT 200°C
TEMPERED 1 HOUR
HARDNESS, Rc
55
50
45
AISI 4330+
0 Si
1.0 WT. % Si
2.0 WT. % Si
3.0 WT. % Si
0 R.T.
200
400
TEMPERING TEMPERATURE (°C)
XBL 768-7375

Fig. 22.

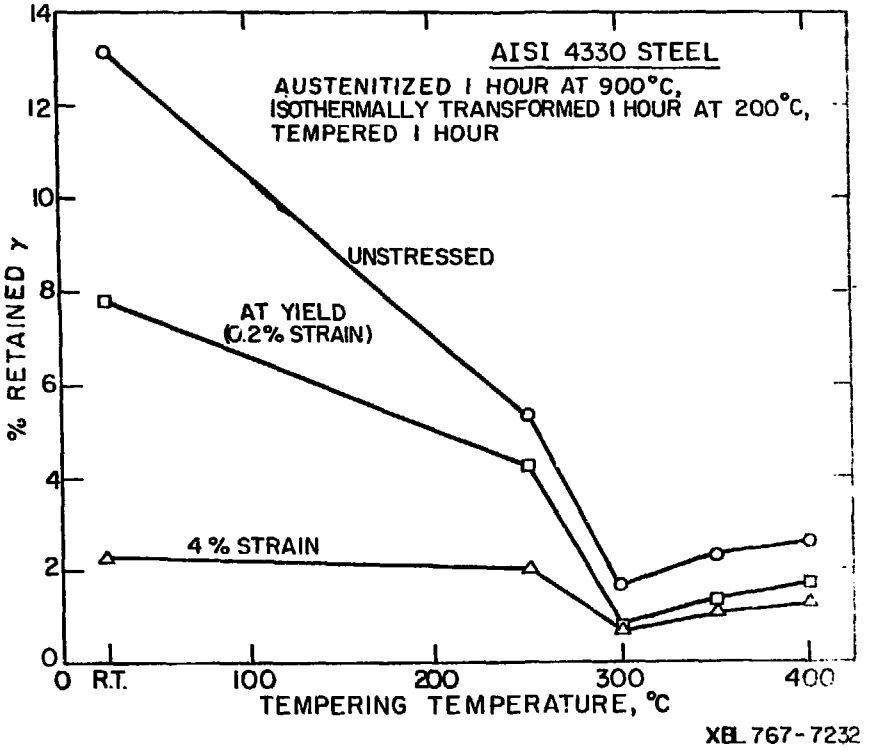
AISI 4330 STEEL
AUSTENITIZED 1 HOUR AT 900°C,
ISOTHERMALLY TRANSFORMED 1 HOUR AT 200°C,
TEMPERED 1 HOUR
UNSTRESSED
AT YIELD
(0.2% STRAIN)
4 % STRAIN
% RETAINED γ
TEMPERING TEMPERATURE, °C
0
2
4
6
8
10
12
14
R.T.
100
200
300
400
XBL 767-7232

Fig. 23.

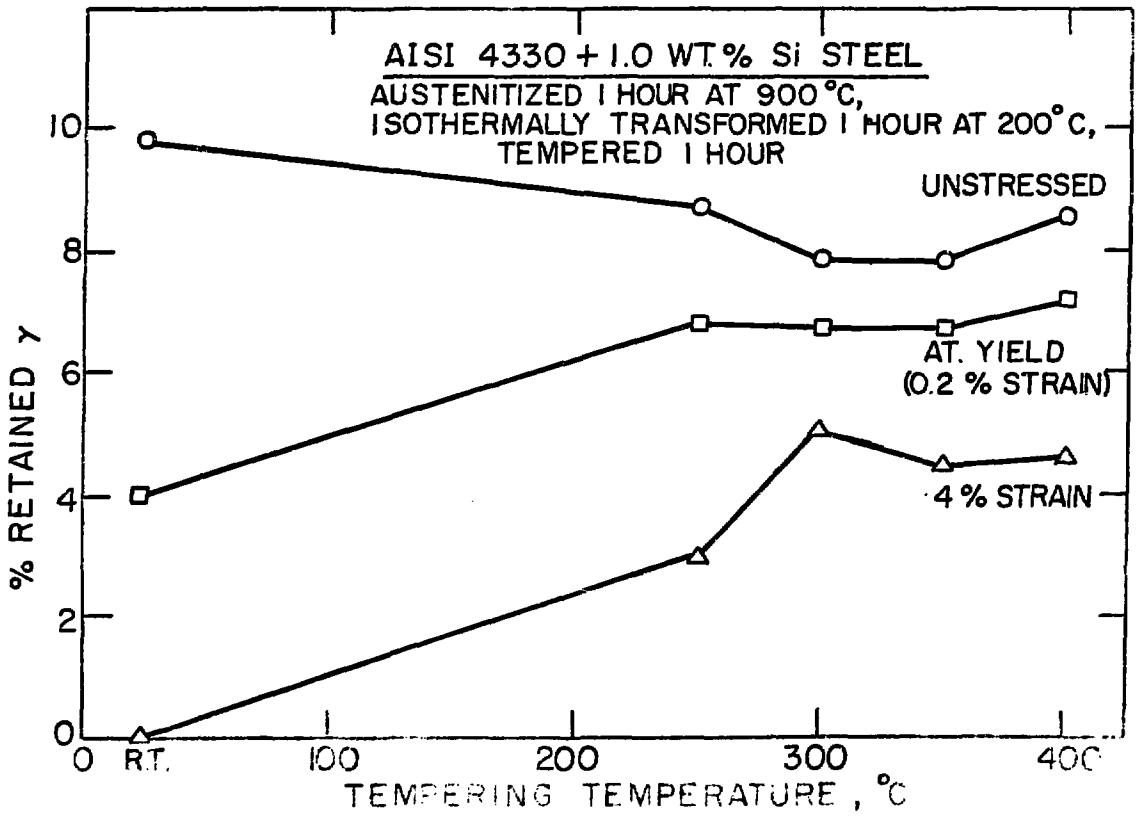

Fig. 24.

XBL 767-7222

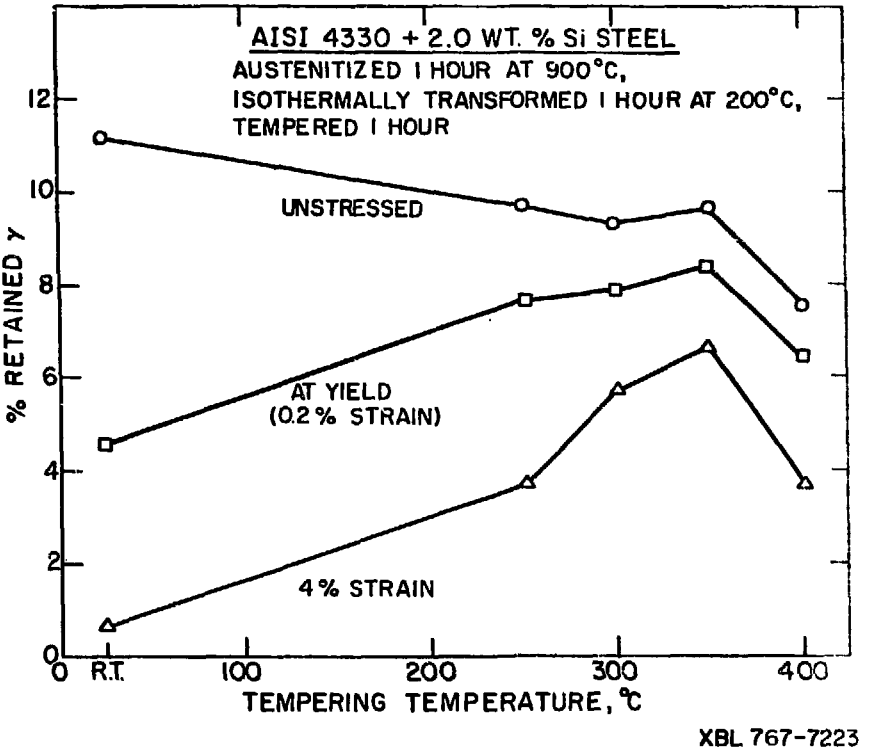
AISI 4330 + 2.0 WT. % Si STEEL
AUSTENITIZED 1 HOUR AT 900°C,
ISOTHERMALLY TRANSFORMED 1 HOUR AT 200°C,
TEMPERED 1 HOUR
UNSTRESSED
AT YIELD
(0.2 % STRAIN)
4 % STRAIN
% RETAINED γ
0
2
4
6
8
10
12
R.T.
100
200
300
400
TEMPERING TEMPERATURE, °C
XBL 767-7223

Fig. 25.

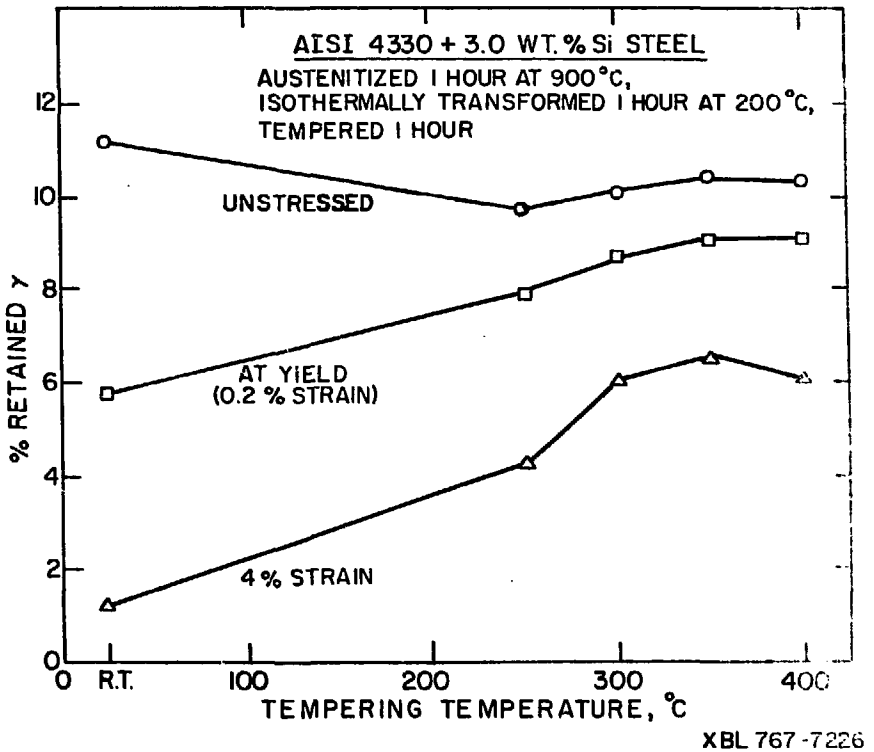
AISI 4330 + 3.0 WT.% Si STEEL
AUSTENITIZED 1 HOUR AT 900°C,
ISOTHERMALLY TRANSFORMED 1 HOUR AT 200°C,
TEMPERED 1 HOUR
UNSTRESSED
AT YIELD
(0.2 % STRAIN)
4 % STRAIN
% RETAINED γ
0
2
4
6
8
10
12
R.T.
100
200
300
400
TEMPERING TEMPERATURE, °C
XBL 767-7226

Fig. 26.

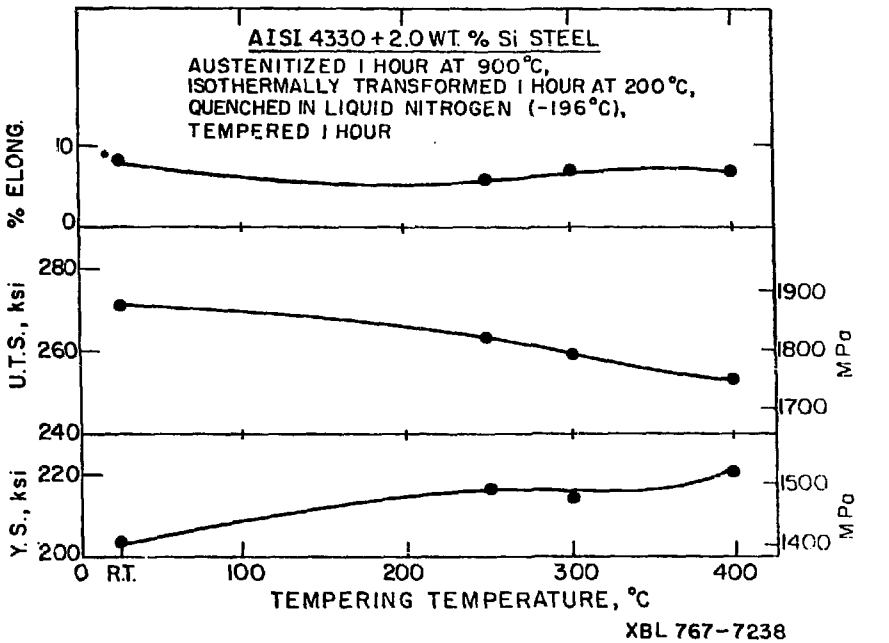
AISI 4330 + 2.0 WT. % Si STEEL
AUSTENITIZED 1 HOUR AT 900°C,
ISOTHERMALLY TRANSFORMED 1 HOUR AT 200°C,
QUENCHED IN LIQUID NITROGEN (-196°C),
TEMPERED 1 HOUR
% ELONG.
10
0
U.T.S., ksi
280
260
240
1900
1800
1700
MPa
Y.S., ksi
220
200
1500
1400
MPa
0 R.T.
100
200
300
400
TEMPERING TEMPERATURE, °C
XBL 767-7238

Fig. 27.

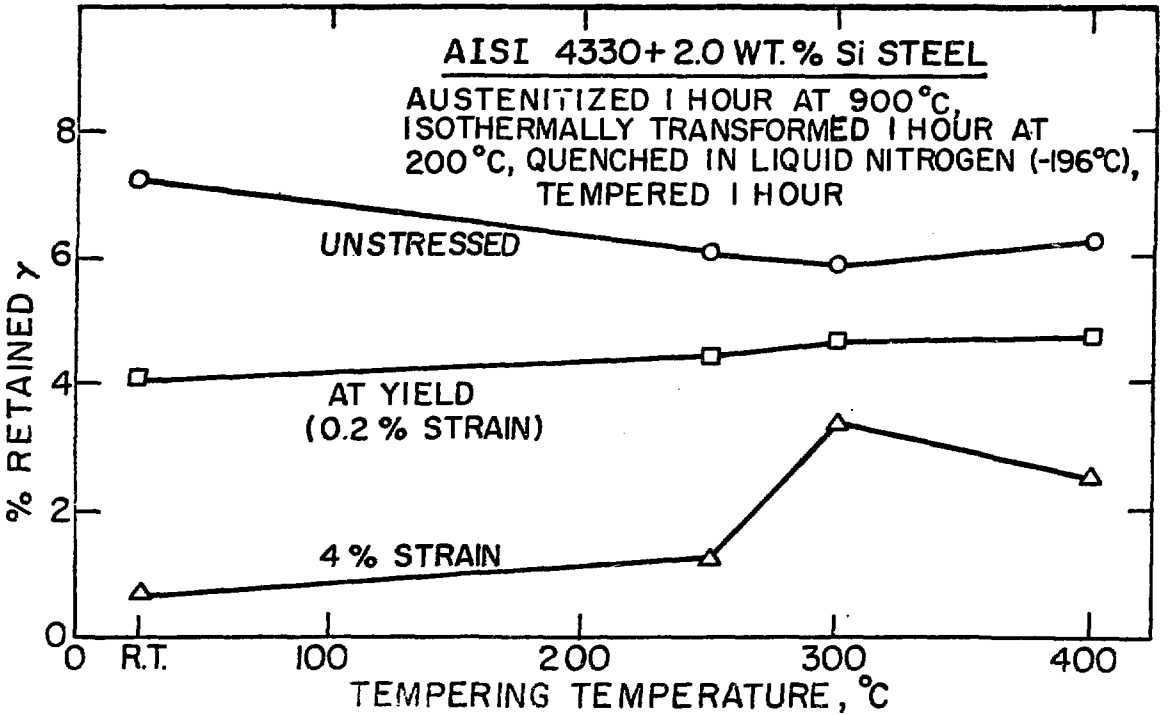

XBL767-7225

Fig. 28.

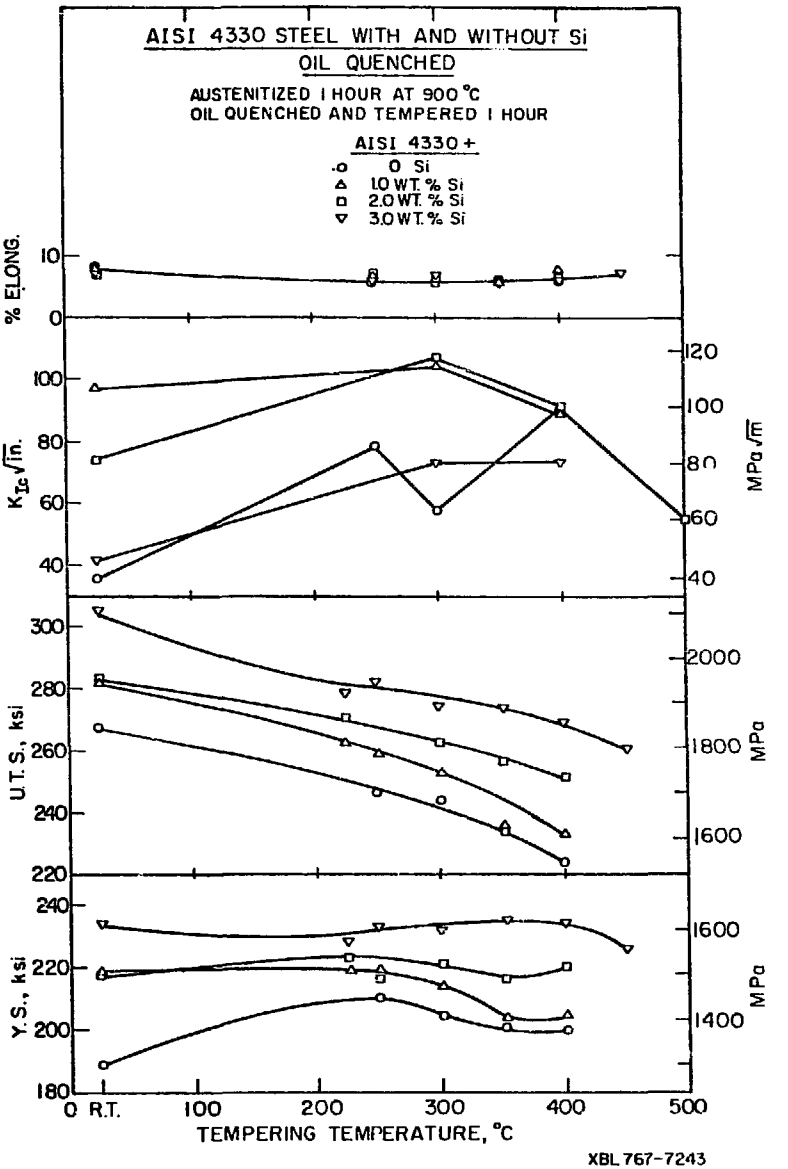
AISI 4330 STEEL WITH AND WITHOUT Si
OIL QUENCHED
AUSTENITIZED 1 HOUR AT 900 °C
OIL QUENCHED AND TEMPERED 1 HOUR
AISI 4330 +
0 Si
1.0 WT. % Si
2.0 WT. % Si
3.0 WT. % Si
% ELONG.
$K_{Ic}\sqrt{in.}$
MPa$\sqrt{m}$
U.T.S., ksi
MPa
Y.S., ksi
MPa
TEMPERING TEMPERATURE, °C
XBL 767-7243

Fig. 29.

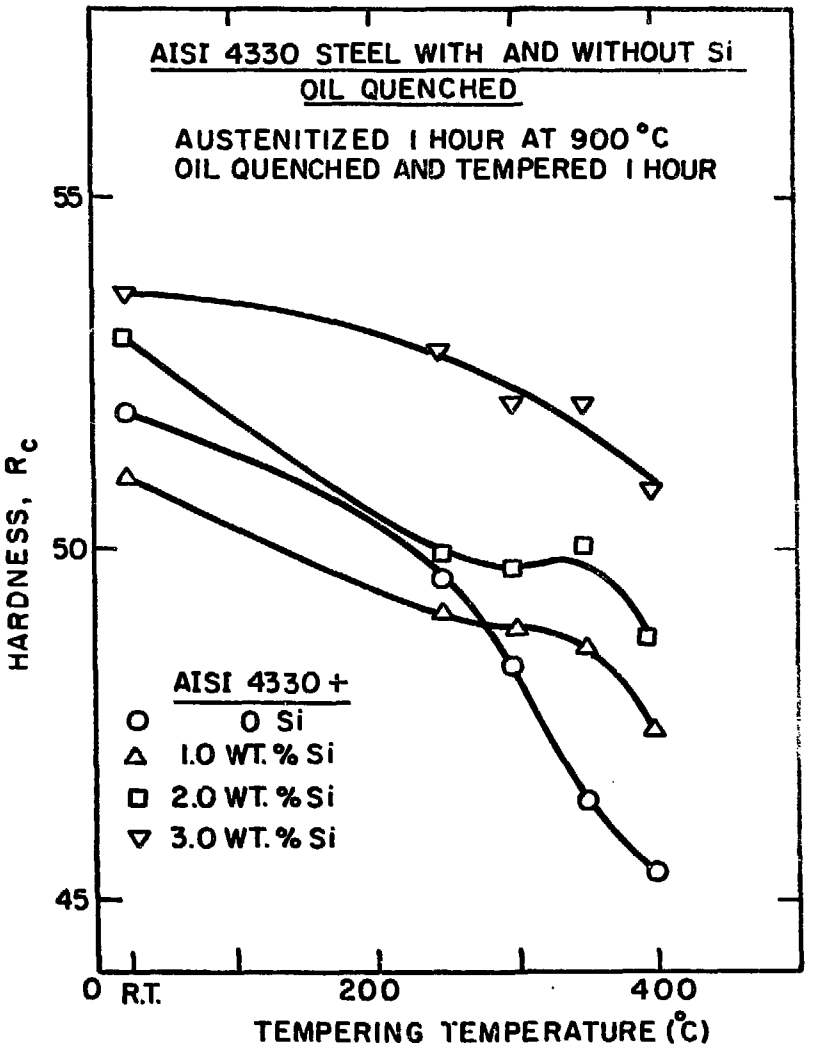

XBL768-7374

Fig. 30.

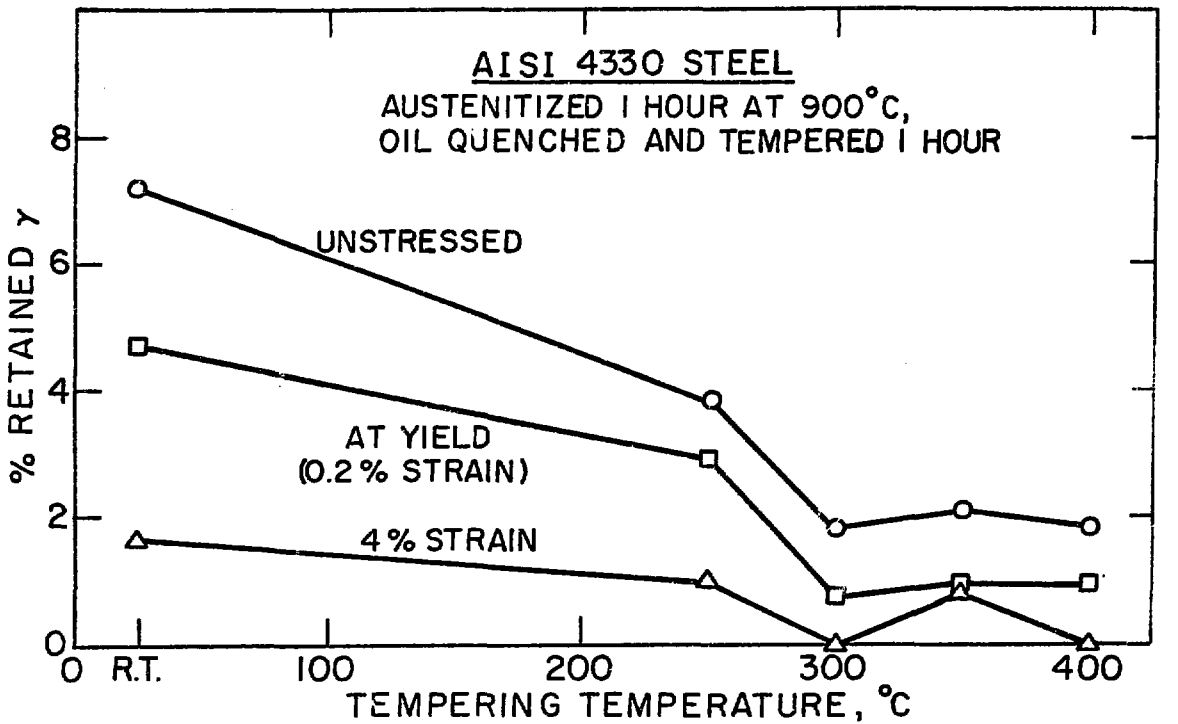
AISI 4330 STEEL
AUSTENITIZED 1 HOUR AT 900°C,
OIL QUENCHED AND TEMPERED 1 HOUR
UNSTRESSED
AT YIELD
(0.2% STRAIN)
4% STRAIN
% RETAINED γ
0
2
4
6
8
0
R.T.
100
200
300
400
TEMPERING TEMPERATURE, °C
XBL 767-7233

Fig. 31.

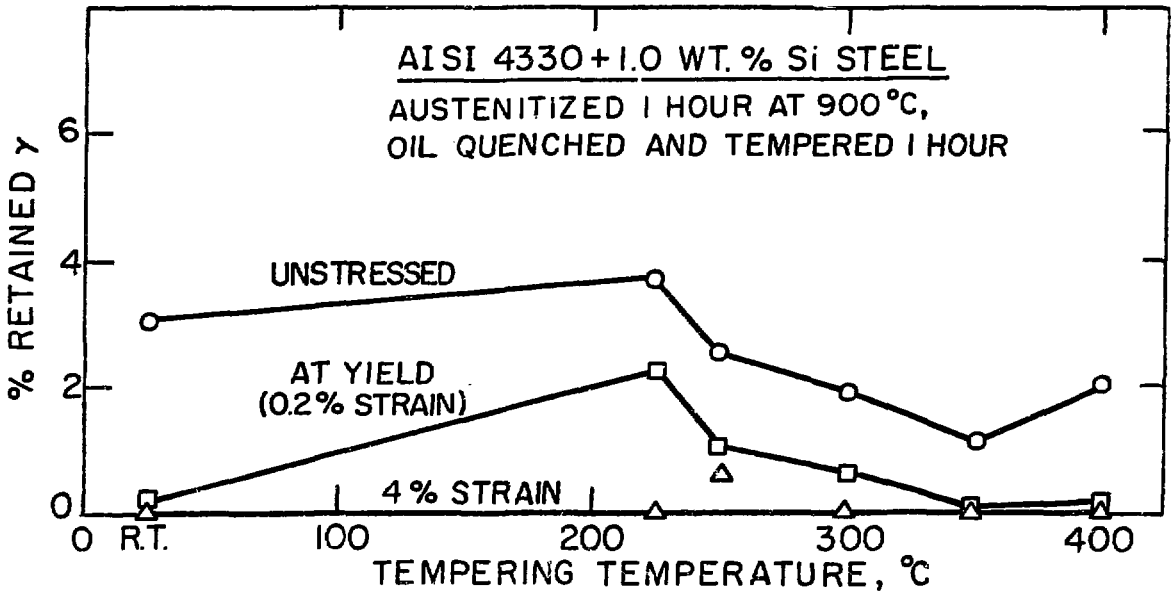
AISI 4330+1.0 WT.% Si STEEL
AUSTENITIZED 1 HOUR AT 900°C,
OIL QUENCHED AND TEMPERED 1 HOUR
% RETAINED γ
6
4
2
0
UNSTRESSED
AT YIELD
(0.2% STRAIN)
4% STRAIN
0
R.T.
100
200
300
400
TEMPERING TEMPERATURE, °C
XBL 767-7229

Fig. 32.

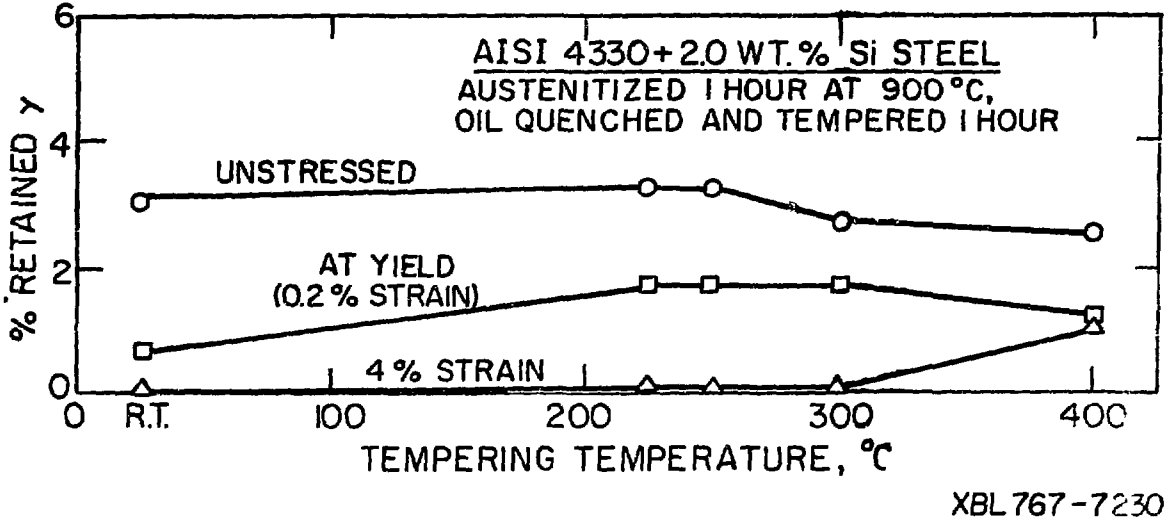
AISI 4330+2.0 WT.% Si STEEL
AUSTENITIZED 1 HOUR AT 900°C,
OIL QUENCHED AND TEMPERED 1 HOUR
UNSTRESSED
AT YIELD
(0.2% STRAIN)
4% STRAIN
% RETAINED γ
TEMPERING TEMPERATURE, °C
0
2
4
6
R.T.
100
200
300
400
XBL 767-7230

Fig. 33.

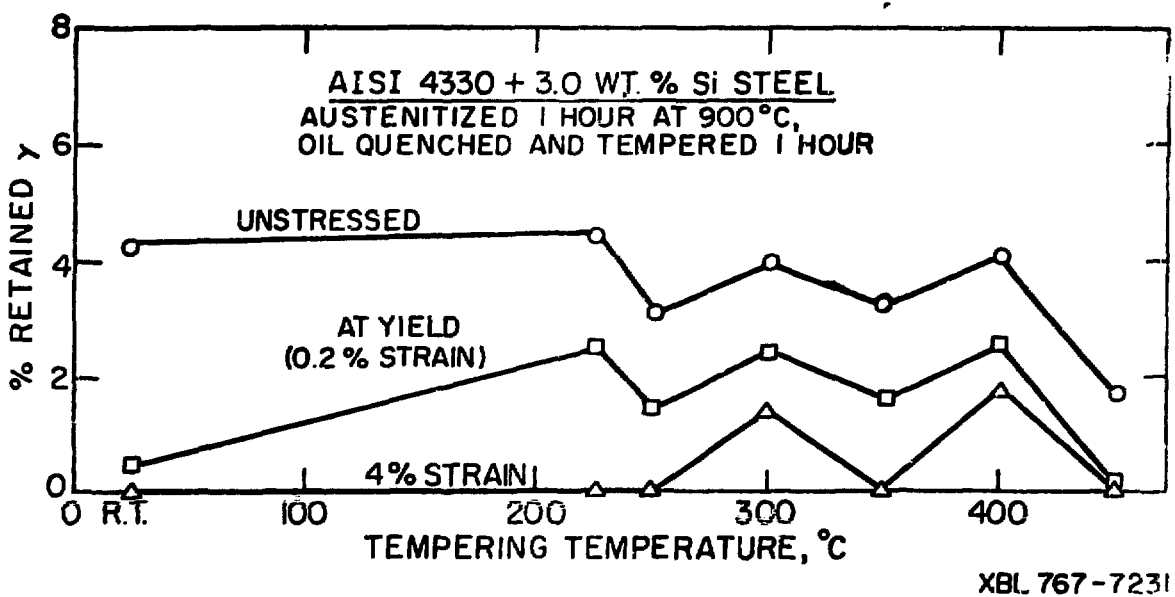
AISI 4330 + 3.0 WT. % Si STEEL
AUSTENITIZED 1 HOUR AT 900°C,
OIL QUENCHED AND TEMPERED 1 HOUR
UNSTRESSED
AT YIELD
(0.2 % STRAIN)
4% STRAIN
% RETAINED γ
0
2
4
6
8
0 R.T.
100
200
300
400
TEMPERING TEMPERATURE, °C
XBL 767-7231

Fig. 34.

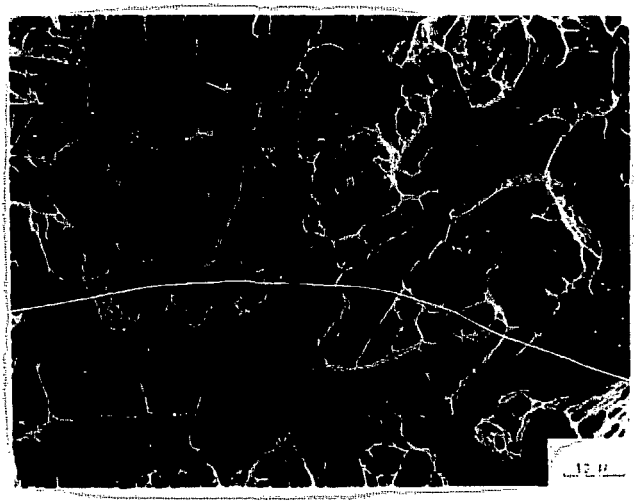

(a)

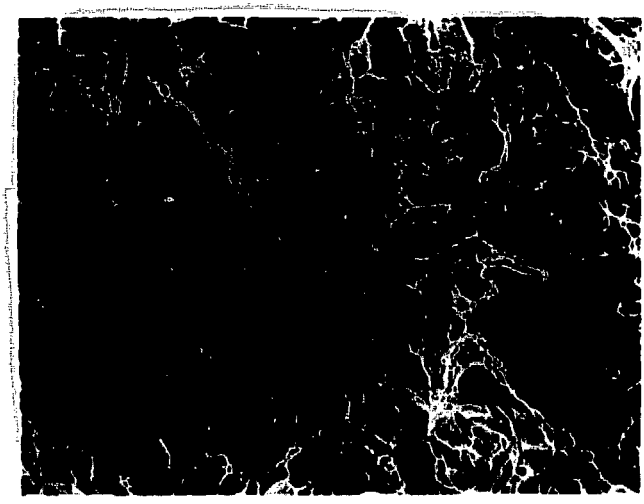

(b) XBB 768-7916

Fig. 35.

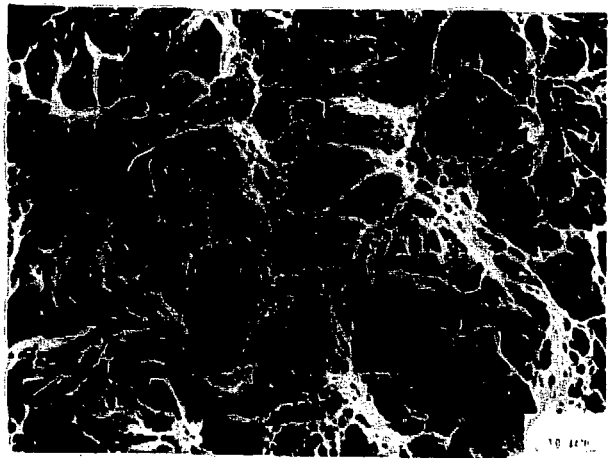

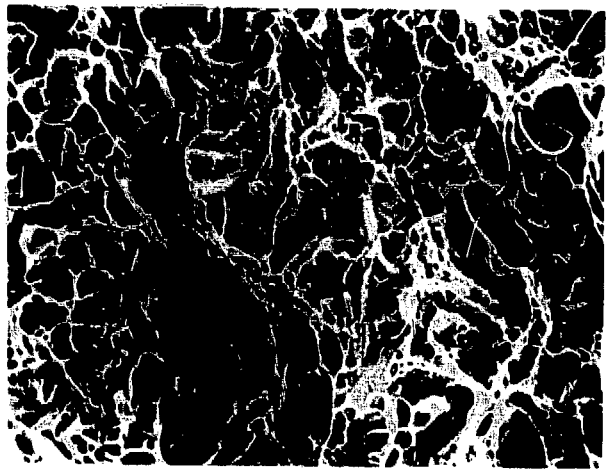

(b) XBB 768-7915

Fig. 36.

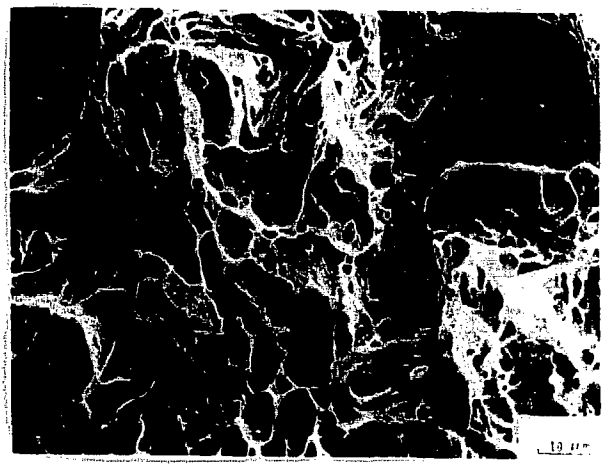

(a)

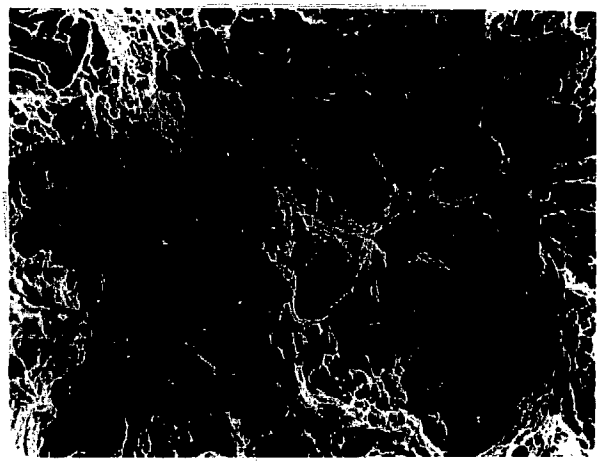

(b) XBB 768-7907

Fig. 37.

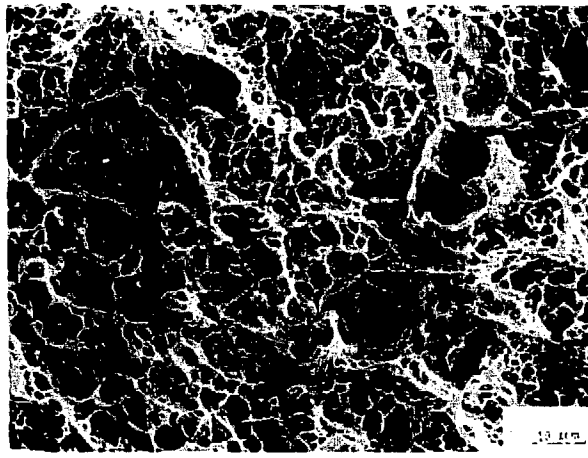

(a)

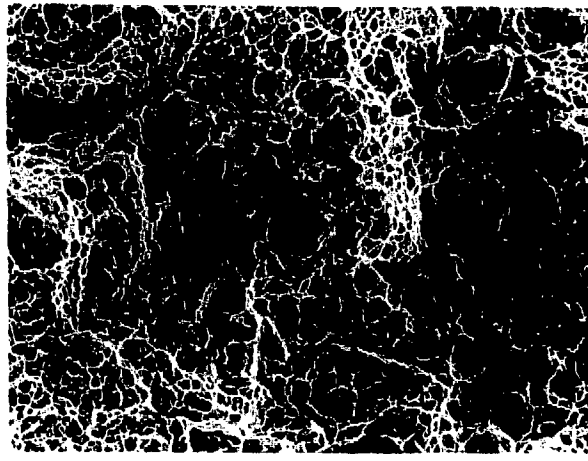

(b) XBB 768-7908

Fig. 38.

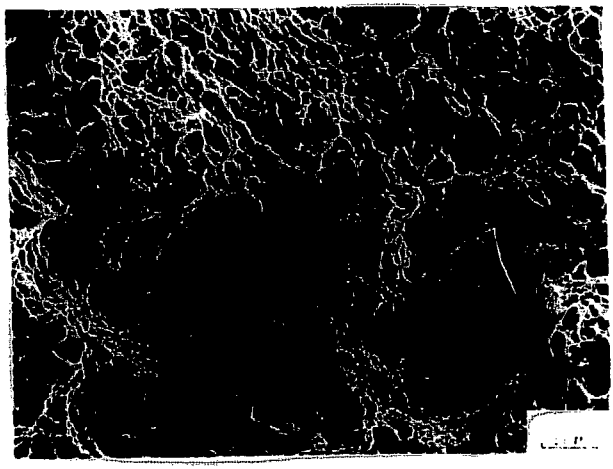

(a)

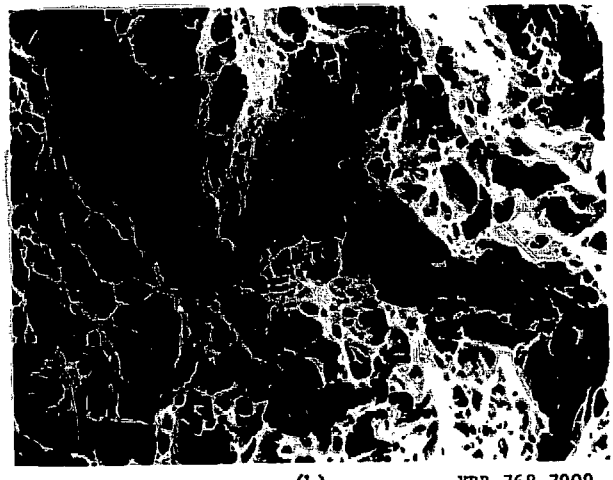

(b) XBB 768-7909

Fig. 39.

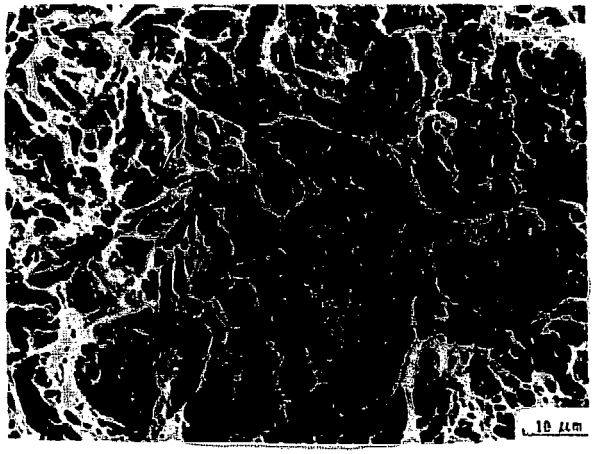

(a)

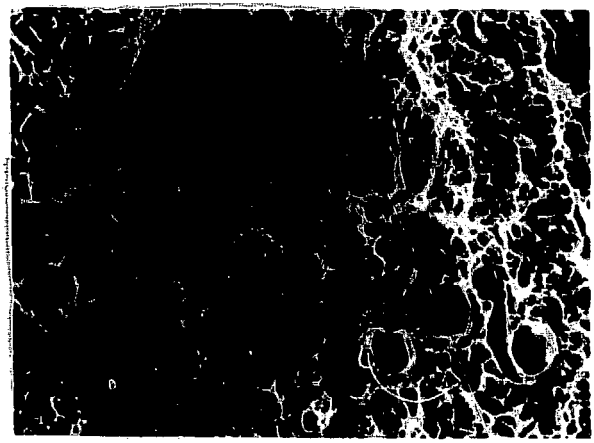

(b) XBB 768-7901

Fig. 40.

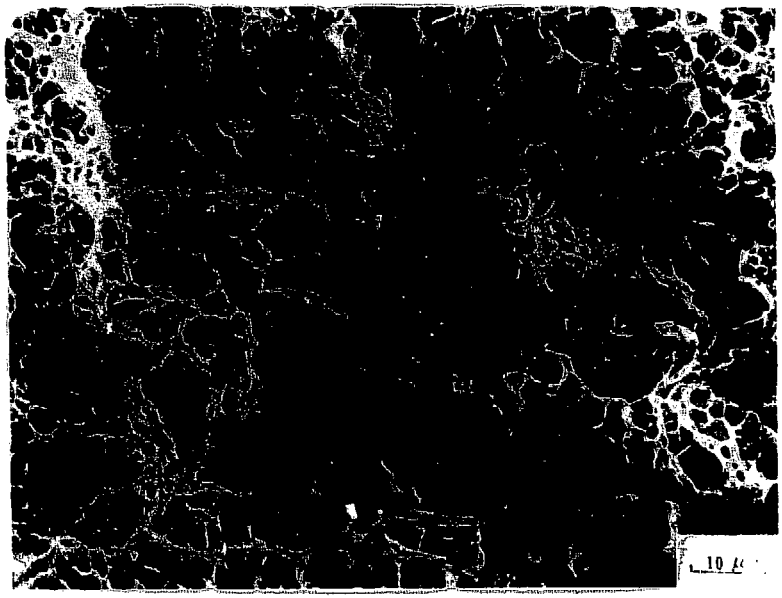

XBB 768-7905

Fig. 41.

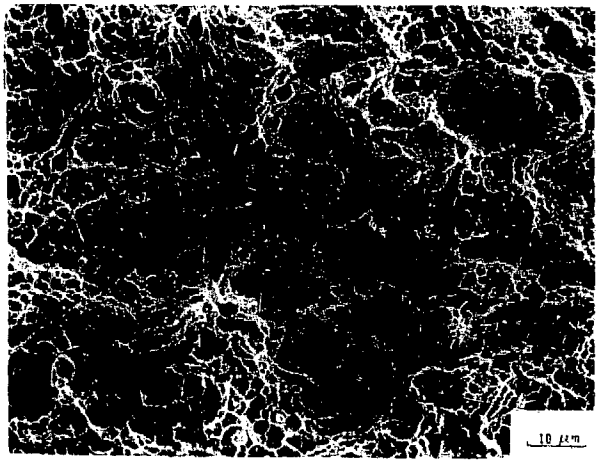

(a)

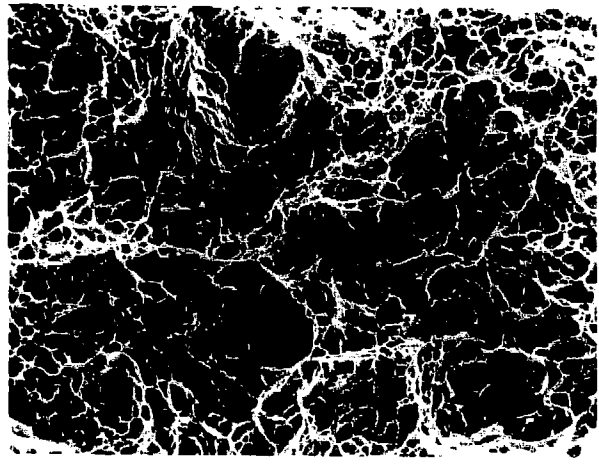

(b) XBB 768-7910

Fig. 42.

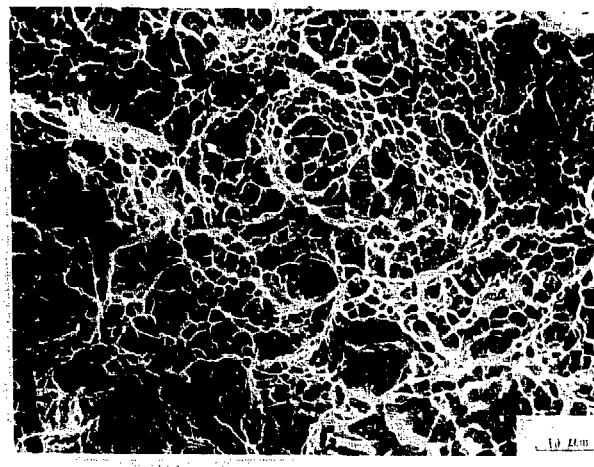

(a)

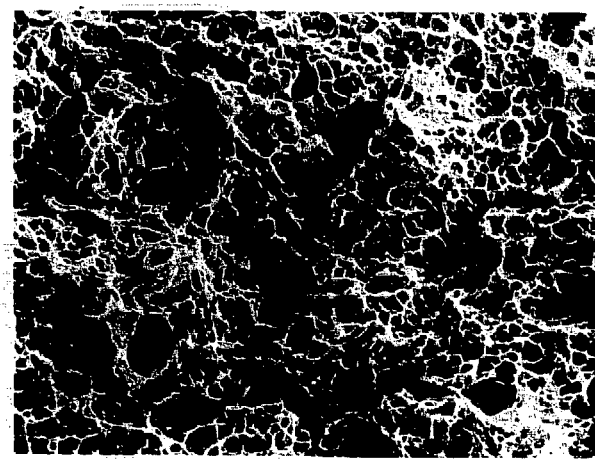

(b) XBB 768-7911

Fig. 43.

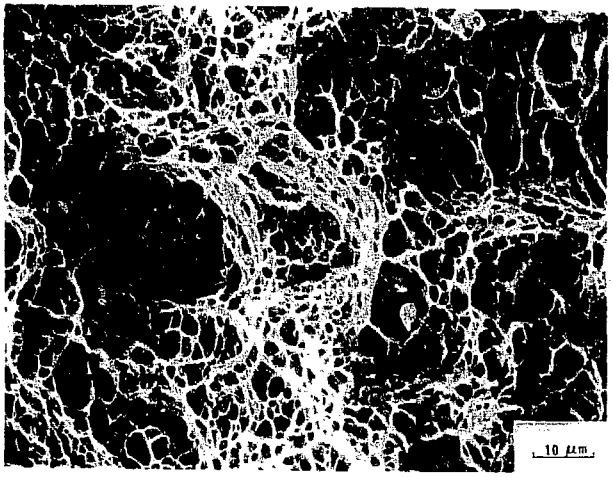

(a)

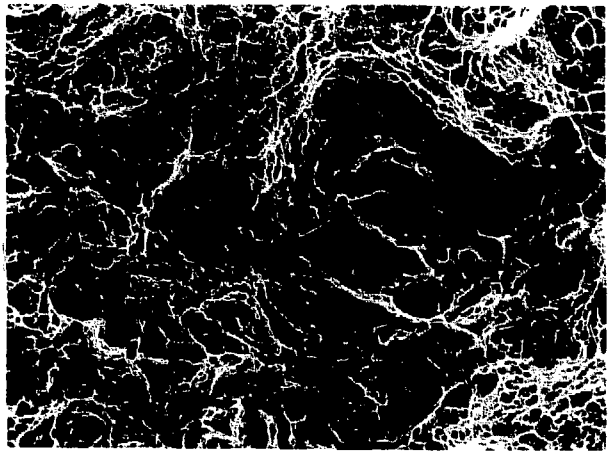

(b)

XBB 768-7900

Fig. 44.

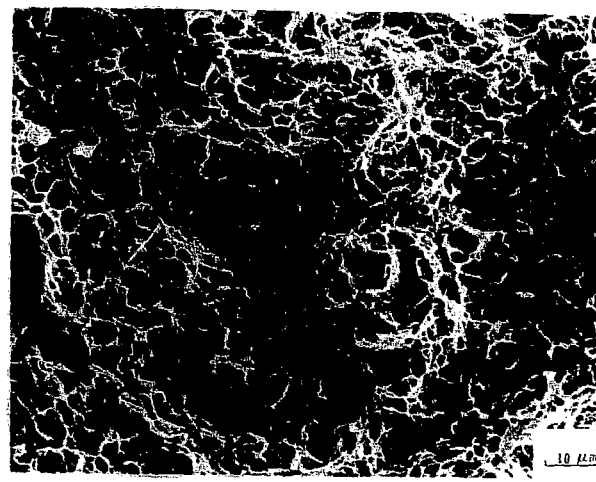

(a)

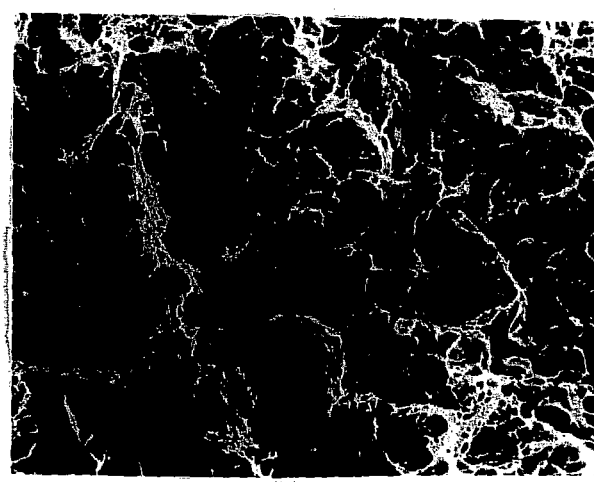

(b)

XBB 768-7902

Fig. 45.

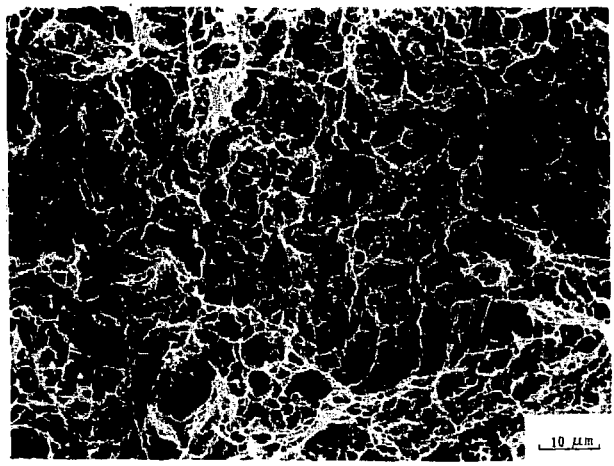

(a)

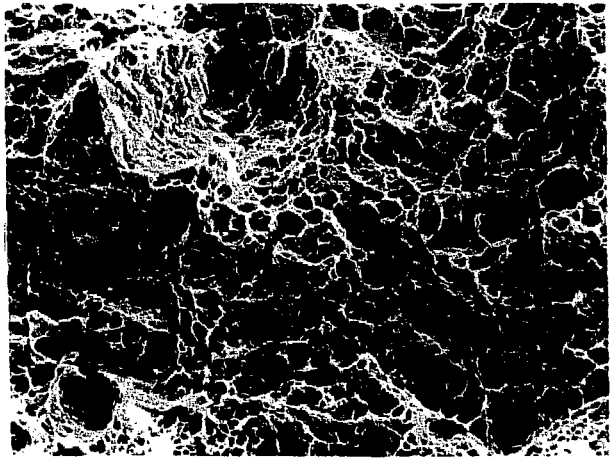

(b) XBB 768-7912

Fig. 46.

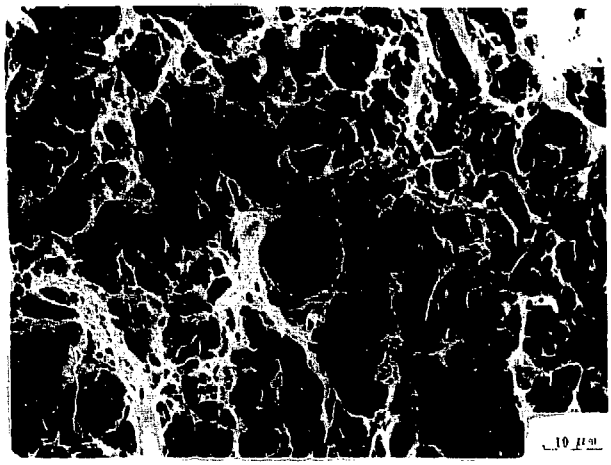

(a)

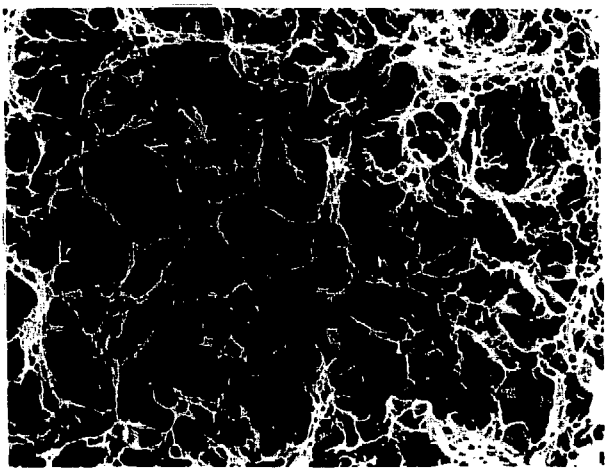

(b) XBB 768-7903

Fig. 47.

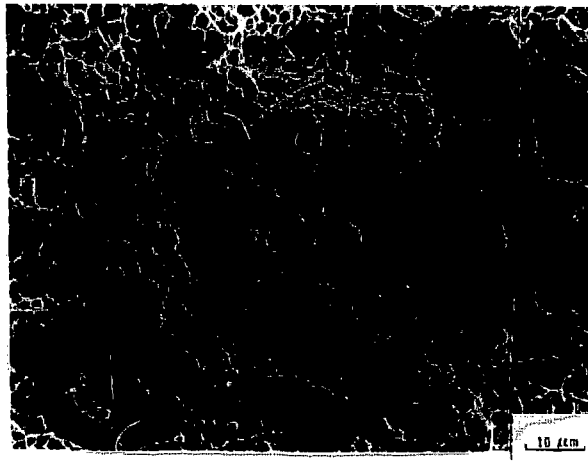

(a)

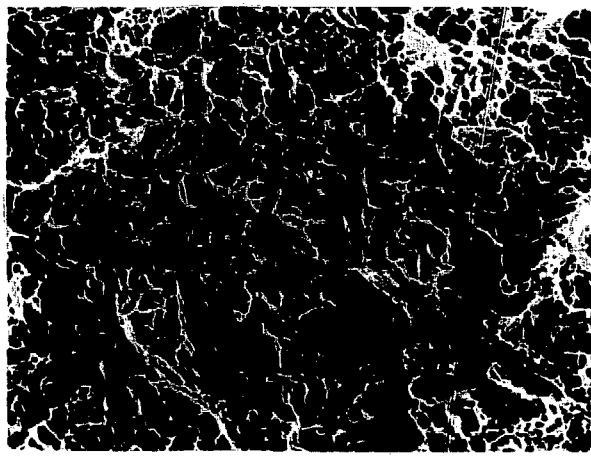

(b)

NBB 768-7914

Fig. 48.

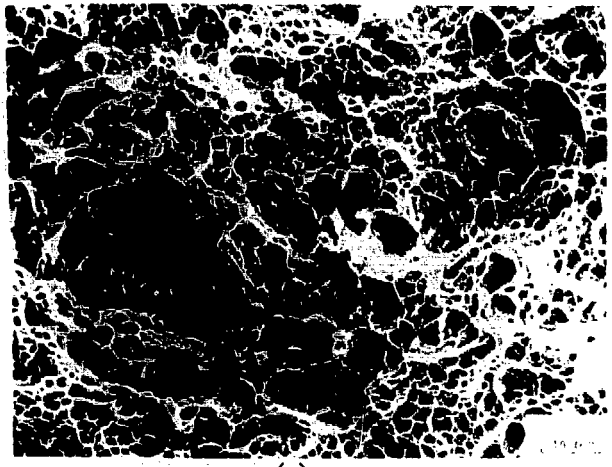

(a)

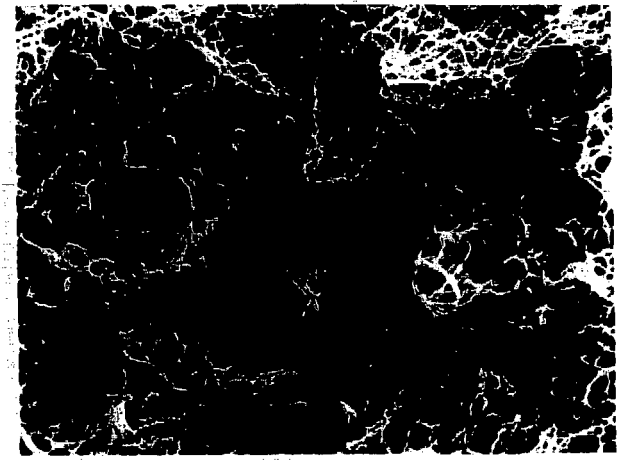

(b) XBB 768-7904

Fig. 49.

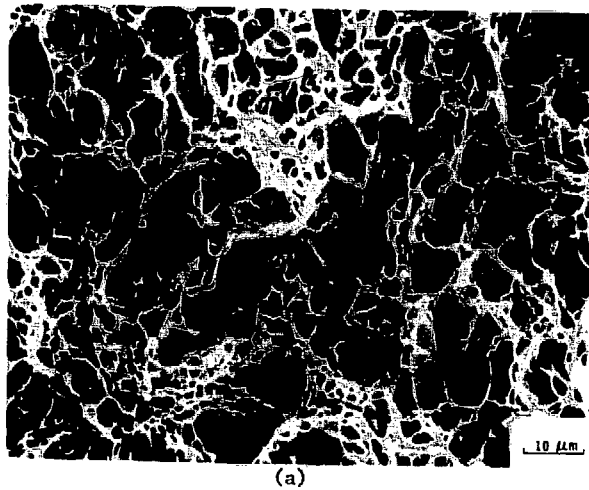

(a)

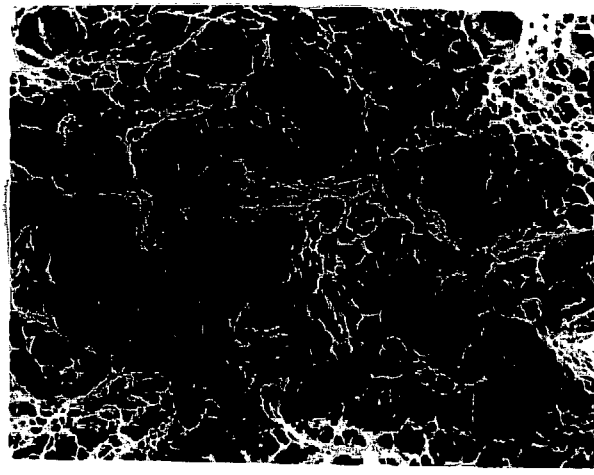

(b)

XBB 768-7914

Fig. 50.

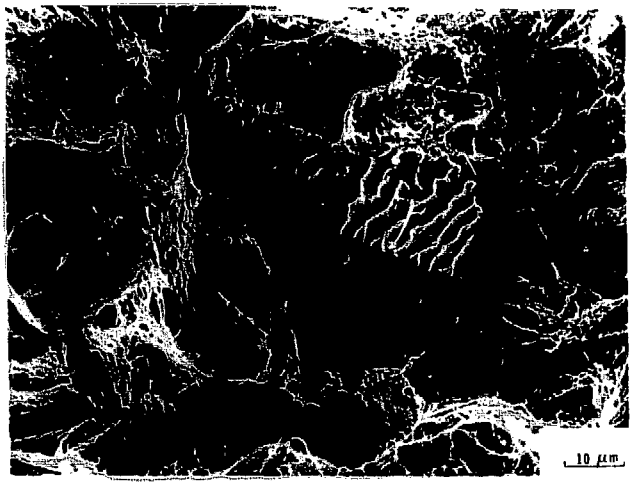

(a)

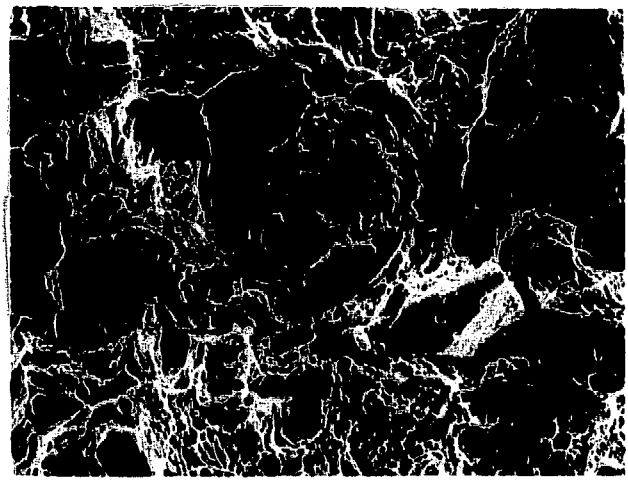

(b)

XBB 768 /917

Fig. 51.

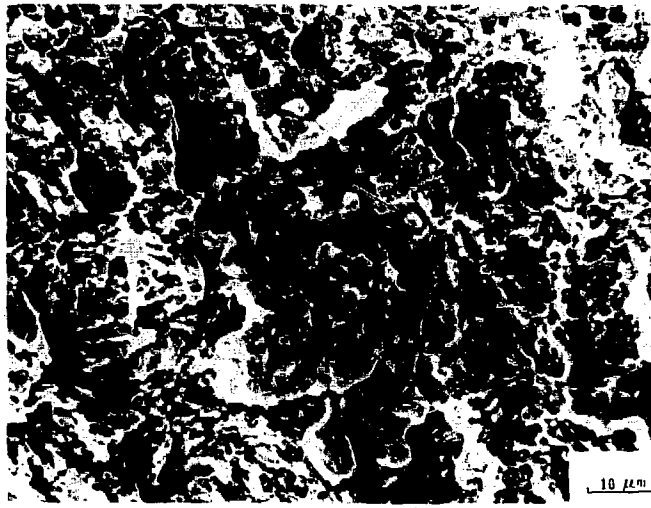

(a)

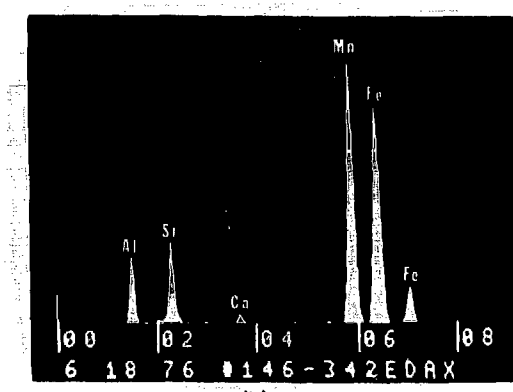

(b) XBB 768-7919

Fig. 52.

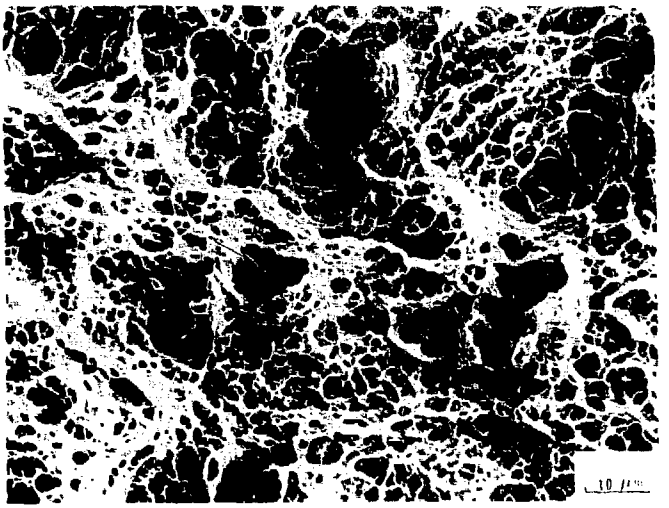

(a)

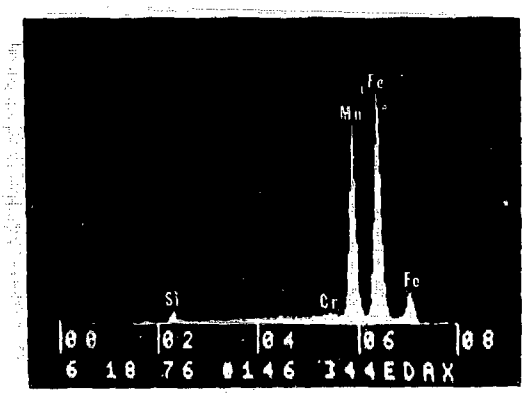

(b) XBB 768-7918

Fig. 53.

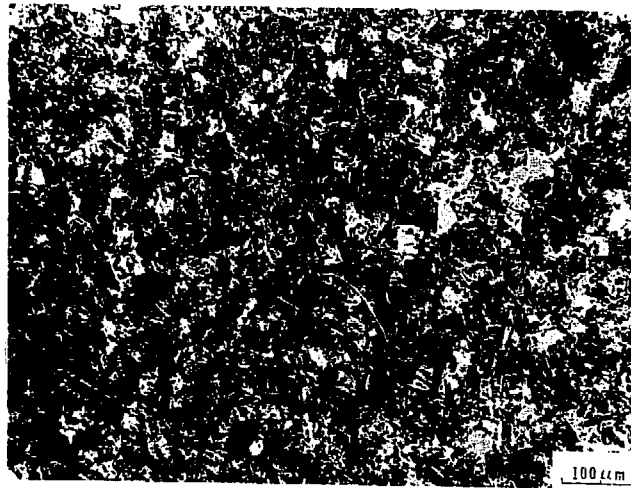

(b)

XBB 768-7922

Fig. 54.

(a)

(b)

XBB 768-7920

Fig. 55.

(a)

(b) XBB 768-7921

Fig. 56.

XBB 768-7906

Fig. 57.

(a)

(b) XBB 768-7899

Fig. 58.

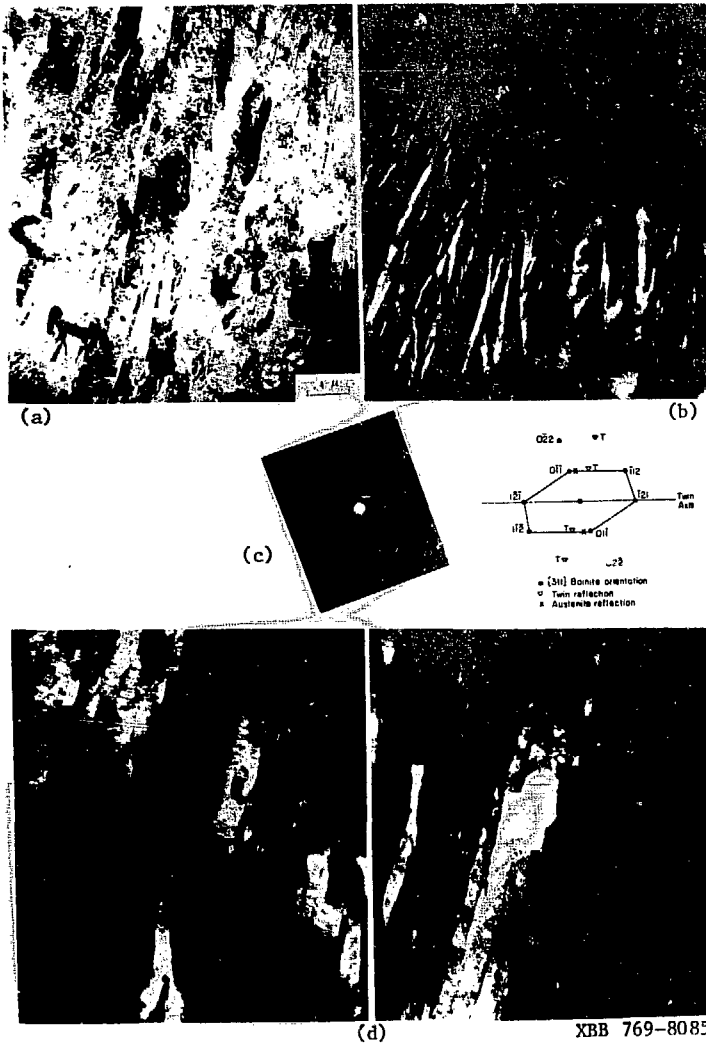
(a)
(b)
(c)
(d)
022
011
112
121
Twin Axis
Austenite reflection
XBB 769-8085

Fig. 59.

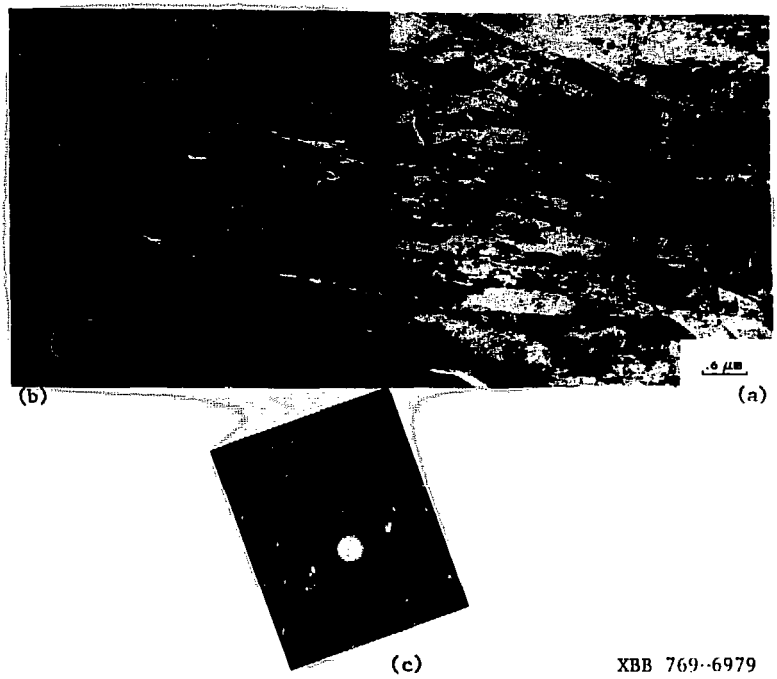

Fig. 60.

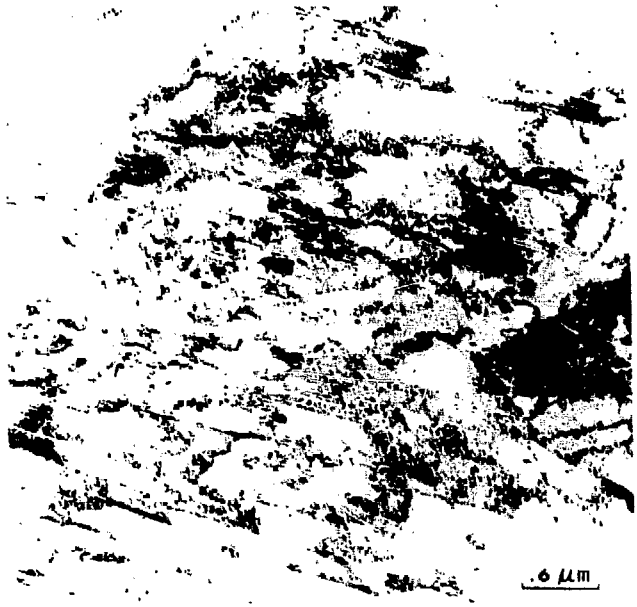

(a)

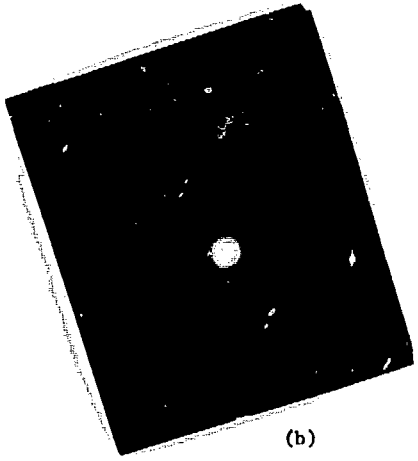

(b)

XBB 769-6982

Fig. 61.

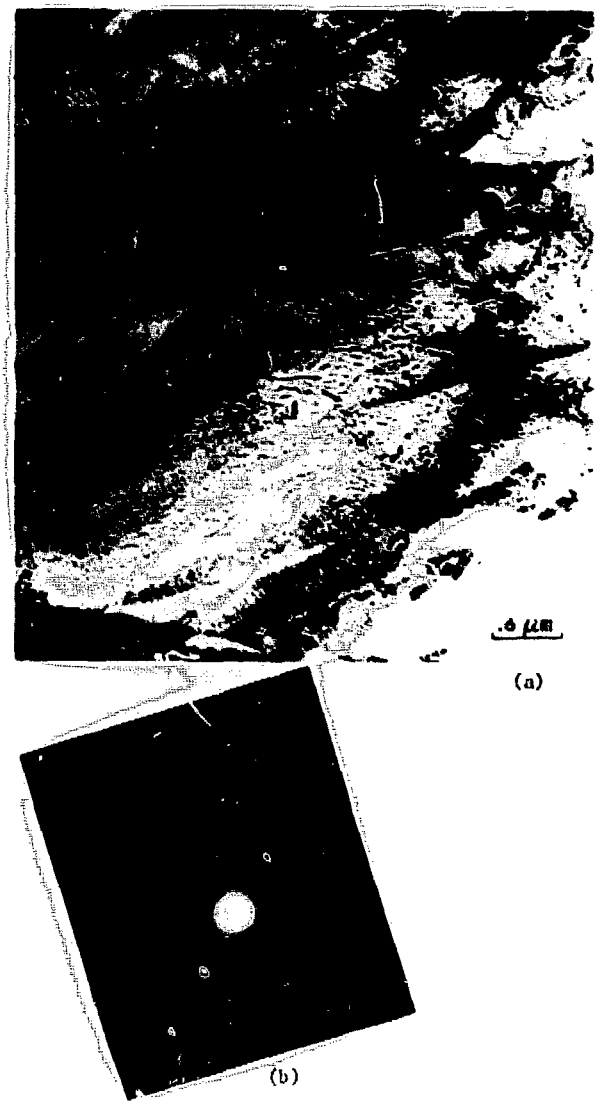

Fig. 62. XBB 769-6977

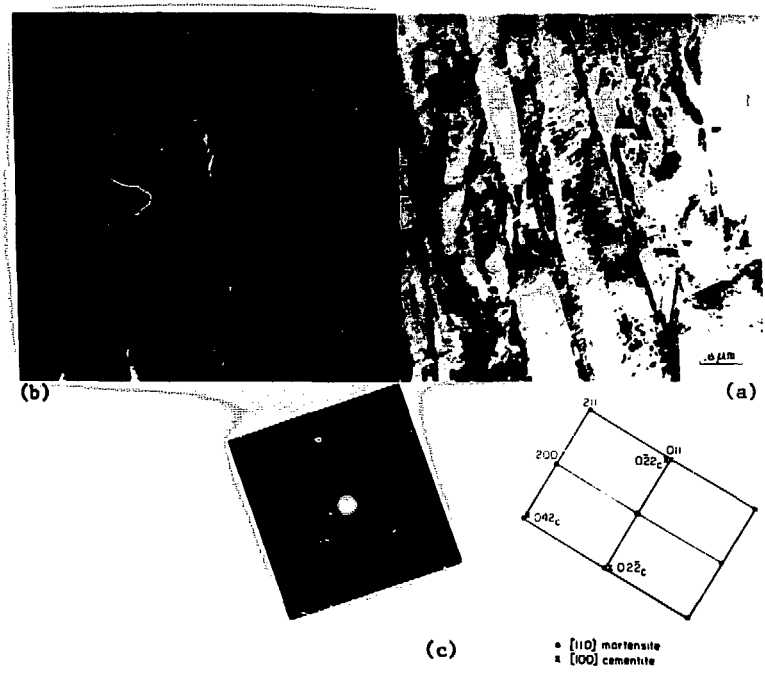

XBB 769-6978

Fig. 63.

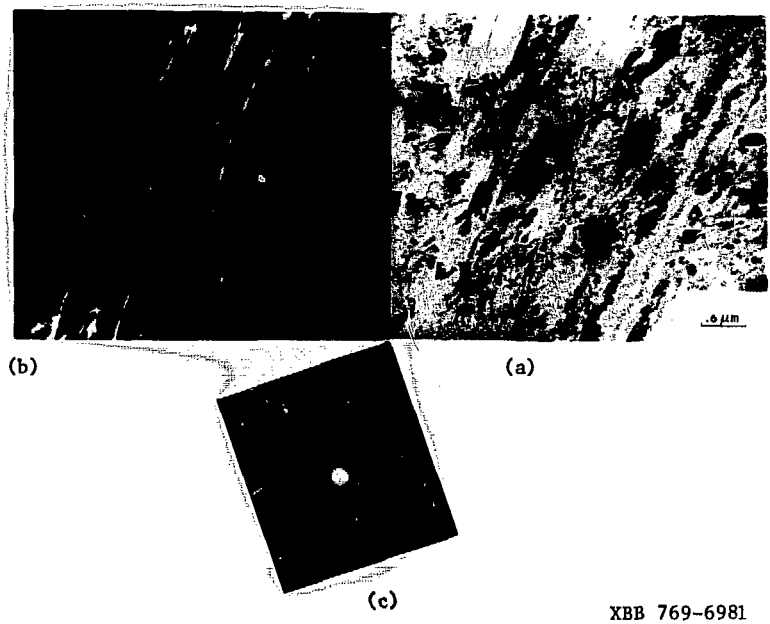

XBB 769-6981

Fig. 64.

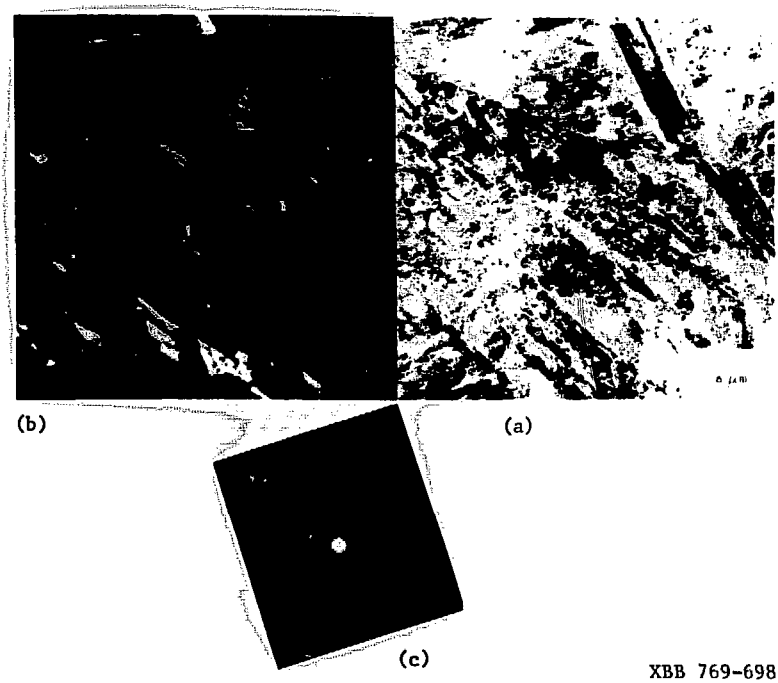

XBB 769-6983

Fig. 65.

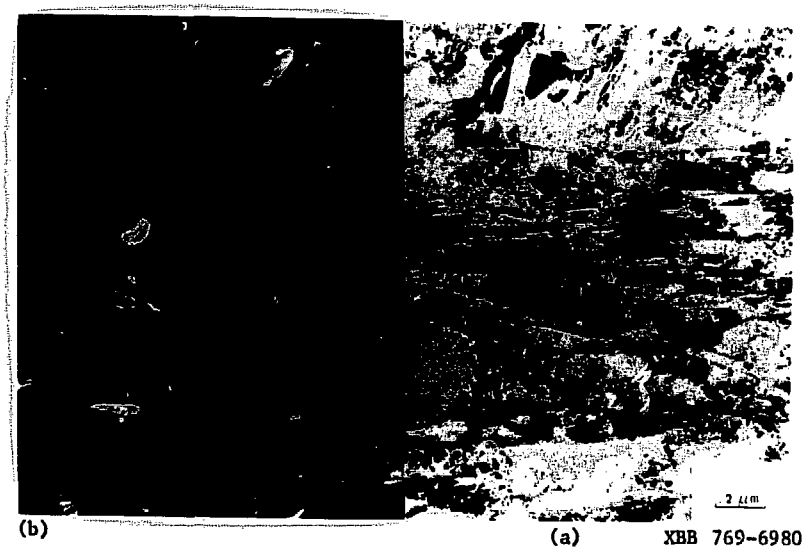

Fig. 66.

(a)

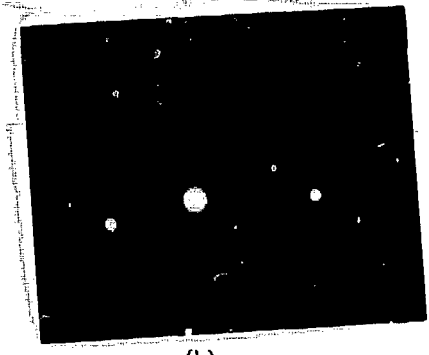

(b)

XBB 769-8086

Fig. 67.

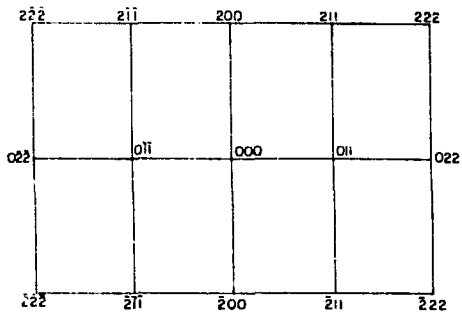

[011] MARTENSITE

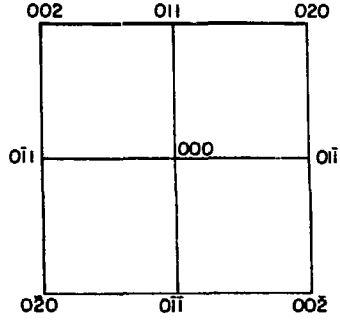

[100] MARTENSITE

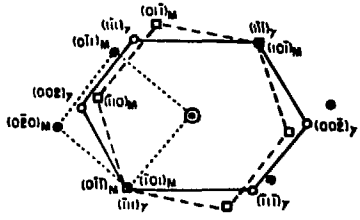

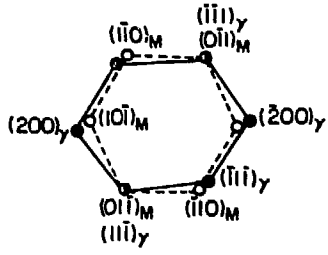

- □ [111] MARTENSITE SPOT
- ○ [110] AUSTENITE SPOT
- ● [100] MARTENSITE SPOT

——— Austenite Orientation $[011]_\gamma$

- - - - - Martensite Orientation $[111]_M$

XBL 768-10277

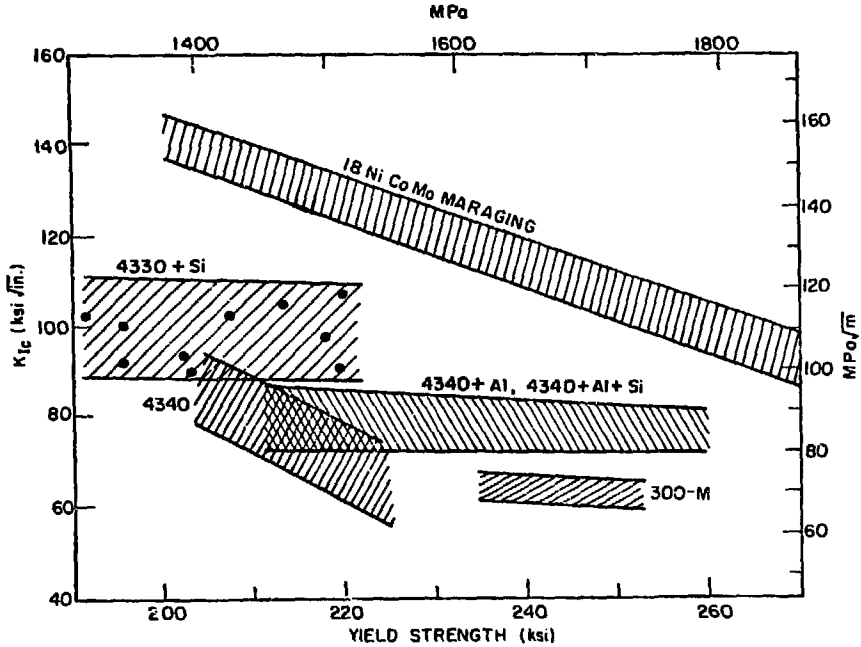
MPa
1400
1600
1800
160
140
120
100
80
60
40
18 Ni Co Mo MARAGING
4330 + Si
4340
4340+ Al, 4340+Al+ Si
300-M
K_{Ic} (ksi $\sqrt{in.}$)
MPa$\sqrt{m}$
200
220
240
260
YIELD STRENGTH (ksi)
XBL 769-7499

Fig. 69.

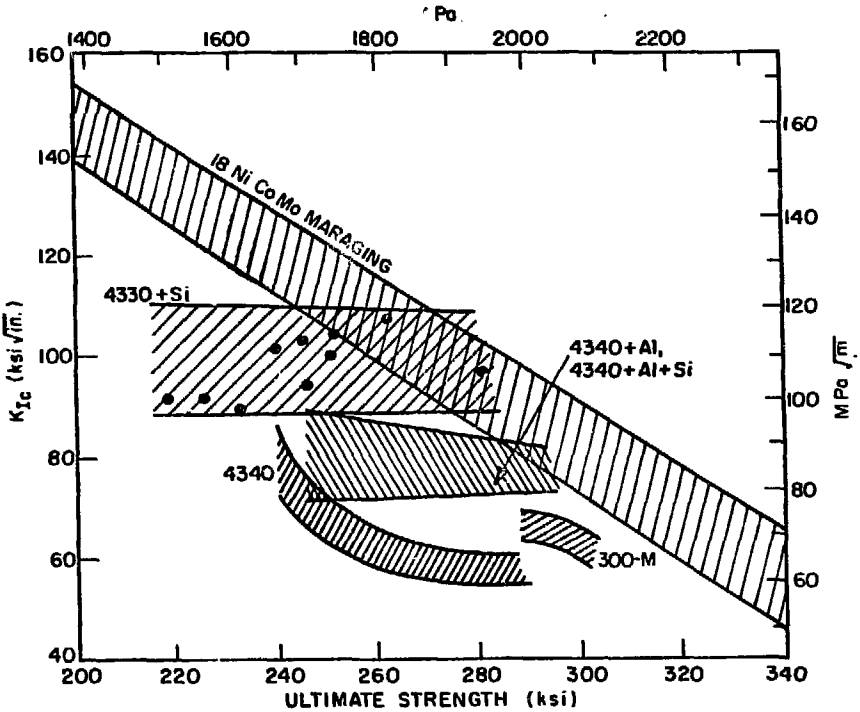

XBL 769-7498

Fig. 70.

ACKNOWLEDGEMENTS

The author wishes to express his deep appreciation to Professors Victor F. Zackay and Earl R. Parker for their continued guidance and encouragement throughout the course of this work. He would also like to express his gratidude to Professors Gareth Thomas and Iain Finnie for helpful discussions and a critical review of the manuscript. Special thanks are extended to Drs. M.S. Bhat, M.D. Bhandarkar and Professors M. P. Dariel and N. Kennon for many discussions and help in the preparation of the manuscript, to Mr. Y. Mishima for his help in electron microscopy and to Mr. G. Haddick for reviewing the manuscript.

The author wishes also to thank all the students of the Parker-Zackay research group for their help and encouragement during the course of his studies at Berkeley.

The valuable assistance of the technical support staff of the Materials and Molecular Research Division is acknowledged, in particular Brian Pope and John Holthius (alloy preparations), Ed Edwards, Julien Patenaude and Duane Newhart (machining), Done Krieger (mechanical testing), James Severns (electronics), Lee Johnson (metallography), Richard Lindberg (scanning microscopy), Sandy Stewart and Paul Stagnaro (purchasing), Gloria Pelatowski (preparation of line drawings) and Alice Ramirez (typing of the manuscript). Special thanks are due to Eric C. Dittmar (student research helper) for his overall valuable assistance in this work. Last but not least, the author is indebted to his wife, Hava, and children without whose constant support and encouragement throughout this investigation this work would not have been acommplished.

This work was done under the auspices of the U.S. Energy Research and Development Administration.